T H E U N I V E R S I T Y O F T U L S A

THE GRADUATE SCHOOL

EXPERIMENTS AND CFD SIMULATIONS OF SAND EROSION AND IMPACT ON PERFORMANCE OF ELECTRICAL SUBMERSIBLE PUMP (ESP)

By
Tanmay Sanjiv Tatu

A thesis submitted in partial fulfillment of

the requirements for the degree of Master of Science

in the Discipline of Petroleum Engineering

The Graduate School

The University of Tulsa

2023

T H E U N I V E R S I T Y O F T U L S A

THE GRADUATE SCHOOL

EXPERIMENTS AND CFD SIMULATIONS OF SAND EROSION AND IMPACT ON PERFORMANCE OF ELECTRICAL SUBMERSIBLE PUMP (ESP)

by
Tanmay Sanjiv Tatu

A THESIS

APPROVED FOR THE DISCIPLINE OF

PETROLEUM ENGINEERING

By Thesis Committee

Hong-Quan Zhang, Chair
Paul Song
Haiwen Zhu

ABSTRACT

Tanmay Sanjiv Tatu (Master of Science in Petroleum Engineering)

Experiments and CFD simulations of sand erosion and impact on performance of Electrical Submersible Pump (ESP)

Directed by Drs. Hong-Quan (Holden) Zhang and Haiwen Zhu

69 pp., Chapter 5 : Conclusions and Recommendations

(403 words)

Artificial lifting is the process of providing external energy to producing wells when the natural drive of the reservoir is insufficient to produce fluids by itself. Among different lifting methods, Electrical Submersible Pumps (ESPs) are one of the most widely used in the oil and gas industry. However, ESPs are very susceptible to the presence of gases or solid particles like sand, which heavily affect the pump performance and run life. The maintenance and overhauling of an ESP in a producing well are not economical, thus extending or maintaining its operational life is important. Predicting the degradation in the pump performance is crucial in estimating the workability and overall life of an ESP.

To evaluate the sand effect on ESPs, sand erosion testing was performed at the Tulsa University Artificial Lift Projects (TUALP) experimental site on two multi-stage mixed flow ESPs (14-stage ESP1 and 8-stage ESP2). The testing was carried out at their individual Best Efficiency Points (BEPs) at 1750 BPD and 6000 BPD, respectively, for a total of 64 hours/per pump in intervals of 8, 8, 16, and 32 hours. The sand was replaced every two hours, and the flow loop was flushed with water to get rid of any residual sand, dust, rust, or unwanted particles before starting

the next test. The performance parameters such as head, efficiency, and horsepower were measured before and after each test interval to observe the change in hydraulic performance. After each test interval, the pump was removed and opened to observe the dimensional changes and weight loss of its internal parts.

It was observed that over the entire 64-hour test period, the head of both pumps reduced by 15%, and the efficiency decreased by 7-15%. The geometry also showed a clear trend of change over the testing. The seal clearances increased by almost 10 times the original value. The weight loss in the stages of ESP2 was much more than the stages in ESP1, possibly due to the much higher operational flow rate in the former. The results of testing such as the dimensional changes and performance parameter deterioration are presented in detail in this paper. The results are comparable with previous similar experiments. This study validates the previous experiments and the data presented help better understand the wear and process of erosion in ESPs and predict the change in performance over a set period of operation of the ESPs under a sandy flow environment.

ACKNOWLEDGEMENTS

This document is a result of constant inspiration, knowledge, and encouragement provided by my advisor Dr. Hong-Quan Zhang, who has guided me throughout the Master's program. I would also like to extend my gratitude to Dr. Haiwen Zhu, for help with my testing, simulation, and writing skills. I am grateful to them for trusting me and allowing me to be a part of the Tulsa University Artificial Lift Projects (TUALP)

I wholeheartedly appreciate the opportunity to work on an actual field project provided to me by the ChampionX UNBRIDLED ESP Systems and TUALP. The advice I received during the project regarding the experimenting, analysis and managing time from TUALP senior members, Dr. Zhang and Dr. Zhu and the ChampionX team engineers, David Baillargeon, Gayla Iron-West, Dr. Paul Song, is very valuable and has helped me gain technical knowledge about ESPs.

I happily thank my TUALP fellow colleagues and team members Dayo Tychus, Sai Praveen Adiraju and Umair Hasan who have always inspired me to do better in a very positive and conducive work environment. I would like to thank Mr. Bryan Sams for technical advice on operating the experimental flow loop and Ms. Donna Trankley for her administrative work.

I acknowledge and appreciate the comments provided to me regarding the thesis from Dr. Siamack Shirazi and post-doctoral associate Dr. Farzin Darihaki for his help in the CFD simulations regarding inlet velocity profile development.

Finally, I would like to appreciate the love and support from my parents, Mr. Sanjiv Tatu and Mrs. Niraja Tatu, who inspire me to be a better person and are role models in this journey.

TABLE OF CONTENTS

LIST OF FIGURES

LIST OF TABLES

INTRODUCTION

The secondary recovery, including using artificial lift equipment, arises when the natural drive of producing wells depletes due to continuous production. Among the various artificial lift options available, the Electrical Submersible Pump (ESP) stands out as the most widely and globally used equipment in the industry. ESPs can be operated under low bottom-hole pressures and under multi-phase flow conditions that include the presence of gas, water, or sand during the production of crude from a well. However, the presence of sand or gas deeply impacts the life and performance of any ESP. Gas can lead to deliverable head degradation, and the formation of gas pockets within the ESP further hampers overall efficiency. On the other hand, solid particles, especially fine-grade sand, pose a serious concern for the ESP's integrity. Despite the use of gravel packs with mesh filters to prevent larger particles from entering, fine-grade sand manages to infiltrate the pump along with the produced fluids. This results in erosion-abrasion problems, causing operational difficulties.Sand causes a combined effect of abrasion and erosion on the internal parts of the pump. Abrasion is the process of loss of material when two surfaces of different roughness get in contact with each other or through an external body whereas erosion is caused due to mechanical impact of particles on the solid surfaces of rigid bodies. The repair, maintenance, or replacement of an ESP from its installed position is economically draining. Thus, it is very crucial that the functional life of an ESP stays intact or at least does not get reduced and measures are taken to extend the workable life of an ESP.

To investigated sand effect on ESPs, two multi-stage ESP pumps were sand tested individually for a total of 64 hours in time intervals of 8, 8, 16, and 32 hours under single-phase

conditions using water as the medium of transport. A single test is carried out for a total of 2 hours with a 15-minute draining and refilling routine before starting the next test with a fresh batch of sand. Parameters such as torque and temperature were noted during the testing and performance parameters such as head delivered, efficiency, and horsepower were calculated after the completion of each test interval.

CFD simulations were also conducted on a 2-stage diffuser-impeller geometry of an ESP pump and Discrete Phase Model (DPM) tracking was applied to observe the impact of injected sand particles and the rebound effect on the walls of the impeller-diffuser geometry for 2 stages. Erosion Rate (ER) was predicted in Kg/m^2-s using 6 erosion models available in the literature encoded in a User Defined Function (UDF) to calculate the amount of material eroded from a surface per unit area per unit of time. The UDF also provides particle impact information such as the impact velocity, impact angle, and the frequency of impact which is also crucial in understanding the wear process. Each stage of the 2-stage geometry has a purpose in the simulation, the 1^{st} stage is used to generate a stable convergent flow field and the 2^{nd} stage is the main stage where we observe the erosion patterns and calculate the amount of erosion. The UDF was modified to account for the inlet pre-rotation effect by considering the inlet velocity data. This data is obtained as velocity-position from the 2^{nd} stage of the geometry at the impeller-2 inlet and was used as an input parameter in the 1^{st} stage impeller inlet. The new and old UDF-generated simulation results are compared both qualitatively and quantitatively and it was observed that the modified UDF shows improvement on the old previous simulation as the results obtained are more comparable to reality. The new UDF although more accurate, still shows some aberrant results and needs improvement to further model the erosion on the geometry more accurately.

CHAPTER 1

LITERATURE REVIEW

Artificial lift involves supplying external energy to reservoirs with insufficient pressure to produce fluids independently and economically. Various types of artificial lift equipment are utilized in production operations, and their selection is influenced by factors like wellbore conditions, fluid properties, reservoir type, characteristics, and environmental considerations. Apart from these technical factors, there are other economic factors as well dictating the choice of an artificial lift method. The objective of any artificial lift method is to maximize production out of the wells and hence maximizing the revenue while minimizing the cost of production. There exist a variety of artificial lifting equipment currently in the oil and gas industry (Brown, 1982):

1) Sucker rod pumps
2) Electrical Submersible pumps
3) Gas lift
4) Plunger lift
5) Progressive cavity pumps
6) Reciprocating pumps

Electrical submersible pumps are one of the most commonly used equipment globally for the specific reasons of highly efficient and reliable production operation in the oil and gas industry.

1.1 Overview of ESPs

ESPs are surface downhole equipment and are in general centrifugal fluid-moving pumps

that can be operated both in onshore and offshore conditions. It is a versatile lifting equipment with an operational range from 100 to 30,000 BPD, while that of other equipment is more limited. ESPs are good to use in wells with low bottom hole pressure, low GOR, and high water cut. Figure 1.1 shows an installed ESP assembly with its surface and subsurface components.

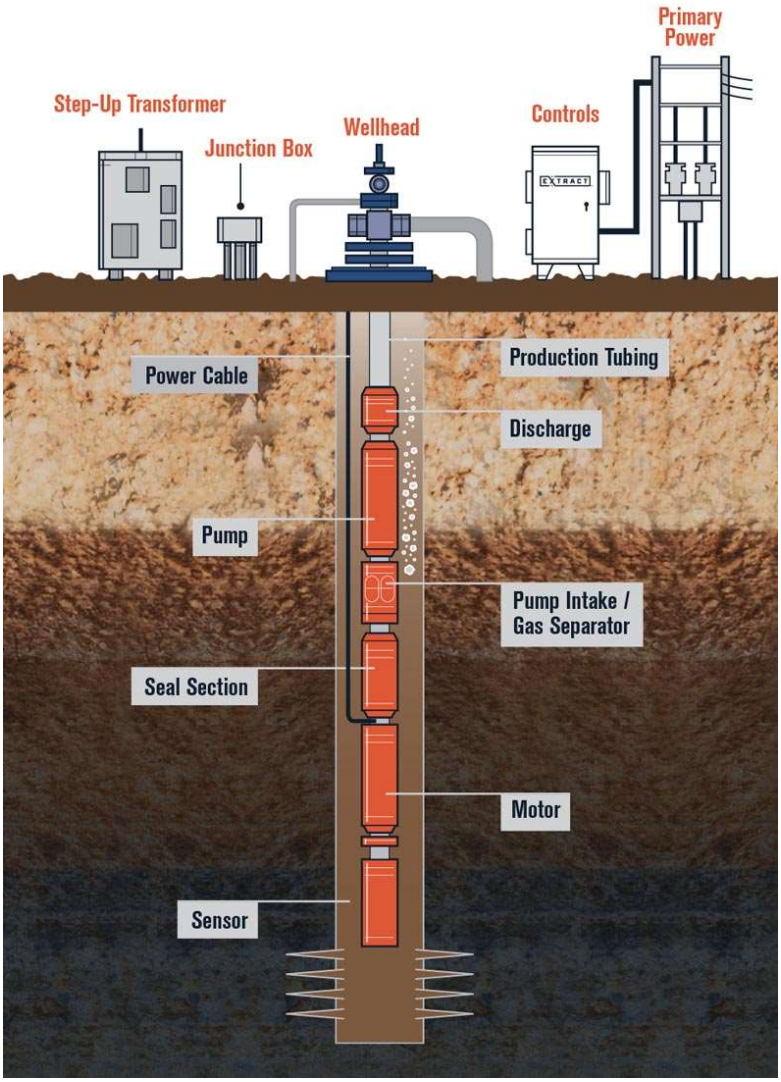

Figure 1.1: ESP assembly downhole and surface

ESPs are equipped with vertically stacked, multi-stage pumps that are powered by three-phase electric motors. Every ESP (Electric Submersible Pump) is designed to function optimally within a particular speed range, which is determined by factors like the maximum deliverable head and the number of stages. As seen in Figure 1.2, there exists a point at which the pump achieves

its highest efficiency, which is referred to as the Best Efficiency Point (BEP). Operating the pump at or near the BEP ensures optimal efficiency and reliable operation. By operating at the BEP, the pump can deliver fluids effectively while minimizing power consumption and maximizing the lifespan of the equipment. Proper understanding and control of the ESP's operating parameters, including speed, head, and number of stages, are necessary to maintain the pump within its optimal operating region and achieve the desired performance outcomes. Over time, the head delivered and efficiency of an ESP are prone to degradation as a result of hours of operation and other factors, including the presence of external media.

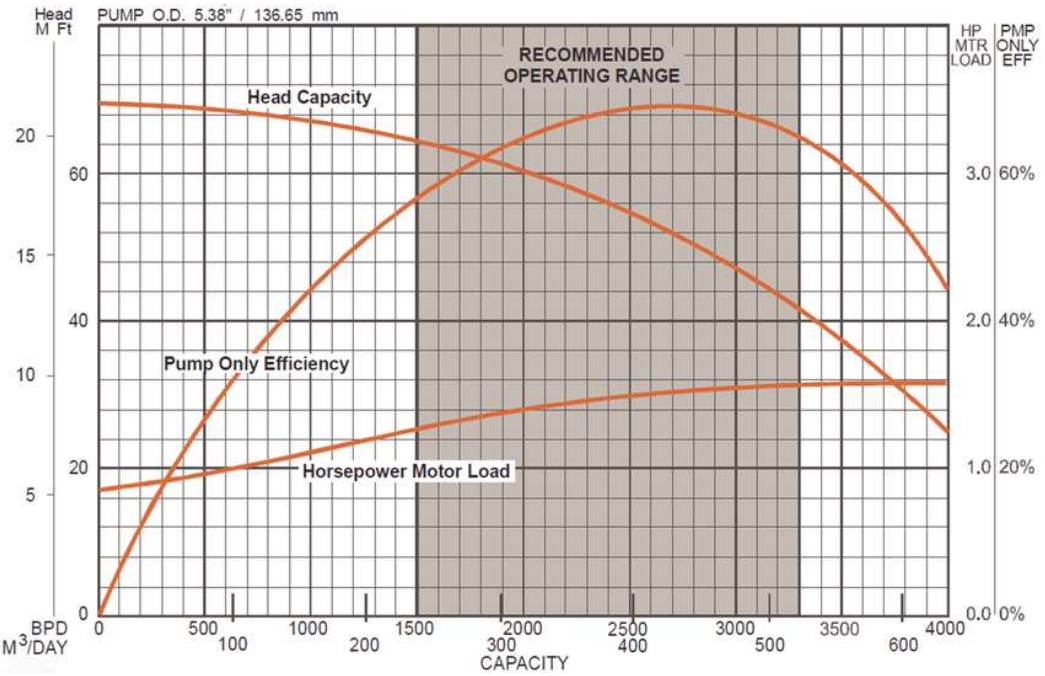

Figure 1.2: ESP performance curve

An ESP stage is composed of a rotating impeller and a stable diffuser. Impellers are critical components of an Electrical Submersible Pump (ESP) and are responsible for imparting energy to the fluid being lifted. Impellers are rotating disks with curved blades that are arranged in series on a common shaft within the pump stages. The primary function of impellers in an ESP is to increase the fluid's energy and pressure as it passes through each stage. As the impellers rotate, the curved

blades push the fluid in a radial direction. This centrifugal force increases the fluid's velocity and kinetic energy. Impellers are generally of 2 types: Mixed flow and Radial flow (Morrison et. al., 2015). They are designed to generate a flow pattern that is a combination of axial and radial directions. The fluid enters the impeller in an axial direction and is then gradually directed toward the radial direction as it passes through the impeller blades. Mixed-flow impellers are typically used in applications where moderate to high flow rates and moderate to high heads are required.

Radial flow impellers generate a radial flow pattern as the fluid enters the impeller axially and is directed outward in a radial direction by the curved blades of the impeller. The high-speed rotation of the impeller imparts kinetic energy to the fluid, increasing pressure as the fluid is forced against the pump casing. Radial flow impellers are commonly used in applications where high flow rates and moderate heads are required. They are well-suited for handling fluids with low viscosity and are efficient in generating pressure for pumping operations.

Impellers are typically made from high-strength materials, such as stainless steel or corrosion-resistant alloys, to withstand demanding downhole conditions. They are designed to handle the specific fluid properties, including temperature, pressure, and viscosity, encountered in the well. In multi-stage ESPs, each impeller stage consists of multiple impellers arranged in series. This configuration allows for successive energy addition and pressure increase as the fluid passes through the stages, facilitating the lifting of fluids from greater depths. An efficient impeller design helps in achieving higher pump efficiencies, maximizing fluid production, and minimizing power consumption. CFD analysis and testing are often employed to optimize impeller design and ensure optimal performance.

A diffuser is a stationary, conical-shaped device located downstream of the pump impellers within the pump stages. The primary function of the diffusers in an ESP is to convert the high velocity kinetic energy of the fluid exiting the impellers into pressure energy. As the fluid flows

through the diffusers, its velocity decreases, and the pressure increases. This pressure conversion helps in further boosting the fluid's energy and facilitating its upward flow towards the well's surface. The design of the diffusers is critical for optimizing the pump's performance. Factors such as the diffuser angle, length, and shape are carefully considered to achieve the desired pressure rise while minimizing energy losses. An efficient diffuser design helps in maintaining a stable flow pattern, reducing hydraulic losses, and improving overall pump efficiency. Diffusers are typically designed to match the impeller geometry and flow characteristics of the ESP. They are made from durable materials such as stainless steel or high-strength alloys to withstand harsh downhole conditions and resist erosion and corrosion.

Stage clearance refers to the radial gap or spacing between the impeller and the pump casing within each stage of the pump. Each stage of an ESP consists of an impeller and a diffuser, and the stage clearance refers to the distance between the outer diameter of the impeller and the inner diameter of the pump casing. Stage clearance is a critical parameter that affects the pump's performance and efficiency. It influences the hydraulic characteristics, flow patterns, and pressure development within the pump stages.

Figure 1.3: ESP stage diffuser and impeller

The shaft connects the motor and the impellers, transmitting power and rotational motion to the pump stages. It is an essential element in maintaining the structural integrity and operational performance of the ESP. The primary function of the shaft is to transmit torque from the motor to the impellers, enabling the rotation of the impellers within the pump stages. The shaft is designed to withstand mechanical stresses, including the rotational forces and fluid loads experienced during pump operation. In some ESP designs, the shaft may incorporate additional components such as radial bearings, thrust bearings, and sleeves. Bearings are used to support the rotating shaft within the ESP and provide a low-friction interface between the shaft and stationary components. They help reduce the wear and mechanical stresses on the shaft and enhance its operational reliability. Sleeves are used to protect the shaft from wear and damage caused by contact with other components or abrasive particles in the fluid. They are usually made of materials with high wear resistance, such as tungsten carbide or ceramic coatings. Sleeves are installed on the shaft in areas where contact or erosion is likely to occur, offering an additional layer of protection and extending the shaft's lifespan.

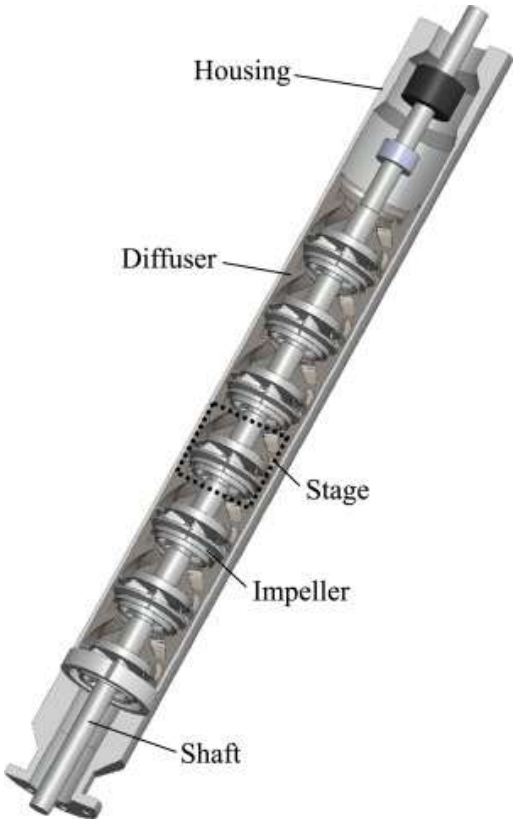

Figure 1.4: ESP inner components

1.2 Operational problems in ESPs

Electrical Submersible Pumps (ESPs) are widely used in the industry for crude oil production. However, the repair, maintenance, or replacement of an ESP can be costly, leading to increased operational expenses. Therefore, it is important to maximize the functional life of ESPs and take measures to extend their workable lifespan.

1.2.1 Intake pressure and Recirculation losses

One key recommendation to improve ESP performance and extend their life is to avoid operating them under low pump intake pressures. Low pressures can adversely affect the pump's efficiency and cause unnecessary wear on its components. Similarly, it is advisable to avoid using

ESPs in multi-phase flow conditions where gas, water, or sand are present.

Leakage losses in a pump refer to the loss of fluid that occurs through small gaps between the rotating and stationary parts of the pump. These gaps can be found at the impeller eye, through balancing holes, and other areas. Takacs (2017) inferenced that the amount of leakage decreases as the flow rate of the liquid increases. The hypothesis was validated in Zhu's (2019) erosion study.

1.2.2 Viscosity effects and gas entrainment

Single-phase test experiments conducted by Shi et al. (2021) proved that the head delivered by an ESP decreases as the viscosity of oil increases. This can be attributed to the fact that as viscosity increases, the fluid becomes thicker and more resistant to flow. This results in higher friction losses within the pump and reduces the overall efficiency of the pump system. Higher viscosity fluids require more energy to pump, leading to decreased pump efficiency and potentially higher power consumption.

ESP Model developed by Zhou et al. (2010) showed that the presence of gas can negatively impact the hydraulic performance of ESPs. The flow behaviors within ESPs when gas is present, such as pressure surges and the formation of gas pockets, can reduce the pump,s ability to provide boosting pressure. Multi-phase flow in ESPs has become common nowadays but the phenomenon is still not clearly understood even with 2-phase testing data widely available in literature.

1.2.3 Vibration

Vibration in ESPs refers to the oscillating motion or movement of the pump components, including the motor, impellers, shaft, and other internal parts. Vibration can occur in ESPs due to various factors and can have both operational and maintenance implications. Experimental work

done by Zhu et al. (2019) took into account the vibrational problem by measuring the vibration of different ESP stages in erosion tests. The vibrations were measured during the erosion testing intervals and were observed to increase in the beginning but stabilize as the testing proceeded.

Reges et al. (2022) developed a novel method of estimating the vibration amplitude using accelerometers that collects vibrational data up to 1000 Hz, using spectrum methods and orbit decomposition theory. The vibration allowance of particular turbomachinery equipment is fixed as per industry and field standards. In literature, historic data has been captured and analyzed to match the vibrational frequencies with the probable causes.

1.2.4 Erosive and abrasive wear due to sand particles

While wells typically have gravel packs to filter out larger particles, fine-grade sand can still infiltrate the pump along with the produced fluids. Formation fluid enters the wellbore caused by poor zonal isolation (Luo et al, 2023, Liu et al., 2023 a, b). The formation fluid may contain corrosive contents, such as carbon dioxide, hydrogen sulfide, and high salinity. The long and often uncased lateral sections found in unconventional wells coupled with the hydraulic fracturing technologies used in these wells contribute to an abundance of solids in well fluid. Shale formation, known by its high heterogeneity, is prone to produce a large quantity of abrasive solids (Zheng et al. 2022 a,b, Zheng et al. 2023a,b). Proppant backflow is another common issue in fracturing wells, and controlling it can be challenging.

Zhu et al. (2021) study of erosion due to sand particles convinced that the solid particles in ESPs can lead to erosion and abrasion problems, causing operational issues. Sand particles cause a combined effect of abrasion and erosion on the internal parts of the pump (Zhu et al., 2019). Abrasion occurs when two surfaces of different roughness come into contact, resulting in the loss

of material. On the other hand, erosion is caused by the mechanical impact of particles on solid surfaces.

Dwycer-Joyce et al. (1994) categorized the abrasive wear as two-body and three-body wear. Two-body wear occurs when two dissimilar surfaces, one smooth and the other rough, come into contact and the rough surface abrades the smooth surface. Three-body wear, on the other hand, involves the presence of external particles that mediate between the two surfaces.

Erosion can be classified into two main types: shock-type and friction-type erosion. Shock-type erosion occurs when particles impact a mechanical surface at a high velocity and a significant angle. Friction-type erosion, on the other hand, happens when particles travel along a surface with high velocity and but at a smaller angle of impact (Kruger et al., 2010). The rate of erosion depends on factors such as sand concentration, particle size, shape, hardness, impact angle, fluid velocity, flow type, and near-wall relative sand particle velocity determined (Pirouzpanah et al, 2014).

In ESPs, both erosive and abrasive wear can be observed. For the sake of clarity, erosive wear is also determined as two-body wear (particle impacts one surface), and abrasive wear is three-body wear (particle presents and be pressurized between two surfaces).

1.3 Erosion test history

There are various sand erosion tests done in the past with a lot of data recorded in literature to understand and analyze the wear mechanism on the ESPs.

Bai (2017) tested a 3-stage ESP for 185 hours with 117 hours of two-phase water-sand flow at first and then continued with 68 hours of three-phase water-air-sand flow. Proximity probes were utilized to monitor vibrational effects on stages during testing. The tests revealed an increase in seal ring clearances and exacerbation of erosion in impeller-diffuser components, resulting in

heightened bearing loads and overall vibration. The presence of air further influenced particle-surface contact. This test was more focused on the vibrational effects during the multi-phase operation of ESPs and the data obtained has been valuable addition to the literature

In a study investigated by Patil et al. (2018), three-phase testing was carried out on a 3-stage ESP with a sand load of 2g/l at two gas volume fraction (GVF), i.e., 0% and 20%. The wear patterns of the diffuser, impeller, and seal were compared under two GVF testing conditions. Performance parameters were monitored and compared for any deviations. The results showed that the 20% GVF condition led to a significant head degradation of approximately 50% compared to water-only tests. Moreover, the 0% GVF condition resulted in erosion primarily in the secondary flow paths, while increasing the GVF shifted the damage to the primary flow sections.

In their study, Beck et al. (2019) conducted extensive two-phase sand erosion testing on a total of 11 pumps. The pumps are operated within a range of 300 to 1750 BPD at their BEP. Two different bearing styles with varying hardness were used in the pumps. The testing duration for all the pumps combined exceeded 250 hours, providing valuable data on changes in performance parameters. The results showed an average head degradation of 4 feet and a decrement in power of approximately 2 HP. To assess erosion effects, the diffuser-impeller stages were periodically removed and analyzed. Changes in dimensions and weight loss were observed in both the impellers and diffusers, with an average change of 2-3% for each component. Vibrational changes were also monitored using accelerometer data collected from an accelerometer positioned at the midpoint of the pumps. This allowed for the measurement and analysis of vibration patterns and trends during the testing process. The comprehensive testing conducted by Beck et al. (2019) provides valuable insights into the performance degradation, erosion effects, and vibrational characteristics of the tested ESPs under two-phase sand-laden conditions. The findings contribute to a better

understanding of the impact of sand erosion on pump performance and highlight the importance of monitoring and mitigating erosion effects in ESP operations.

Zhu (2019) performed sand tests on the 2-inch TUALP erosion testing flow loop for a 12-stage ESP with a BEP flow of 3100 BPD. To assess erosion effects, the stages of the ESP were coated with paint, and the erosion areas were observed after specific test intervals by examining the paint-removal patches on the surface. Vibration probes were installed on the stages to monitor vibration levels throughout the testing. It was observed that vibrations increased during the initial 16 hours of testing and then reached a stable state. On the other hand, the performance parameters of the ESP, such as head and pump efficiency, experienced degradation of 10% and 12%, respectively, over the 64-hour test period. The analysis of the pump stages focused on examining seal clearance increments, paint removal photos, and weight losses. Weight loss on the diffusers and impellers was compared, and the patterns of abrasion-erosion damage were investigated, which is believed to have a significant impact on the overall deterioration of the ESP. This study provides valuable insights into the erosion effects and performance degradation of the ESP under sand-laden conditions. The findings contribute to the understanding of the mechanisms involved in ESP deterioration and highlight the importance of managing erosion-related issues to maintain optimal performance and longevity of ESP systems.

The presence of sand particles in the flow degrades the efficiency and head delivered by the pump and is a primary cause of ESP failure. Failure analysis of degraded pumps has highlighted areas for improvement in pump design. Boudi (2016) specified that the introduction of mixed flow stages can provide a smoother flow pattern and reduce erosion caused by suspended solid particles. Additionally, the compression lifting of impellers away from the diffusers during assembly helps decrease abrasive wear on washers. Further research on failure analysis suggests the use of

additional shaft components, such as Tungsten Carbide (WC) bushings and inter-stage sleeves, to provide radial support and eliminate the risk of fluid leakage through seal clearances during continuous operations. By implementing these recommendations and improving the design of ESPs, it is possible to extend their operational life, minimize wear and erosion, and optimize their performance during crude oil production

.

CHAPTER 2

EXPERIMENT AND FACILITY

The testing is conducted using the 2-inch closed circulating TUALP ESP erosion flow loop (Figure 2.1a). The flow loop was initially designed and constructed by Dr. Haiwen Zhu for the sand-liquid-gas three-phase ESP erosion test. In this study, two new pumps are provided by the TUALP sponsor company, ChampionX (CHX). The ESP testing bench is modified to fit new pumps, and sand-liquid erosion tests are completed at the BEP of the pumps.

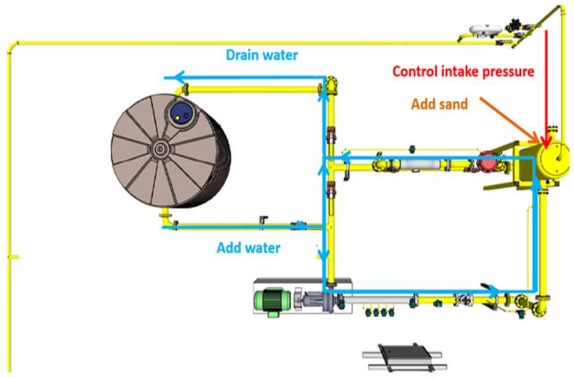

(a)

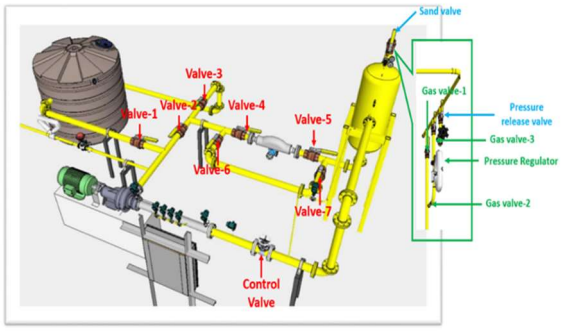

(b)

(c)

Figure 2.1: TUALP ESP flow loop, (a) 2D view, (b) 3D view, (c) Photo

Before the erosion test, the flow loop is firstly flushed and cleaned, then filled up by the water from a supply tank, and water is circulated in a test. The sand is added from the top of the tank through the sand inlet valve with the testing pump running at a low speed (10-15 Hz). To avoid cavitation, the loop is pressurized using compressed air and is maintained above 40 psig (minimum) by a pressure regulator before increasing the pump speed. Once pressurized, the rotational speed is increased to 60 Hz gradually, and the flow rate is manipulated to the BEP flow rate of the pump by adjusting the control valves. Then, the flow is diverted by opening valves 6 and 7 and closing valves 4 and 5 as seen from Figure 2.*1*b to protect the flow meter from the sand particles. A 2-hour test is conducted without any interruptions. Temperature, torque, rotational speed, head, and flow rate were measured during the tests, and efficiency was calculated correspondingly.

Following every 2-hour test, the flow loop is drained and cleaned for 10-15 minutes with fresh water from the water supply tank to remove any residual sand, rust, dust, or solid particles. Then, a new 2-hour test is conducted following the same procedure. The flushing routine is essential for two reasons. Firstly, it removes any residual sand left in the pump from the previous test. Secondly, it helps to lower the temperature of the pump and its internal stages. During the test, sand particles can collide with the pump's parts, causing friction and generating heat, which can lead to an overall increase in temperature as high as 70°C, harmful to both the pump and researchers. The TUALP testing flow loop (Figure 2.1c) contains the test bench, ESP pumps (to be tested), discharge section, vertical separator, and miscellaneous parts such as flow meter and control valves.

2.1 ESP Test Bench

The TUALP test bench consists of a 50 HP electric motor working along with a variable speed drive. The motor is responsible to produce rotational motion in the pump and the variable speed drive (VSD) controls the torque generated by the motor. Another part of the test bench is the ESP thrust chamber which is mainly used to absorb the down thrust generated from the fluid discharge out of the ESP and provide stability to the operation. The shaft of the ESP pump is connected to the motor with the use of a coupling so as to allow the transfer of rotatory motion to the pump.

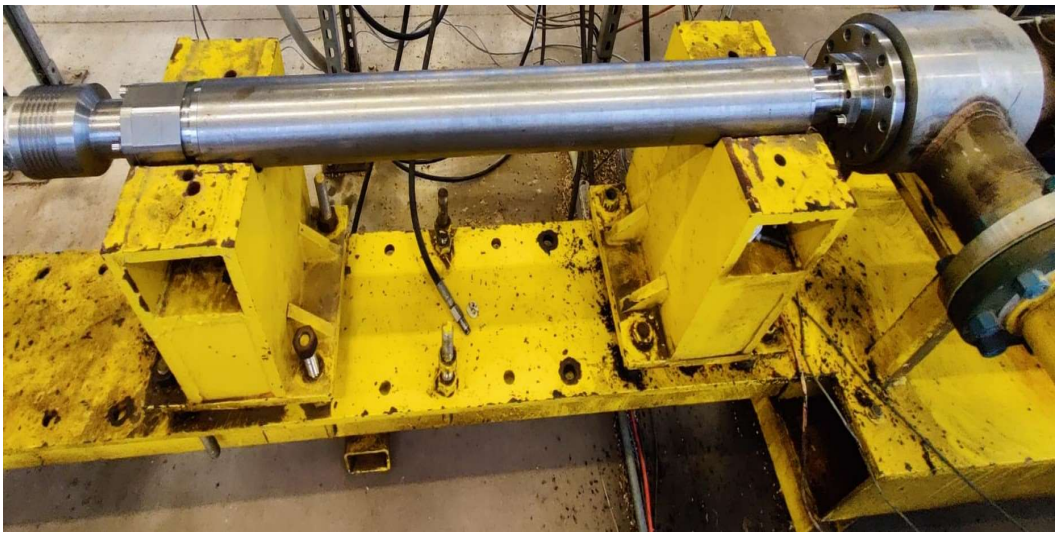

Figure 2.2: ESP test bench

2.2 ESP Pumps

ESP1 and ESP2 are the 2 pumps tested in this study. Both pumps are 43.1 inches in length and have a total of 14 and 8 internal stages respectively. The arrangement of the stages is depicted in Figure 2.3:

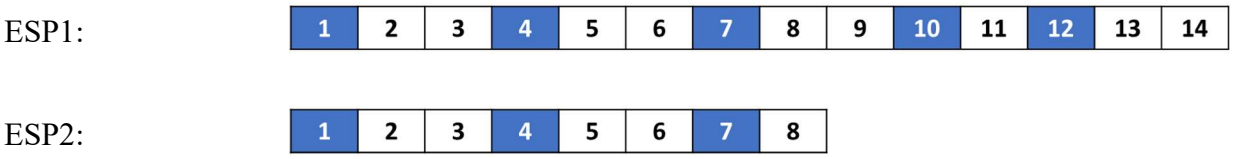

Figure 2.3: Stage arrangement in ESP1 and ESP2

In Figure 2.3, stages marked in blue are the special Abrasion Resistant (AR) stages that employ the use of Tungsten Carbide (WC) sleeves and bushings (1, 4, 7, 10, 12 in ESP1 and 1, 4, 7 in ESP2). The BEP of ESP1 and ESP2 are 1750 BPD and 6000 BPD respectively. ESP1 is designed to operate in the range of 200-2500 BPD and ESP2 is designed to operate in the range of 2000-7500 BPD. The important dimensions of the internal stages of both the pumps such as diameters, boreholes, weight, etc. were measured before and after each test interval. The order in which the stages are arranged in the pumps is fixed and maintained as was after every inspection disassembling and reassembling.

Figure 2.4: ESP1 and ESP2

2.3 Discharge Section

The discharge section connects the other end of the ESP pump to the gas separator and subsequently to the flow loop. The section is built using a pipe nipple with unions on both ends, two gate valves, and a flexible metal hose. A ½" pipe nipple is welded at the pump discharge pipes for pressure sensor installation. The gate valves are used as control valves to adjust the flow rate of the fluid in the loop. They can be easily replaced if they get eroded due to sand testing. The 9-inch long SS 321 grade flexible metal hose is used for easy alignment. The discharge section is connected as a separate unit to allow convenient removal and attachment of the ESP pump as and when the testing commences and culminates.

Figure 2.5: Discharge section of the flow loop

2.4 Gas separator and flow-meters

The gas separator can be used for three-phase gas-liquid-solid erosion testing where the gas is injected at the pump intake and separated using the gas separator. For the study, the gas separator is only used as a pressure vessel to maintain the pressure above 40 psig to avoid any cavitation issues in the pump. The discharged slurry from the ESP enters into the separator nearly at its middle and flows through the bottom to the loop. The sand is added through the top valve at the separator. A Coriolis flow meter is used to measure and check the flow rate inside the loop. The flow meter is used initially till the desired flow rate is adjusted and then is bypassed to protect it from the solids.

(a) (b)

Figure 2.6: (a) Gas separator, (b) Coriolis flow meter

CHAPTER 3

EXPERIMENTAL RESULTS AND DISCUSSION

The pumps are subjected to 1% sand by weight during the experiment and operated at their BEP flow rate to observe the performance deterioration and geometrical changes. The pumps are performance tested after sand erosion testing interval to calculate the efficiency and head degradation. To maintain the homogeneity of the results and reduce equipment replacement time, the testing of ESP2 is started only after the completion of the 64-hour testing of ESP1.

3.1 ESP1

This section provides the performance and dimensional changes in ESP1 due to sand erosion testing for various test intervals

3.1.1 Performance

The ESP1 is exhaustively tested for 64 hours in total and performance monitoring tests are conducted before and after each testing interval.

3.1.1.1 Initial testing: The pump is performance tested before starting the sand testing to verify the performance metrics are comparable to those found during the company's performance testing of the same pump

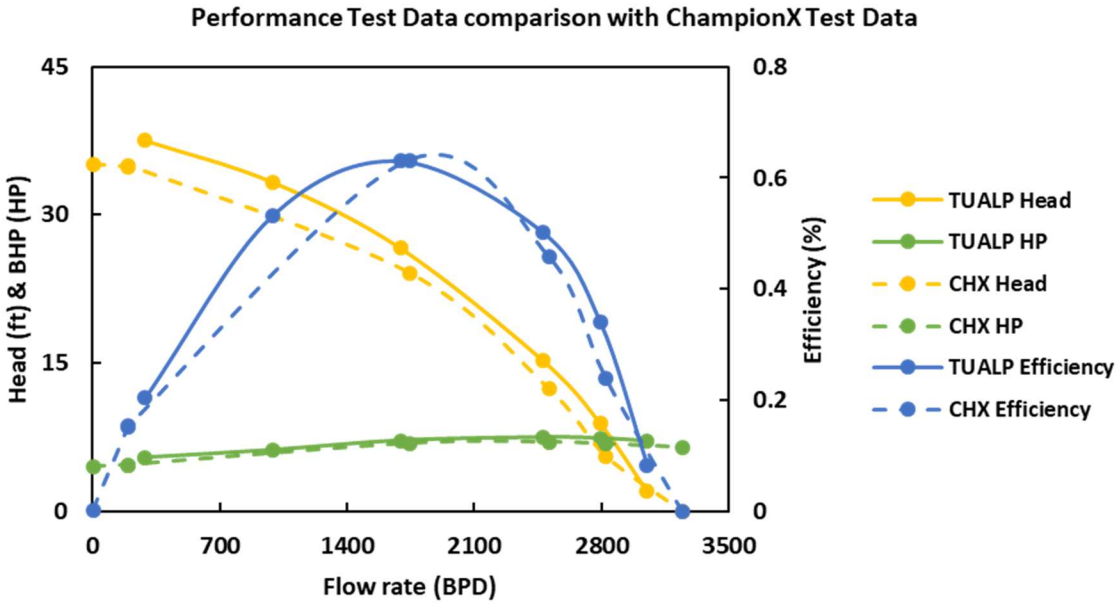

Figure 3.1: ESP1 performance test data comparison with CHX data

As is seen from, the performance results are comparable and validates the fact that TUALP test facility can provide reproducible results and the pump is workable and at its catalog properties. The performance results are tabulated in. The pump has a deliverable head of 26 ft. and efficiency of around 63% at its BEP of 1750 BPD.

Table 3.1: ESP1 test data TUALP and CHX

TUALP Flow (BPD)	TUALP Head (ft.)	TUALP Efficiency	TUALP Power (HP)	CHX Flow (BPD)	CHX Head (ft.)	CHX Efficiency	CHX Power (HP)
290.61	37.5228	20.37%	0.3875	3.1	35.1	0.3%	0.321
988.55	33.337	53.14%	0.4416	196.5	34.8	15.2%	0.333
1694.51	26.6238	63.02%	0.51	1742.2	24.1	63.2%	0.491
2477.74	15.2398	50.21%	0.5324	2513.6	12.4	45.8%	0.501
2793.68	8.8722	34.07%	0.5258	2826.7	5.6	23.9%	0.487
3052.13	1.9634	8.31%	0.5065	3245.9	0	0%	0.462

3.1.1.2 TUALP Performance tests: Head, efficiency, horsepower and torque are the 4 parameters under observation after every testing interval and is presented in this sub-section. The continuous performance monitoring data can be found in Appendix C

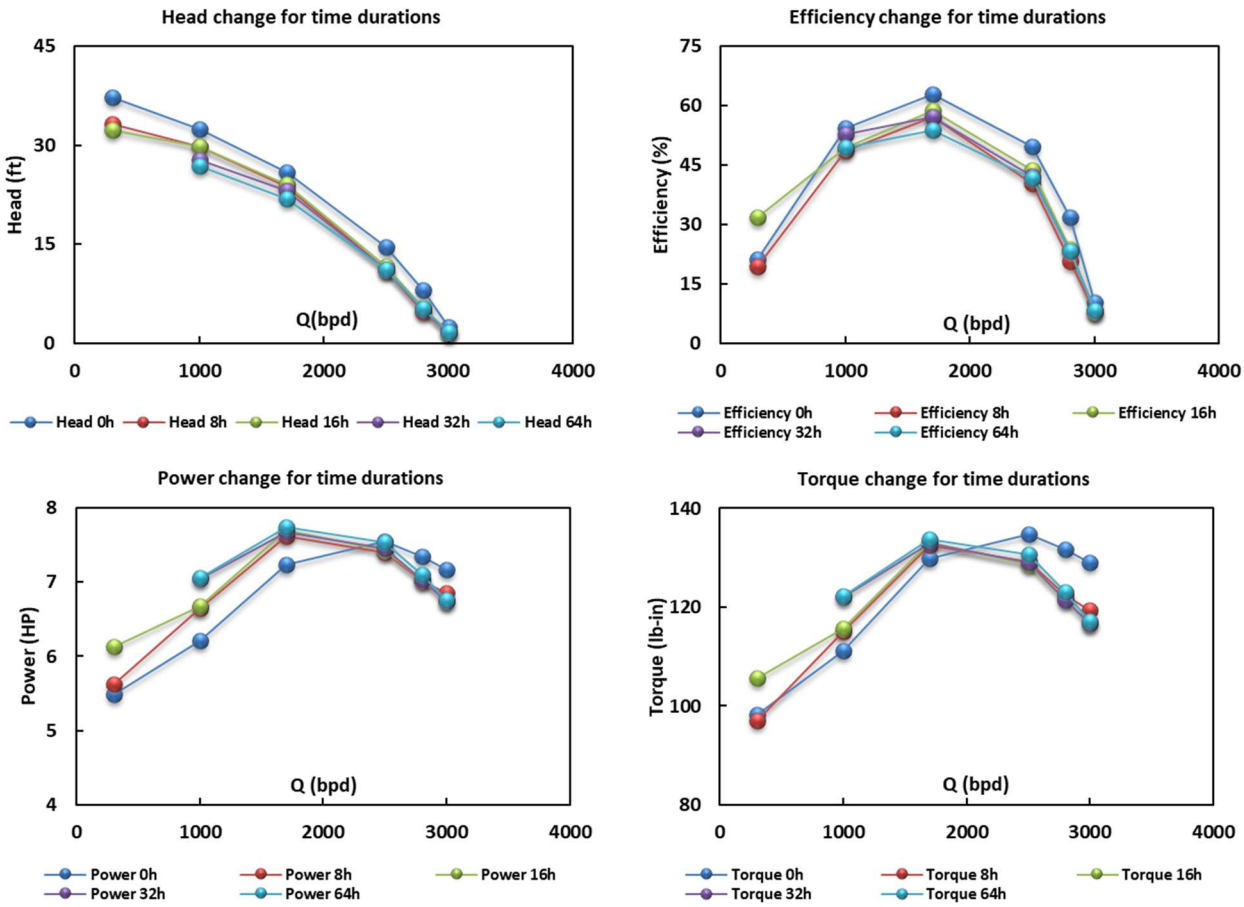

Figure 3.2: ESP1 performance test parameters over various time periods

As seen from, the deliverable head and efficiency suffer severe deterioration over the 64-hour testing period. Brake Horsepower and torque exhibit only a slight increase from their initial values. The fact that the power remains relatively unchanged indicates that the stage impellers are still capable of boosting the fluid flow, despite the erosion and abrasion caused by the sand testing.

3.1.1.3 Cumulative performance degradation comparison: the initial and final pump performance curves are compared at the TUALP test flow loop and also at the CHX testing site to verify the percentage degradation of ESP1 and compare the differences between the results obtained.

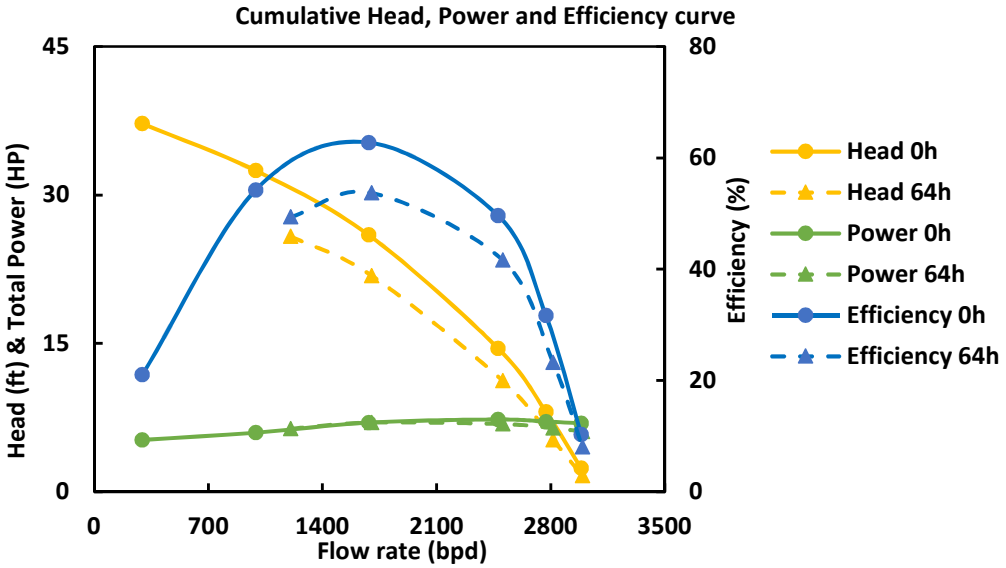

Figure 3.3: ESP1 cumulative performance degradation from TUALP

Table 3.2: ESP1 TUALP initial and final performance parameters

TUALP Flow (BPD) 0h	TUALP Head (ft.) 0h	TUALP Efficiency 0h	TUALP Power (HP) 0h	TUALPFlow (BPD) 64h	TUALP Head (ft.) 64h	TUALP Efficiency 64h	TUALP Power (HP) 64h
290.61	37.5228	20.37%	0.3875	-	-	-	-
988.55	33.337	53.14%	0.4416	1205.01	25.82	48.37%	0.46
1694.51	26.6238	63.02%	0.51	1702.18	21.84	50.14%	0.50
2477.74	15.2398	50.21%	0.5324	2505.62	11.23	41.61%	0.49
2793.68	8.8722	34.07%	0.5258	2814.24	5.24	23.23%	0.46
3052.13	1.9634	8.31%	0.5065	2994.44	1.62	8.06%	0.44

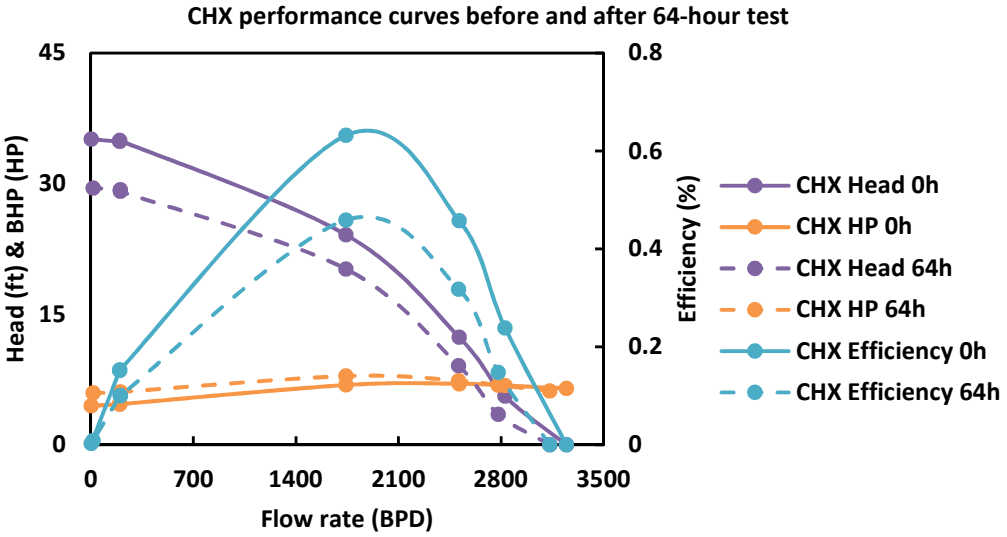

Figure 3.4: ESP1 cumulative performance degradation from CHX

Table 3.3: ESP1 CHX initial and final performance parameters

CHX Flow 0h (BPD)	CHX Head 0h (ft)	CHX Efficiency 0h	CHX Power 0h (HP)	CHX Flow 64h (BPD)	CHX Head 64h (ft)	CHX Efficiency 64h	CHX Power 64h (HP)
3.1	35.1	0.3%	4.492	17.0	29.5	0.9%	6.188
196.5	34.8	15.2%	4.662	200.7	29.3	10.1%	6.860
197.9	35.0	15.3%	4.666	202.1	29.1	10.0%	7.378
1742.2	24.1	63.2%	6.869	1740.6	20.2	45.9%	7.896
2513.6	12.4	45.8%	7.010	2509.5	9.1	31.80%	6.062
2826.7	5.6	23.9%	6.818	2780.3	3.5	14.80%	6.006
3245.9	0.0	0.0%	6.470	3132.9	0	0.00%	5.964

According to TUALP results in Table 3.2, ESP1 experiences a 16% decrease in delivered head, dropping from 26 ft to 21.8 ft. In addition, the efficiency of ESP1 degrades by 17.3%, going from an initial value of 63% to around 50%. However, the change in horsepower is minimal, with power remaining nearly constant during testing. Furthermore, there is a 6% increase in Brake Horsepower (BHP) for ESP1. The parameters show a sharp change within the first 8-16 hours of sand testing, and this trend is consistent with the three-body abrasion damage pattern.

By looking at the CHX results in Table 3.3, it is observed that there is a significant drop in

the delivered head from 24 ft to 20 ft, while the efficiency of ESP1 experiences a degradation from its initial value of 63% to approximately 46%. Despite this, the change in horsepower is minimal, with power remaining almost constant throughout testing. The difference between the final and initial values of horsepower is 1 HP.

3.1.2 Dimensional changes, seal clearances and weight loss

The stage diffusers of ESP1 contain 8 vanes and the impellers have 6 blades and balance holes. Initially, the geometries of both pumps are measured and used as reference values that are nearly equivalent to the design values. Dimension A-F exhibit less than a 1% change from their initial values, whereas the impeller hub outer diameter (Dimension G) experiences a significantly higher variation of 6.6% in ESP1, indicating more trapped sand in that area. Most geometries undergo rapid changes in the first 8-16 hours of testing, with the changing trend flattening out over time. The three-body abrasion wear mechanism suggests that abrasion rates are linked to the force between abrasive solids and the surface being targeted. Carbide sleeves and bearings used in ESPs aid in maintaining rotational stability, reducing the force responsible for abrasion. The similar trend in changes to abrasion damage and performance deterioration indicates that the decline in pump performance is more likely due to three-body damage on the seal clearance.

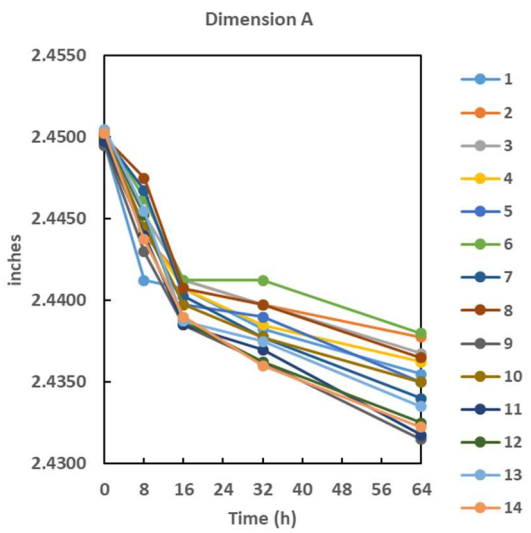

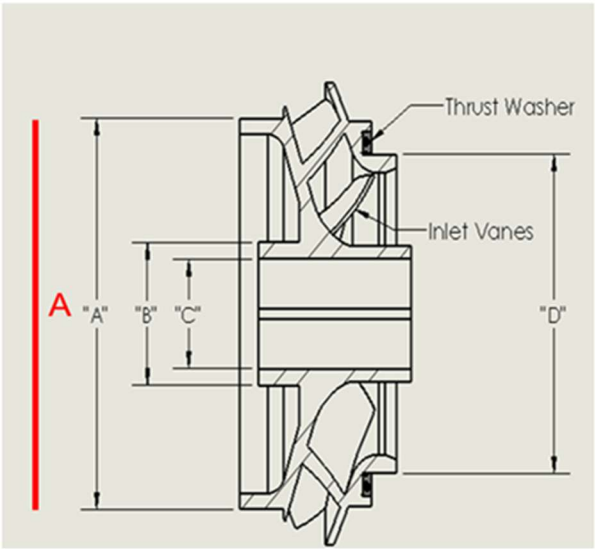

(a) (b)

Figure 3.5: Trend in change of impeller balance ring OD (Dimension A), (a) ESP1, (b) Reference geometry

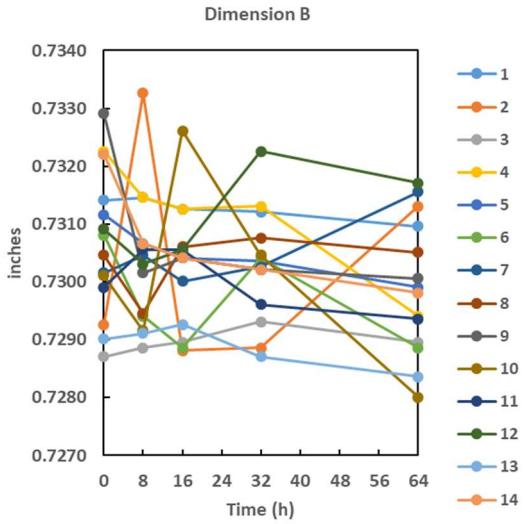

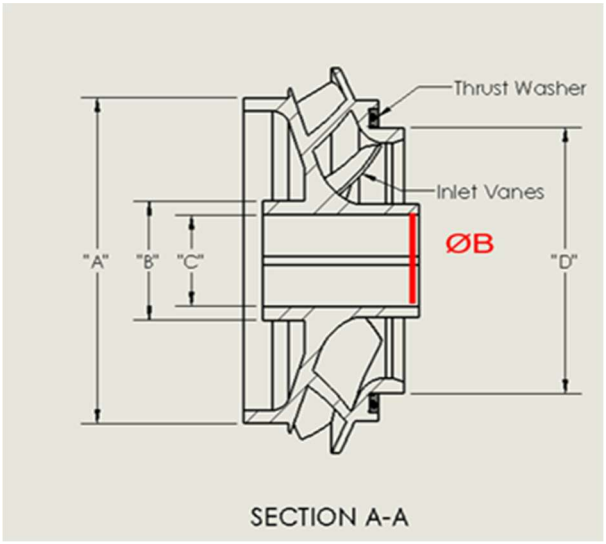

(a) (b)

Figure 3.6: Trend in change of impeller hub ID (Dimension B), (a) ESP1, (b) Reference geometry

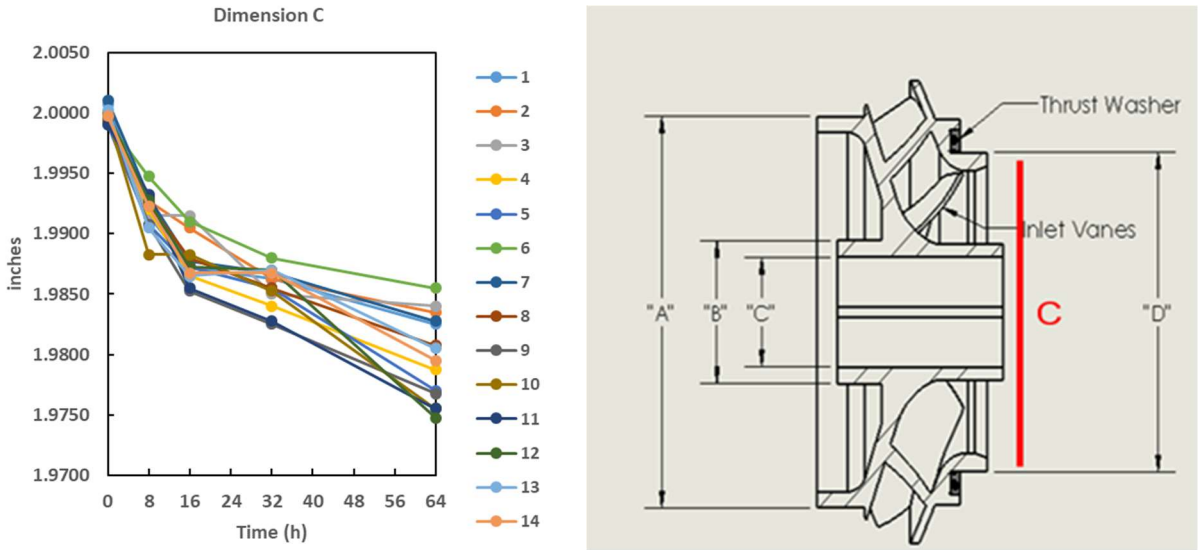

(a) (b)

Figure 3.7: Trend in change of impeller skirt ring OD (Dimension C), (a) ESP1, (b) Reference geometry

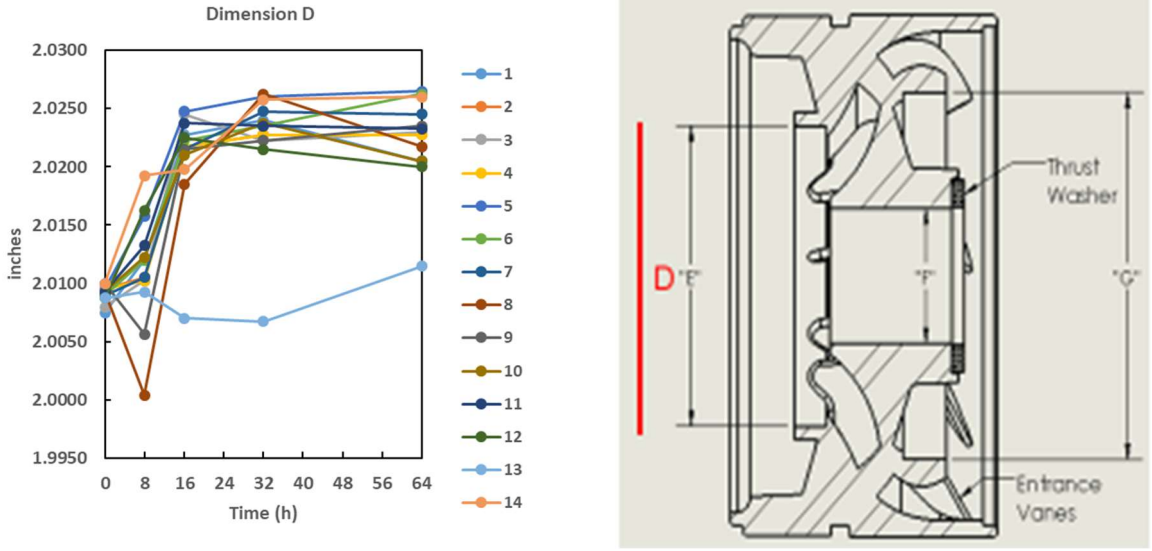

(a) (b)

Figure 3.8: Trend in change of diffuser skirt ring ID (Dimension D), (a) ESP1, (b) Reference geometry

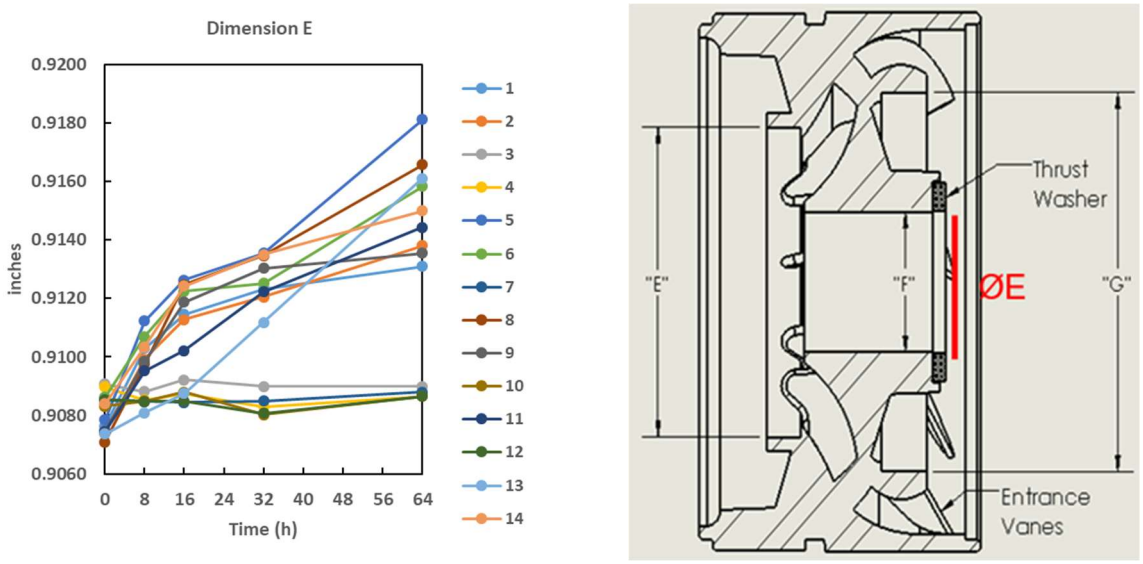

(a) (b)

Figure 3.9: Trend in change of diffuser hub ID (Dimension E), (a) ESP1, (b) Reference geometry

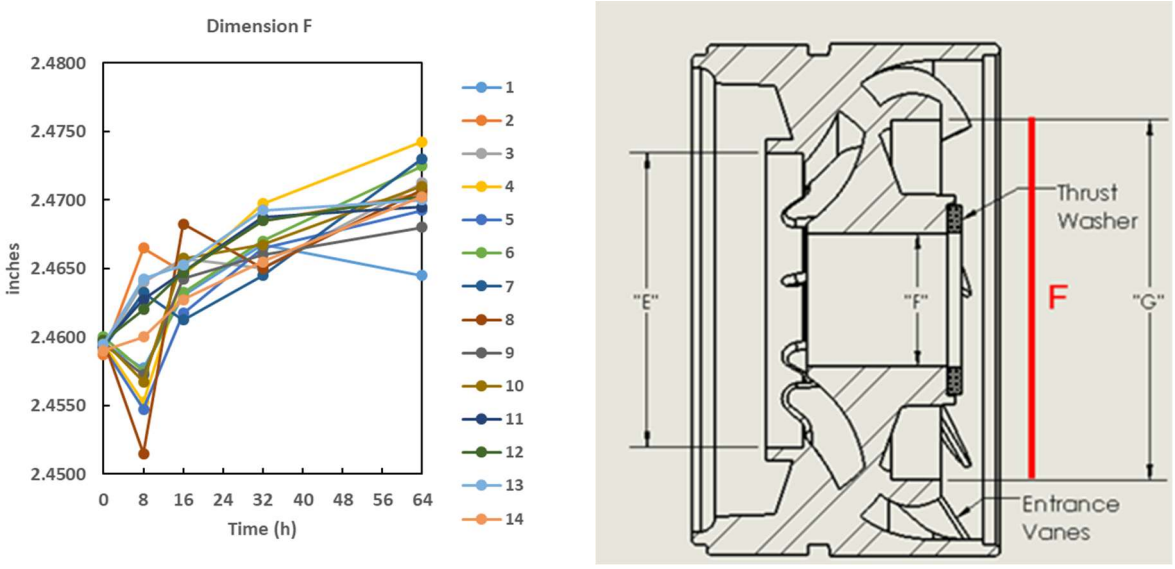

(a) (b)

Figure 3.10: Trend in change of diffuser balance ring ID (Dimension F), (a) ESP1, (b) Reference geometry

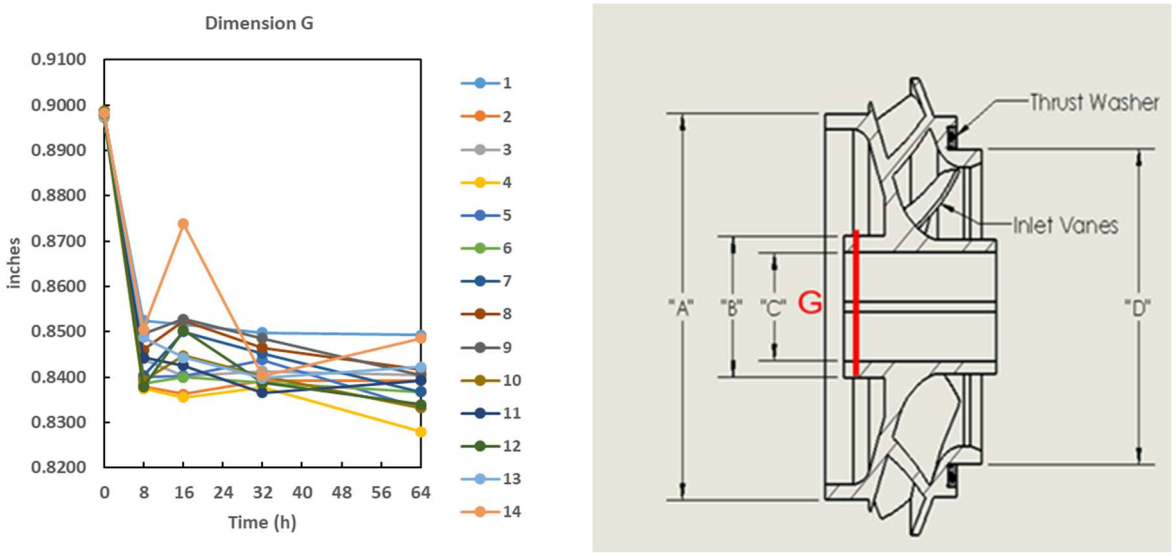

(a) (b)

Figure 3.11: Trend in change of impeller hub OD (Dimension G), (a) ESP1, (b) Reference geometry

Clearance refers to the gap between the inner diameter of the diffuser and the outer diameter of the impeller geometries. As erosion wear occurs, the clearances gradually increase over time, creating a secondary flow channel that allows fluid to seep in and cause severe damage. The balance ring clearance is the difference between the diffuser balance ring ID and the impeller balance ring OD, while the skirt ring clearance is the difference between the diffuser hub ID and the impeller skirt ring OD. For ESP1, both clearances display a similar, homogeneous increasing trend. Initially, the clearances increase drastically in the first 8-16 hours, following the pattern of three-body abrasion wear. However, the rate of change stabilizes over time.

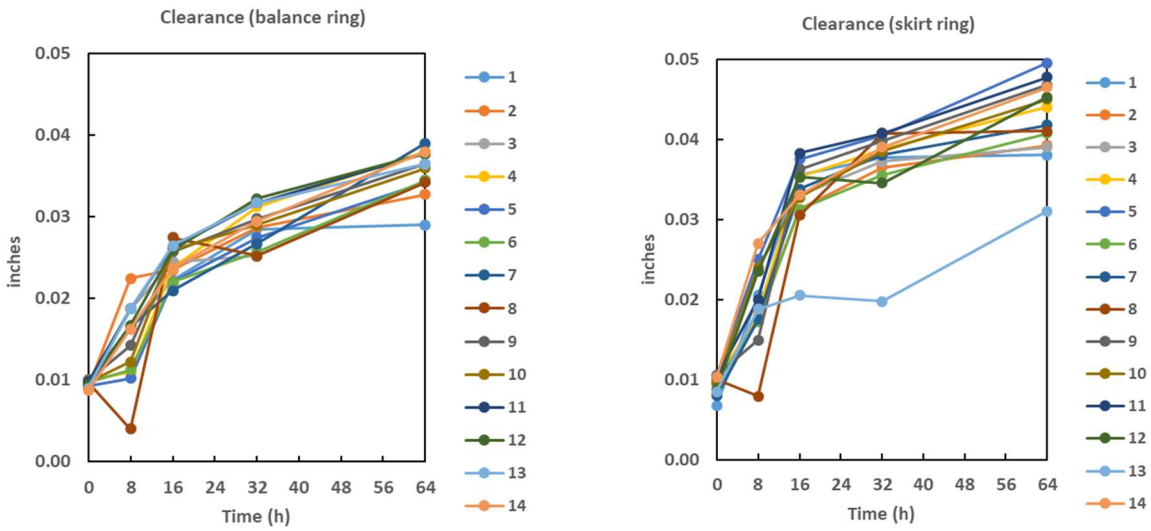

(a) (b)

Figure 3.12: ESP1 seal ring clearances, (a) balance ring, (b) skirt ring

Weight loss in the stages is due to both abrasion and erosion wear. Abrasion damage causes significant weight loss in the stages in the first 8-16 hours of testing, which then stabilizes. However, a constant linear weight loss persists, presumably due to erosion damage. ESP1's diffusers experience a weight loss of 12 g, while the average impeller weight loss is around 8 g.

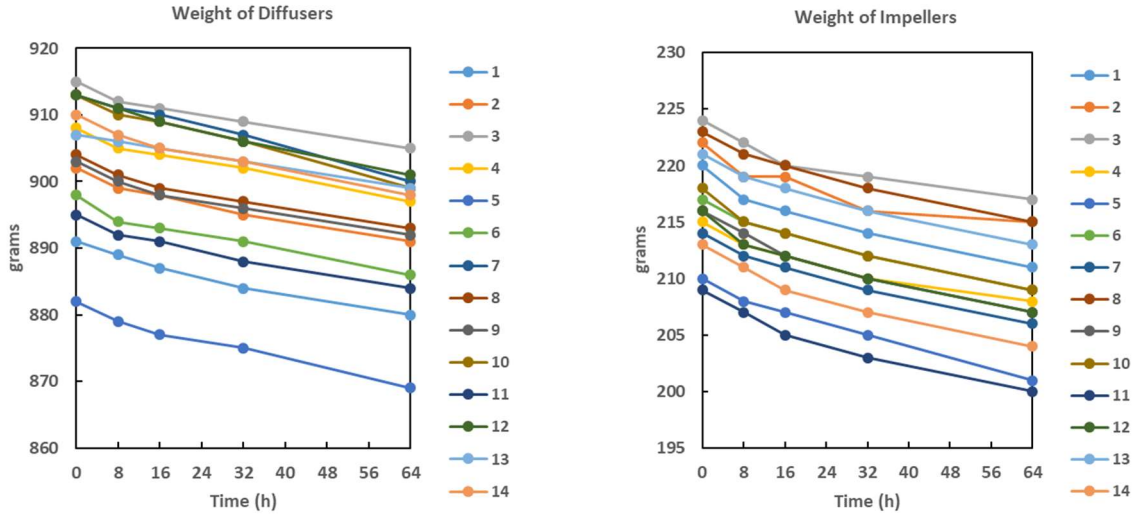

(a) (b)

Figure 3.13: ESP1 loss in weight, (a) Diffusers, (b) Impellers

The balance holes on the stage impellers are designed to minimize axial thrust and balance pressure on the up-thrust and down-thrust sides of the impellers. However, the diameter of these holes is measured using a low-accuracy hit-and-trial instrument, making it difficult to identify a clear trend. During the 64-hour test, recirculation of particles through the balance chamber causes an increase in diameter from their original values.

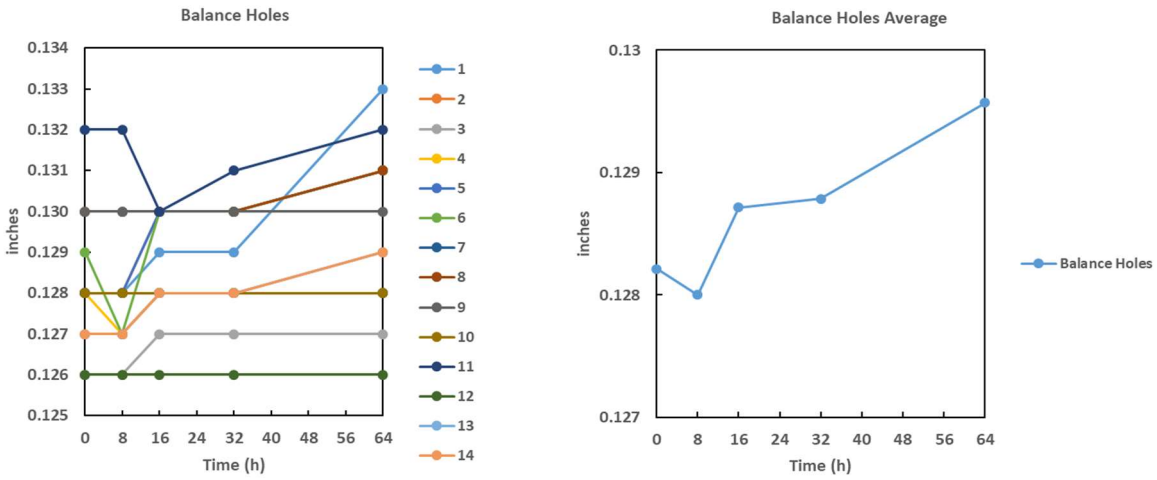

(a) (b)

Figure 3.14: ESP1 impeller balance hole diameter change, (a) Stage-wise, (b) Average

3.2 ESP2

This section presents the performance and dimensional alterations observed in ESP2 as a result of sand erosion testing conducted at different intervals.

3.2.1 Performance

The ESP2 undergoes a rigorous 64-hour testing process, during which its performance is thoroughly evaluated through pre- and post-testing performance monitoring assessments.

3.2.1.1 Initial Testing: Before commencing sand testing, a performance test is carried out

on the pump to confirm that its performance metrics are consistent with those recorded during the company's previous performance testing of the same pump.

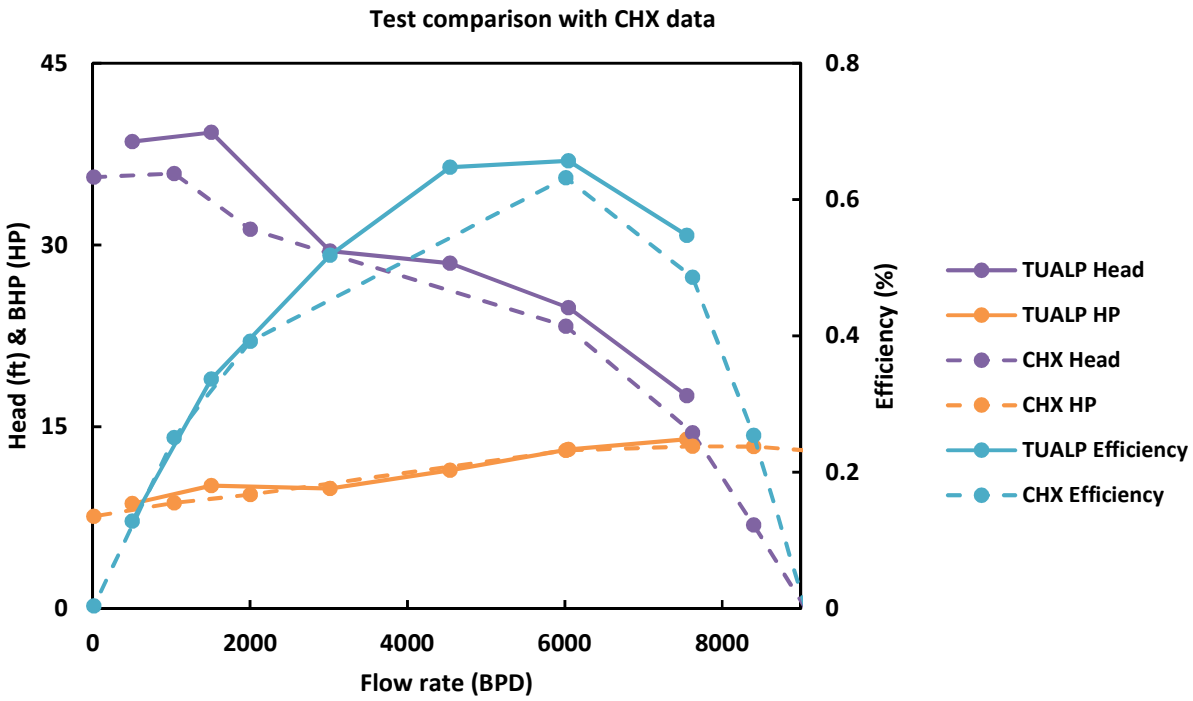

Figure 3.15: ESP2 performance test data comparison with CHX data

The TUALP test facility has demonstrated its ability to provide reproducible results, as evidenced by the comparable performance results. These results validate that the pump is functional and operating within its catalog properties, with a deliverable head of 25 ft. and an efficiency of approximately 65% at its best efficiency point (BEP) of 6000 barrels per day (BPD) as is tabulated below.

Table 3.4: ESP2 test data TUALP and CHX

Flow (BPD)	Head (ft)	Efficiency	Power (HP)	CHX Flow (BPD)	CHX Head (ft)	CHX Efficiency	CHX Power (HP)
7424.10	16.18	52.45%	1.67	9061.1	0	0.00%	1.633
5986.59	24.19	65.24%	1.62	8400.8	6.9	25.40%	1.671
4972.25	26.81	64.37%	1.51	7625.4	14.5	48.60%	1.673
3982.15	27.82	59.59%	1.36	6015	23.3	63.20%	1.633
2988.30	28.44	50.78%	1.22	2001.8	31.3	39.20%	1.177
1986.76	31.19	38.94%	1.15	1033.5	35.9	25.10%	1.09
996.49	36.63	24.36%	1.10	15.5	35.6	0.40%	0.951

3.2.1.2 TUALP Performance tests: Similar to the ESP1, testing was done on ESP2 at its BEP flow of 6000 BPD and the head, efficiency, torque and horsepower are displayed over a range of time intervals against the different flow rates in Figure 3.16 as shown below.

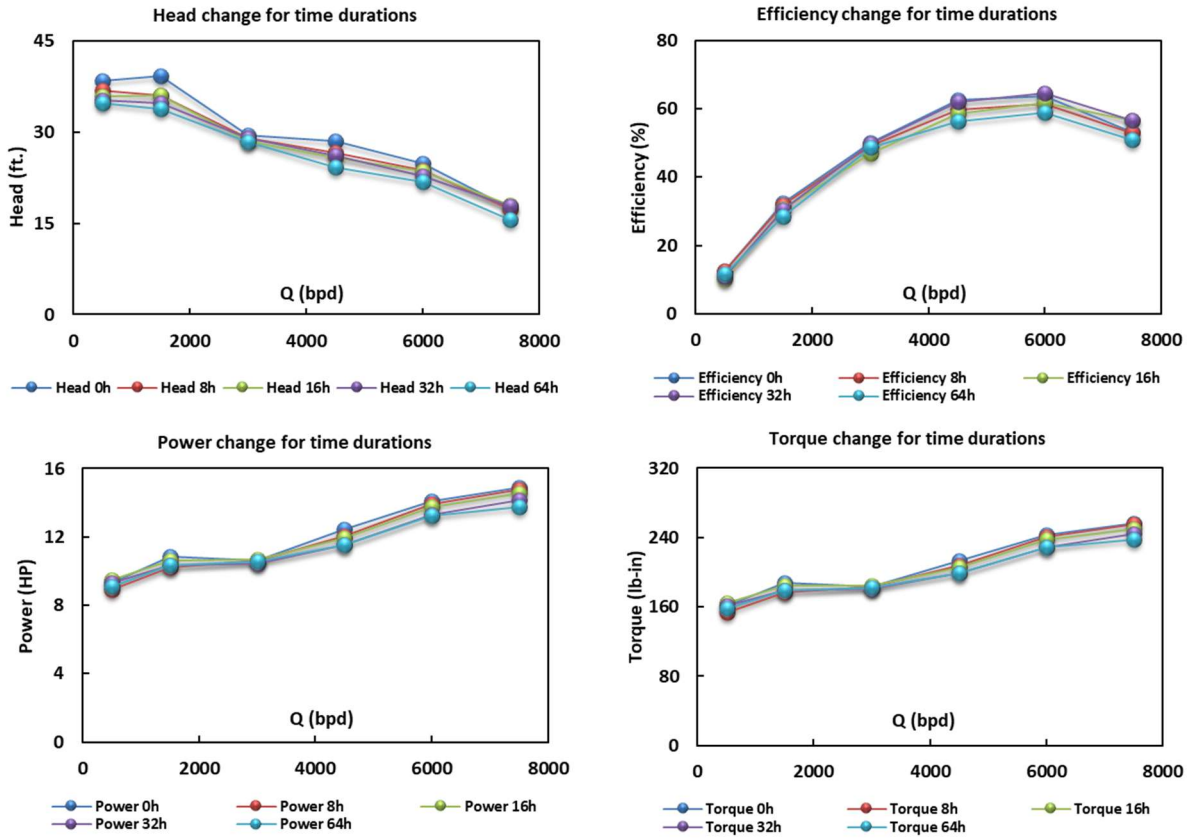

Figure 3.16: ESP2 performance test parameters over various time periods

3.2.1.3 Cumulative performance degradation comparison: To determine the percentage degradation of ESP2 and compare the results obtained, both the initial and final pump performance curves were compared at both the TUALP test flow loop and CHX testing site.

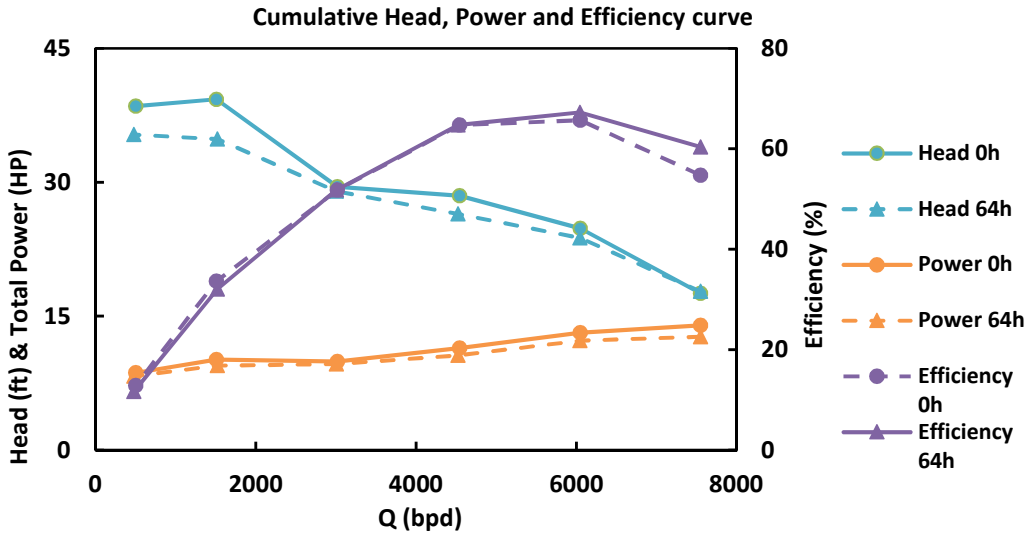

Figure 3.17: ESP2 cumulative performance degradation from TUALP

Table 3.5: ESP2 TUALP initial and final performance parameters

TUALP Flow (BPD) 0h	TUALP Head (ft.) 0h	TUALP Efficiency 0h	TUALP Power (HP) 0h	TUALP Flow (BPD) 64h	TUALP Head (ft.) 64h	TUALP Efficiency 64h	TUALP Power (HP) 64h
7500	17.57	53.23	14.86	7500	15.57	50.97	13.74
6000	24.83	63.69	14.08	6000	21.83	59.38	13.23
4500	28.5	62.46	12.43	4500	24.23	56.34	11.51
3000	29.51	49.94	10.62	3000	28.35	48.49	10.54
1500	39.29	32.45	10.86	1500	33.76	28.28	10.34
500	38.53	12.33	9.3	500	34.81	11.73	9.11

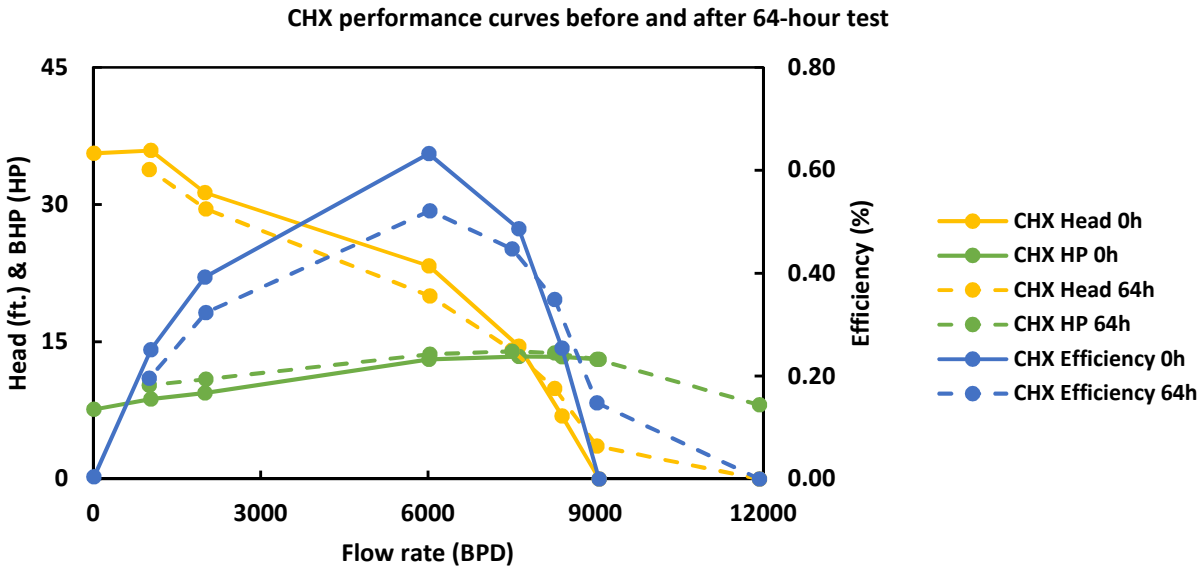

Figure 3.18: ESP1 cumulative performance degradation from CHX

Table 3.6: ESP2 CHX initial and final performance parameters

CHX Flow 0h (BPD)	**CHX Head 0h (ft)**	**CHX Power 0h (HP)**	**CHX Efficiency 0h**	CHX Flow **64h (BPD)**	CHX Head 64h **(ft)**	**CHX Power 64h (HP)**	**CHX Efficiency 64h**
/	/	/	/	11933.8	0	1.012	0.00%
9061.1	0	1.633	0.00%	9021.4	3.6	1.633	14.80%
8400.8	6.9	1.671	25.40%	8269.7	9.9	1.72	34.90%
7625.4	14.5	1.673	48.60%	7507.2	14.1	1.744	44.70%
6015	23.3	1.633	63.20%	6029.2	20	1.702	52.10%
2001.8	31.3	1.177	39.20%	2020	29.5	1.362	32.30%
1033.5	35.9	1.09	25.10%	1006.7	33.8	1.278	19.60%
15.5	35.6	0.951	0.40%	/	/	/	/

Results from TUALP indicate that ESP2 experiences a 12% decrease in delivered head, dropping from 24.8 ft to 21.8 ft, and a 6.78% degradation in efficiency, from an initial value of 65% to around 59%. Despite these changes, the horsepower for ESP2 remains almost constant during testing, with only a minimal change. Furthermore, while ESP1 shows a 6% increase in Brake Horsepower (BHP), there is a 6% decrease in BHP for ESP2. These parameters exhibit a significant change within the first 8-16 hours of sand testing, consistent with the three-body

abrasion damage pattern.

The results in from CHX tests that indicate a significant drop in the delivered head of ESP2, from 23 ft to 20 ft, along with a degradation in efficiency from an initial value of 63% to approximately 52%. Despite these changes, the horsepower for ESP2 remains constant during testing, with negligible change of 0.1 HP.

3.2.2 Dimensional changes, seal clearances and weight loss

Both ESP2,s stage diffusers and impellers have specific geometries: 10 vanes and 9 blades with balance holes, respectively. At the start of testing, the pumps' geometries were measured and used as reference values, which closely matched the design values. Dimension A-F underwent negligible changes, whereas Dimension G (the impeller hub outer diameter) exhibited a significant 4.4% variation in ESP2, possibly due to trapped sand. Similar to the ESP1, the abrasion trend followed in ESP2 as well since most geometries showed rapid changes within the initial 8-16 hours, but trends eventually leveled out. Carbide sleeves and bearings, which maintain rotational stability, help reduce abrasion forces. The declining pump performance,s similarity in changes to abrasion damage indicates that three-body damage on the seal clearance is likely the cause.

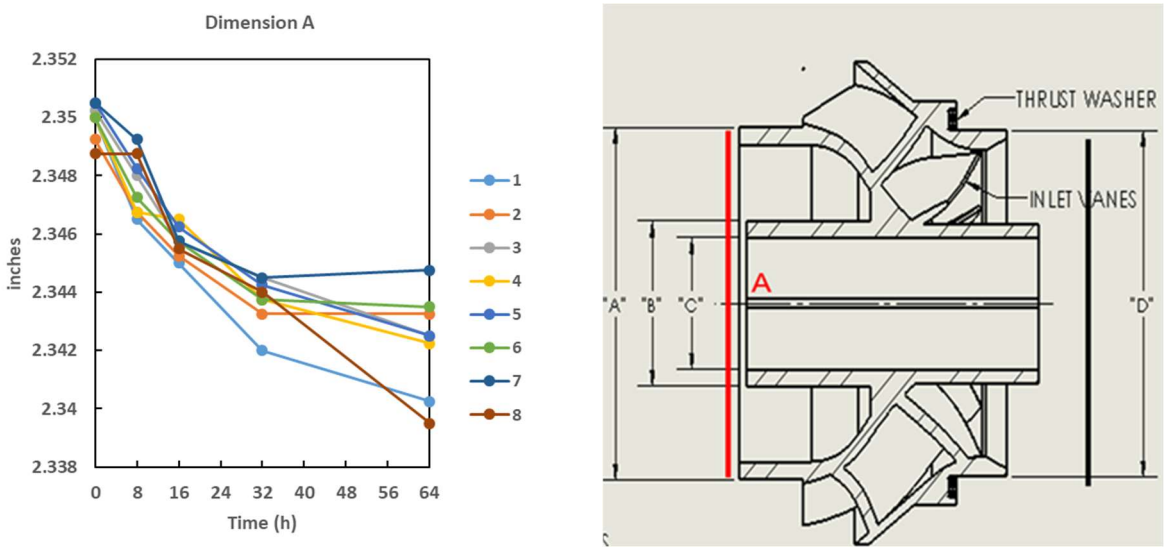

(a) (b)

Figure 3.19: Trend in change of impeller balance ring OD (Dimension A), (a) ESP2, (b) Reference geometry

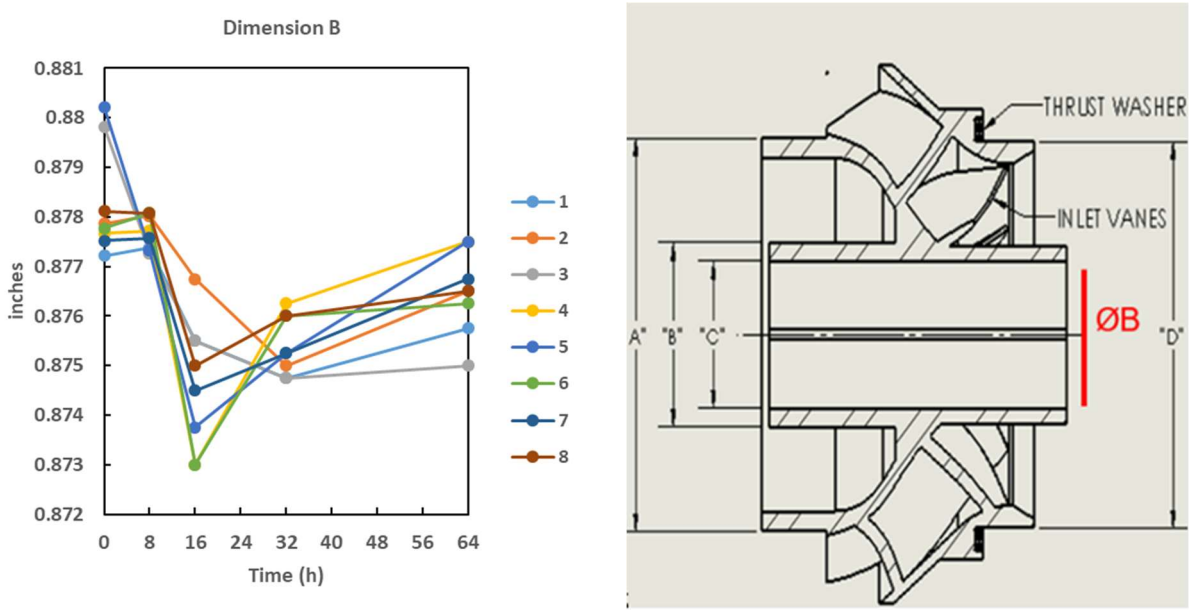

(a) (b)

Figure 3.20: Trend in change of impeller hub ID (Dimension B), (a) ESP2, (b) Reference geometry

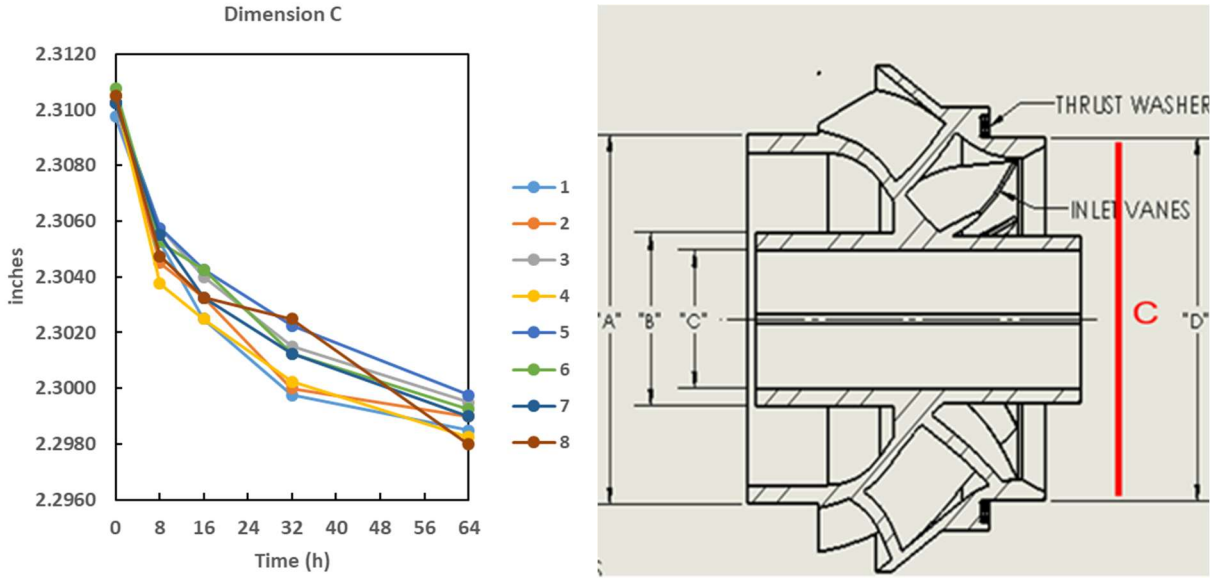

(a) (b)

Figure 3.21: Trend in change of impeller skirt ring OD (Dimension C), (a) ESP2, (b) Reference geometry

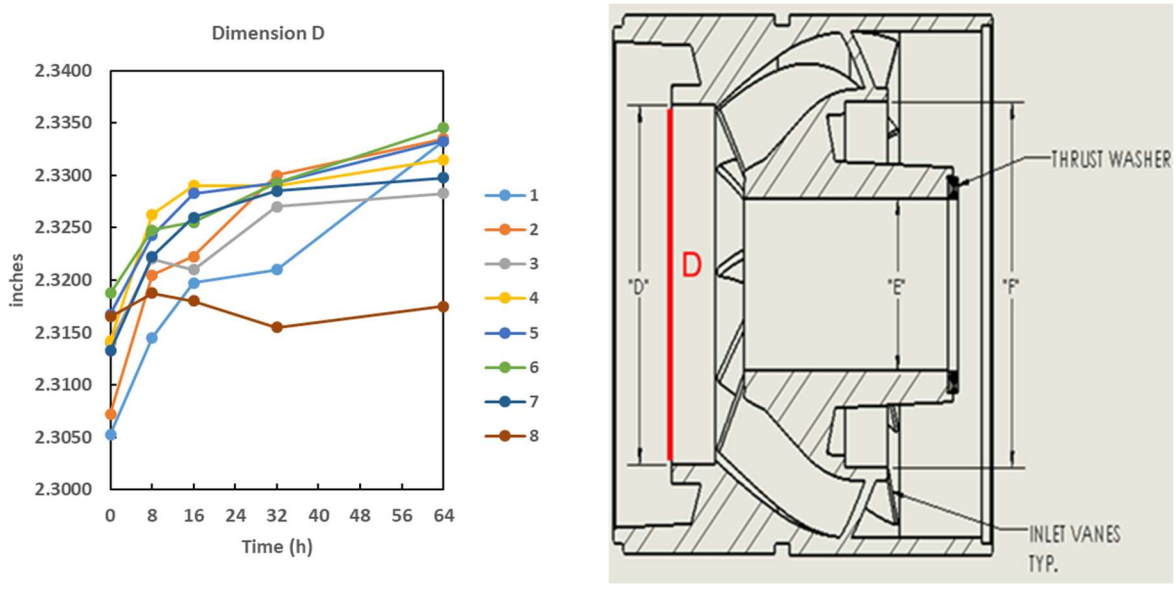

(a) (b)

Figure 3.22: Trend in change of diffuser skirt ring ID (Dimension D), (a) ESP2, (b) Reference geometry

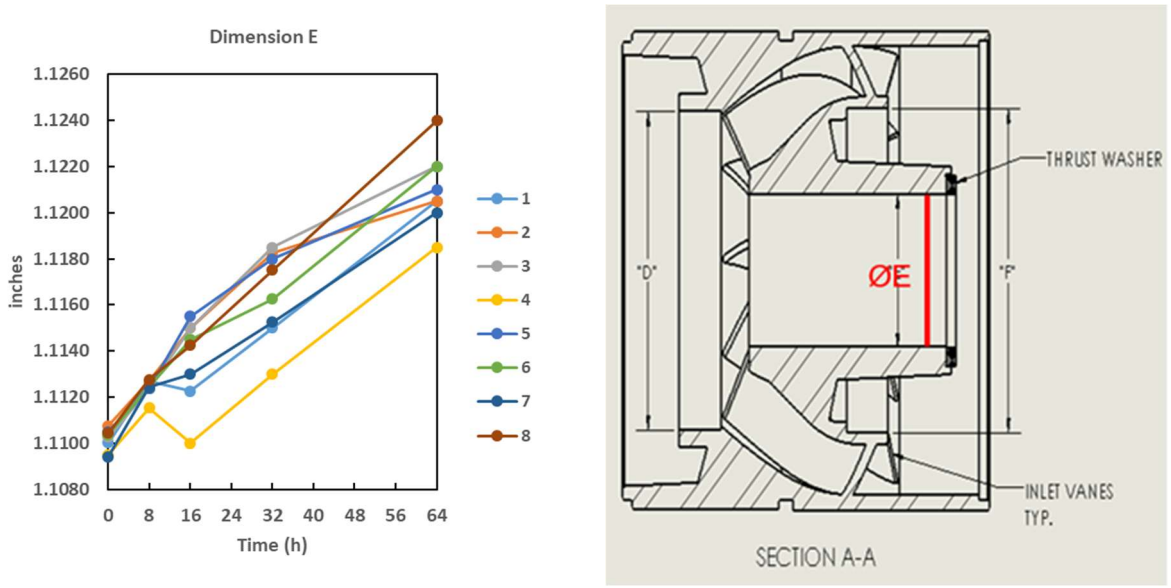

(a) (b)

Figure 3.23: Trend in change of diffuser hub ID (Dimension E), (a) ESP2, (b) Reference geometry

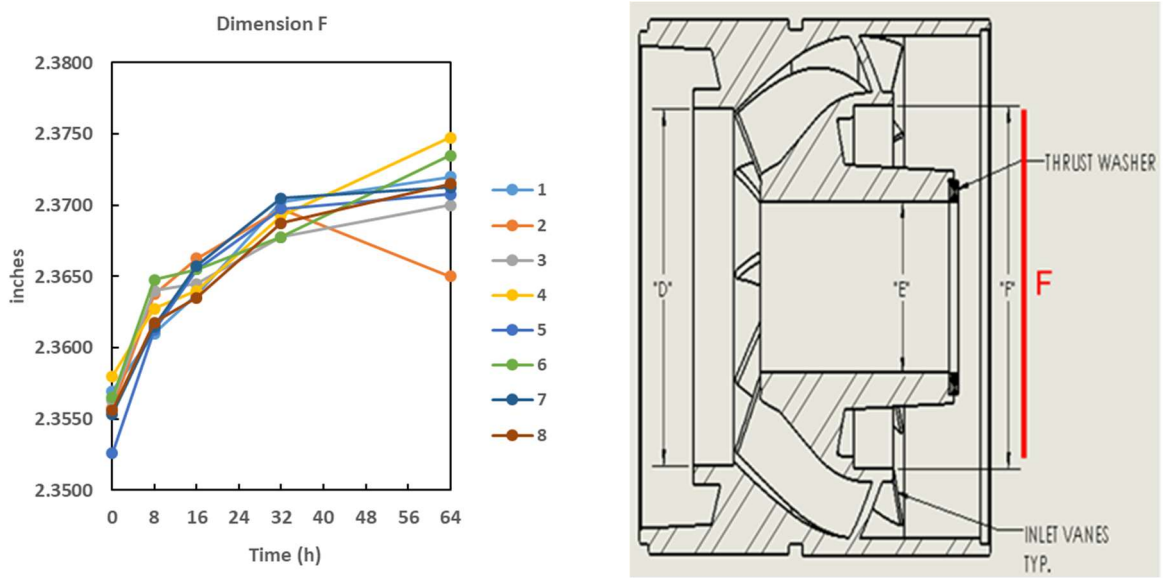

(a) (b)

Figure 3.24: Trend in change of diffuser balance ring ID (Dimension F), (a) ESP2, (b) Reference geometry

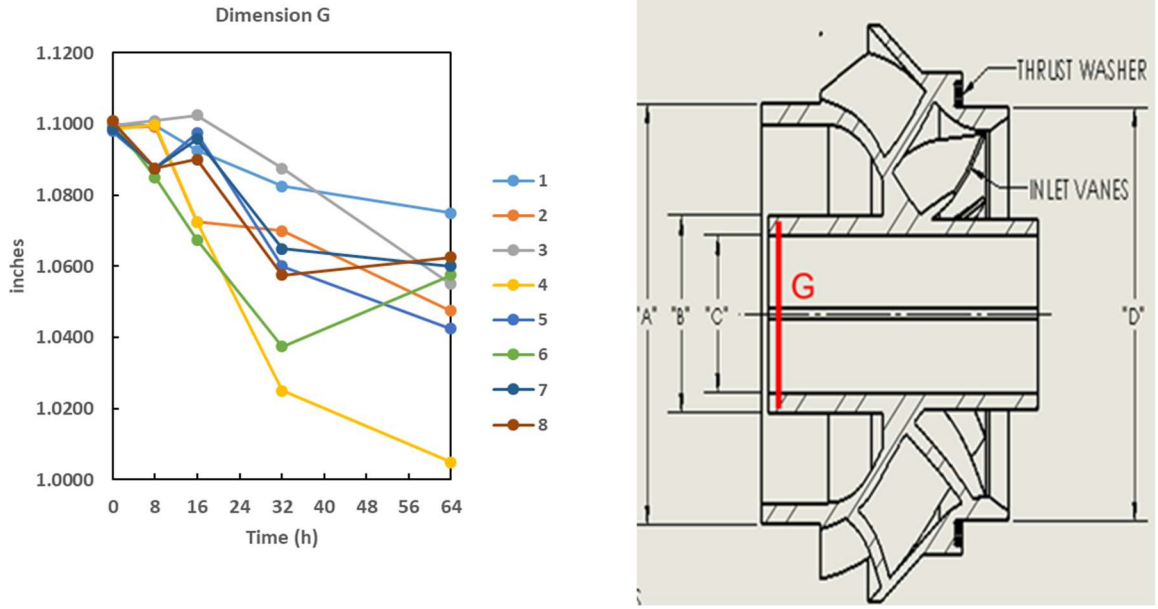

(a) (b)

Figure 3.25: Trend in change of impeller hub OD (Dimension G), (a) ESP2, (b) Reference geometry

The increasing trend of seal clearances is similar to that in ESP1 but the difference in the original and final value is lesser in ESP2. Contrary to the expected result of higher flow rate producing more damage to the ESP stages due to abrasion, the change in seal clearance is actually lesser in ESP2 with 6000 BPD than in ESP1 with 1750 BPD.

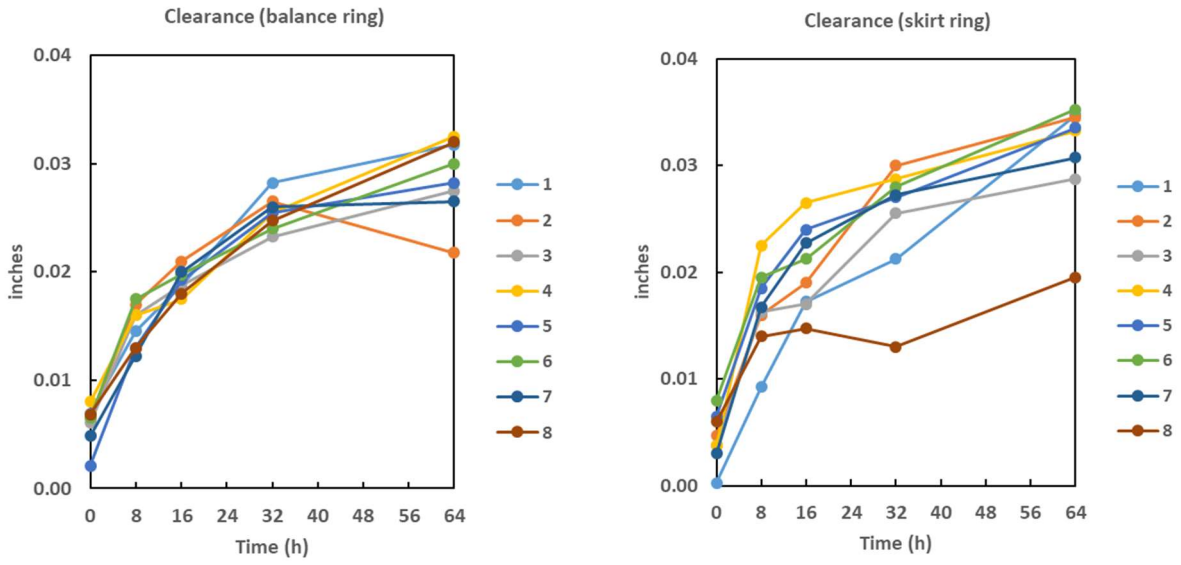

(a) (b)

Figure 3.26: ESP2 seal ring clearances, (a) balance ring, (b) skirt ring

The average weight loss on diffusers of ESP2 is 30 g and for impeller is 15 g which is almost twice the weight loss as compared to ESP1. The most probable explanation for this is the fact that both the pumps undergo similar abrasion damage in the early periods of testing as the weight decreases drastically in the beginning and then the erosional wear is responsible for the further loss in weight and causes a decreasing trend. This erosional damage is more in the case of ESP2 due to the higher operating flow rate that provides higher frequency of particles (hits number) contacting the stage surfaces and thus reducing the weight more than that in ESP1

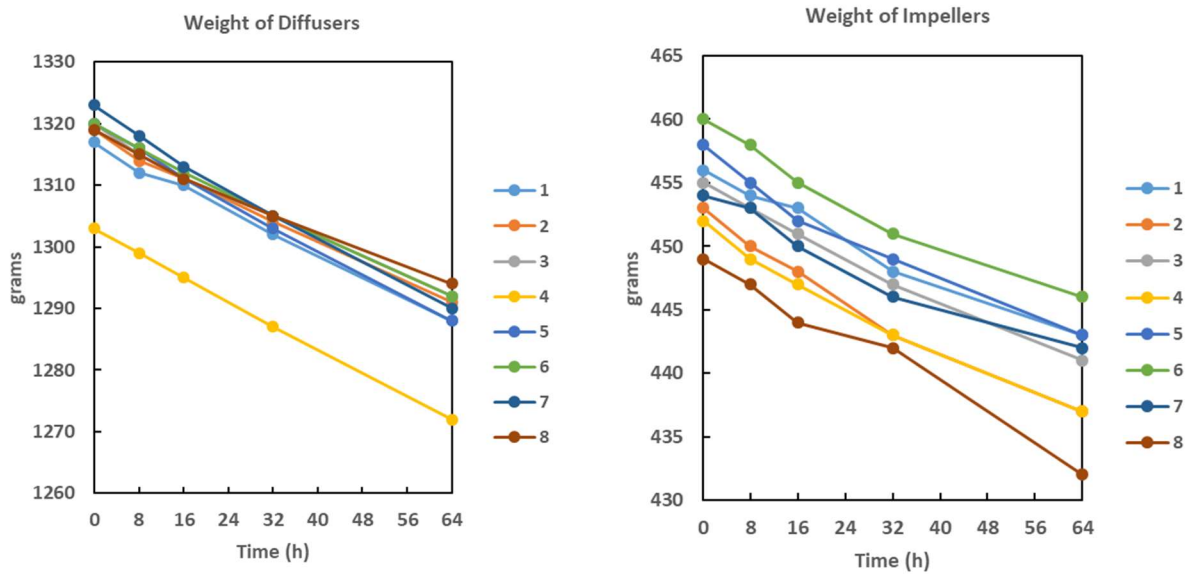

(a) (b)

Figure 3.27: ESP2 loss in weight, (a) Diffusers, (b) Impellers

The diameter of balance holes of the impellers shows an increasing trend which matches the trend observed in ESP1 due to the reason of sand particle recirculation in the balance chambers that causes rise in balance hole diameters

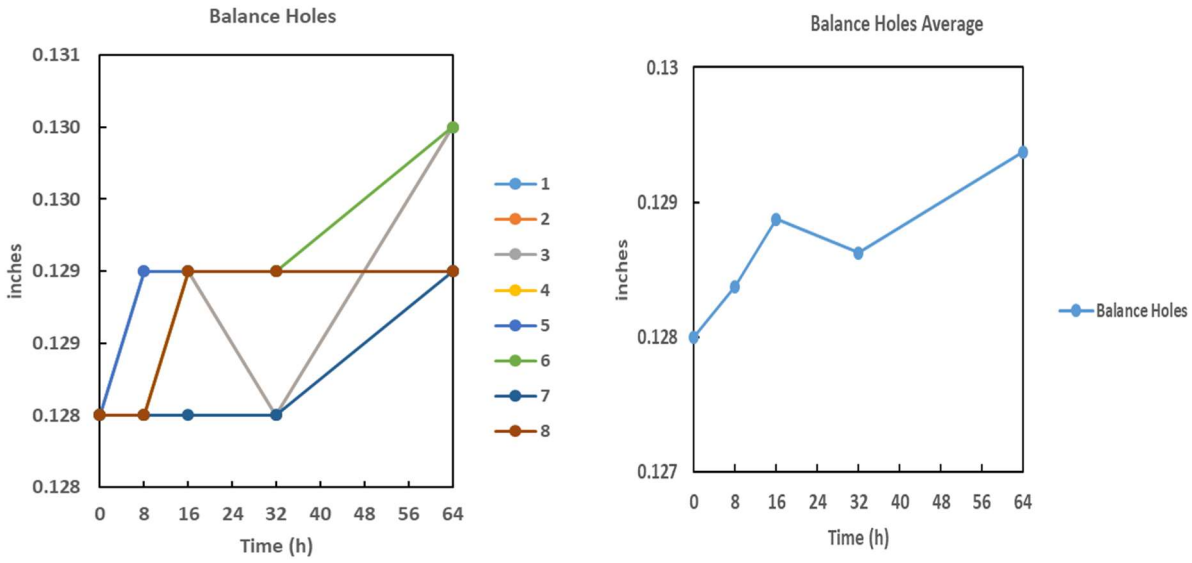

(a) (b)

Figure 3.28: ESP2 impeller balance hole diameter change, (a) Stage-wise, (b) Average

3.3 Experiments summary

The 64-hour testing of ESP1 and ESP2 was completed in 75 days and about 60 Kg of sand was used in the experimenting (approx. 30 Kg per ESP pump). Both the pumps degrade over the period of 64-hour testing and the degradation in performance quantifies the pumps as inoperable in the real field application due to the sub-standard performance and worn out inner stages.

A tabulated summary of the change in individual dimensions for both the pumps is given below in Table 3.7

Table 3.7: Summary of changes in dimensions of the stages of ESP1 and ESP2

Quantity	ESP1			ESP2		
	Original (Avg)	Final (Avg)	% Change (Avg)	Original (Avg)	Final (Avg)	% Change (Avg)
Impeller balance ring OD (Dimension A)	2.45”	2.4347”	-0.62%	2.35”	2.342”	-0.32%
Impeller hub ID (Dimension B)	0.7306”	0.73”	-0.1%	0.8783”	0.876”	-0.21%
Impeller skirt ring OD (Dimension C)	2”	1.9798”	-1%	2.31”	2.3”	-0.49%
Diffuser skirt ring ID (Dimension D)	2”	2.022”	0.66%	2.3133”	2.33”	0.73%
Diffuser hub ID (Dimension E)	0.908”	0.913”	0.53%	1.11”	1.121”	0.98%
Diffuser balance ring ID (Dimension F)	2.4594”	2.4704”	0.44%	2.356”	2.371”	0.65%
Impeller hub OD (Dimension G)	0.898”	0.8388”	6.6%	1.1”	1.051”	4.44%
Balance Holes	0.128”	0.129”	0.78%	0.128”	0.129”	0.78%
Weight of Diffusers	904 g	892 g	-1.26%	1318 g	1288 g	-2.22%
Weight of Impellers	217 g	209 g	-3.82%	455 g	440 g	-3.19%

A tabulated summary of the change in performance parameters for both the pumps is shown below:

Table 3.8: Summary of change in performance parameters for both the pumps as per TUALP and CHX tests

TUALP						
Performance Parameter	ESP1			ESP2		
	Original (Avg)	Final (Avg)	% Change (Avg)	Original (Avg)	Final (Avg)	% Change (Avg)
Head (ft.)	25.96	21.84	-15.88%	24.83	21.83	-12.07%
Efficiency (%)	62.76	50.14	-17.35%	65.69	59.38	-6.78%
Horsepower (HP)	6.99	7.73	6.88%	14.08	13.23	-6.05%
CHX						
Performance Parameter	ESP1			ESP2		
	Original (Avg)	Final (Avg)	% Change (Avg)	Original (Avg)	Final (Avg)	% Change (Avg)
Head (ft.)	24.1	20.2	-16.18%	23.3	20	-14.16%
Efficiency (%)	63.2	45.9	-27.37%	63.20	52.10	-17.56%
Horsepower (HP)	6.869	7.896	14.95%	1.633	1.702	4.23%

CHAPTER 4

CFD SIMULATIONS AND INLET VELOCITY PROFILE

Running erosion tests on actual ESPs with sand and observing the change after each testing period is an expensive and time-consuming process. Due to the advancements in the technology of Computational Fluid Dynamic (CFD) simulation and dynamic solid particle tracking in the CFD Ansys Fluent software, single-phase steady-state simulations were run to predict the Erosion Rate in Kg/m^2-s on the CFD impeller-diffuser geometry. Erosion rate can be defined as the amount of material eroded from the solid geometry due to the incumbent solid particles (sand) per unit area of the geometry per unit of time. In literature, there exist various models based upon detailed experimental data for the prediction of erosion rate. The generalized equation for calculating the erosion rate can be simply written as

$$ER = K \times {V_p}^n \times F(\phi),$$

where ER is Erosion rate in Kg/m^2-s, V_p is Particle velocity (m/s), ϕ is Angle of impact (degrees), and K, n are constants determined by experimental data.

These ER predicting models are encoded in a specific User Defined Function (UDF) that can be compiled and used in Ansys Fluent to generate the desired erosion results and can be used to visually observe the affected parts of the geometry as per the specified solid particles being injected.

Figure 4.1: 2 stage Diffuser-Impeller geometry

4.1 Case setup and results

The case setup was done in Ansys Fluent for a steady-state single-phase simulation. The parameters of interest that were used to set up the CFD case are mentioned below in Table 4.1

Table 4.1: Case setup parameters

Material	Sand
Density	2660 Kg/m^3
Diameter	0.0003 m
Diameter distribution	Rosin-Rammler type
Injection type	Surface
Drag Law	Spherical
Turbulence	Discrete Random Walk model
Viscous Law	SST k-ω model
Particle tracking	Discrete Phase model (DPM)
Solution method	SIMPLEC
Inlet velocity	3.5 m/s
Mass flow rate	0.055 Kg/s

The general simulation methodology process consists of 3 main steps:

1) Flow field generation: Simulating the given case file to generate a converging flow field

before injecting and tracking the particle. The convergence criteria are kept low (1e-3) and thus the system is stabilized before injecting the particle.

2) DPM particle tracking: Particles are inserted in the geometry in the converged fluid flow field and are tracked as they move through the system geometry.

3) User-Defined function (UDF): The UDF is coded with various erosion rate predicting models to get the erosion rate and the particle impact parameters such as impact velocity and angle and the frequency of impact. The calculation of erosion rate in the UDF is based on different models in literature and the results of the simulation yielded the following erosion patterns on the 2nd diffuser in the geometry. As seen from the results in Figure 4.2 below, the Amir Air model predicts the highest erosion rate on the diffuser geometry whereas the DNV model predicts the least amount of erosion.

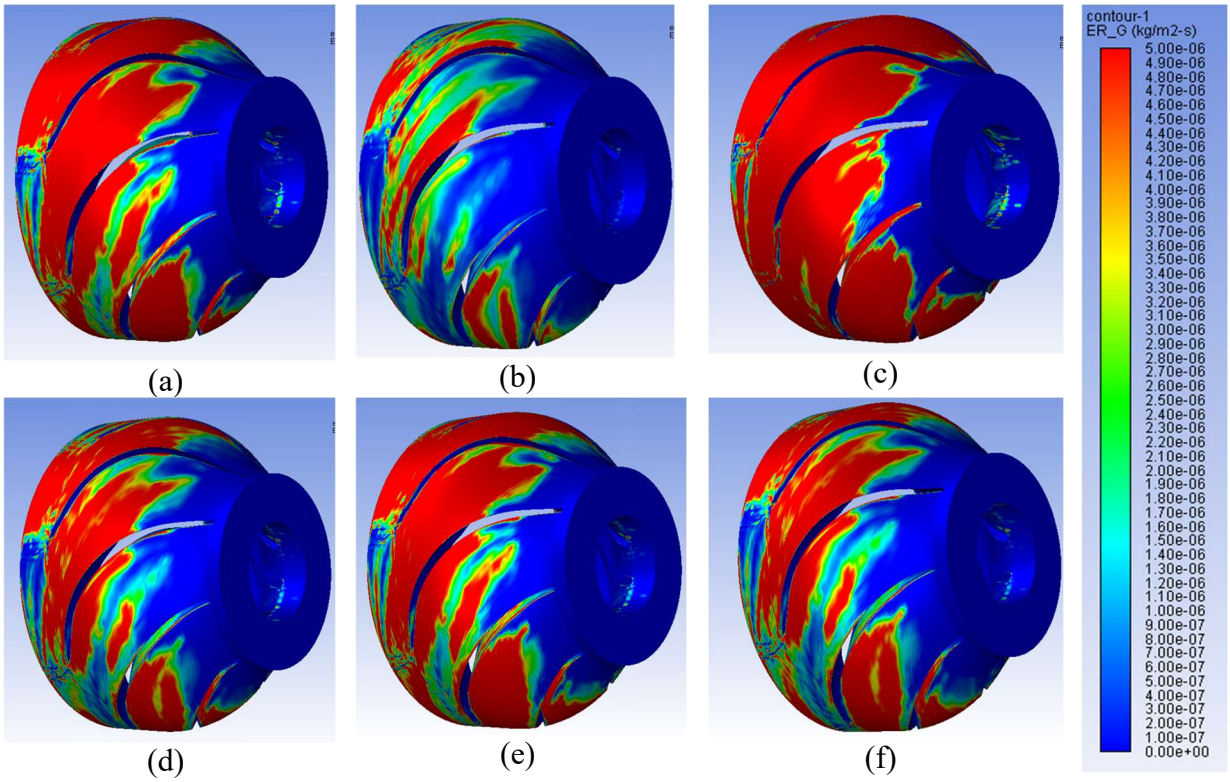

Figure 4.2: Erosion rate from various models on diffusers, (a) Hadi, (b) DNV, (c) Amir-Air, (d) Amir-Water, (e) Oka, (f) Zhang

The erosion results on the impeller geometry show a similar trend as that in the diffusers. Based on the results depicted in Figure 4.3, it can be observed that the Amir Air model predicts the highest rate of erosion on the diffuser geometry, while the DNV model predicts the lowest erosion rate. The worst impacted areas on the impeller geometry are impeller blades and shroud.

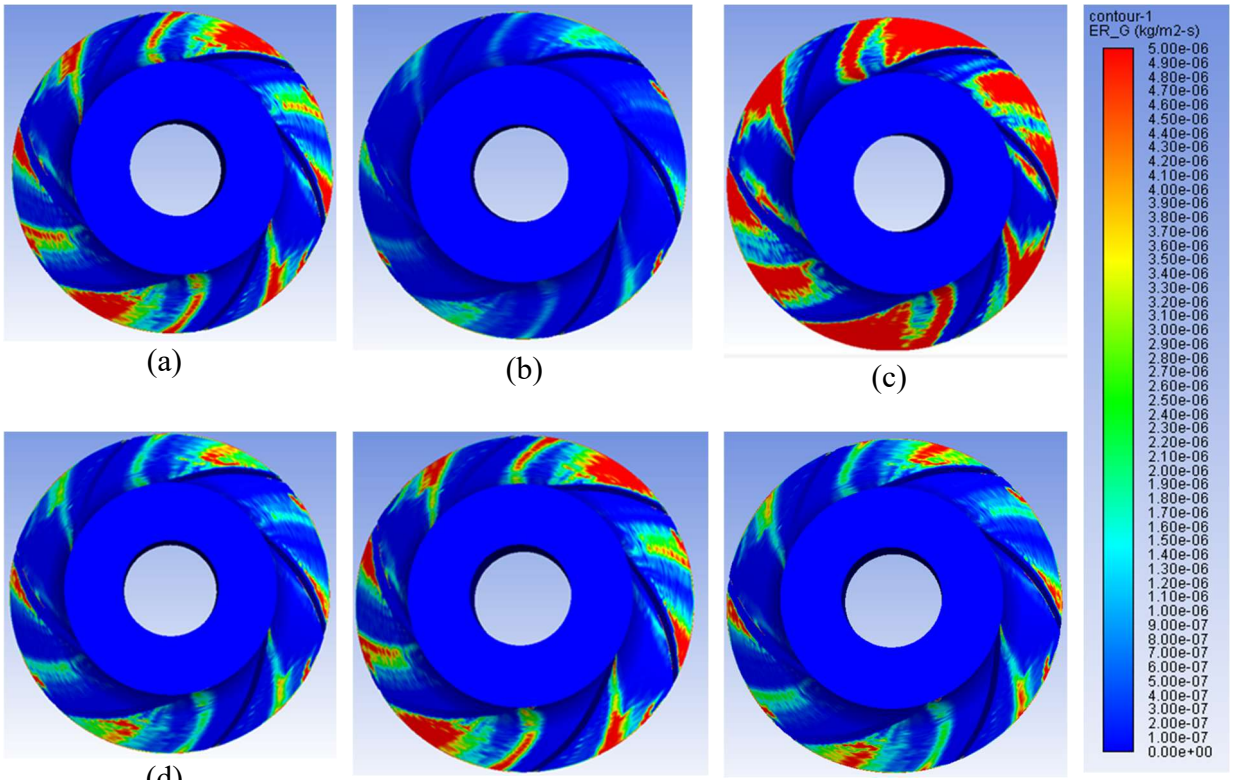

(a) (b) (c)

(d) (e) (f)

Figure 4.3: Erosion rate from various models on impellers, (a) Hadi, (b) DNV, (c) Amir-Air, (d) Amir-Water, (e) Oka, (f) Zhang,

The ER values predicted by the six models are numerically compared to observe the minimum and maximum erosion.

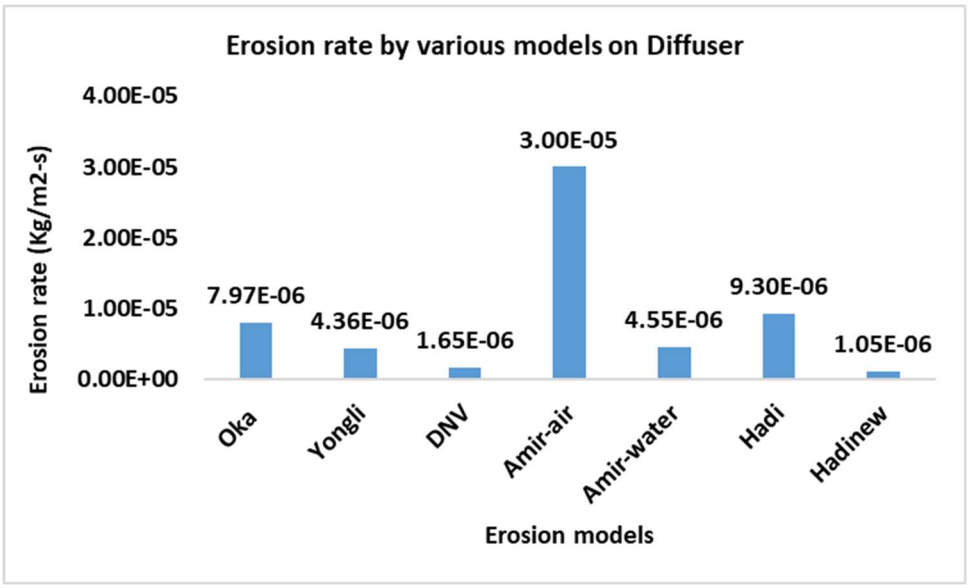

(a)

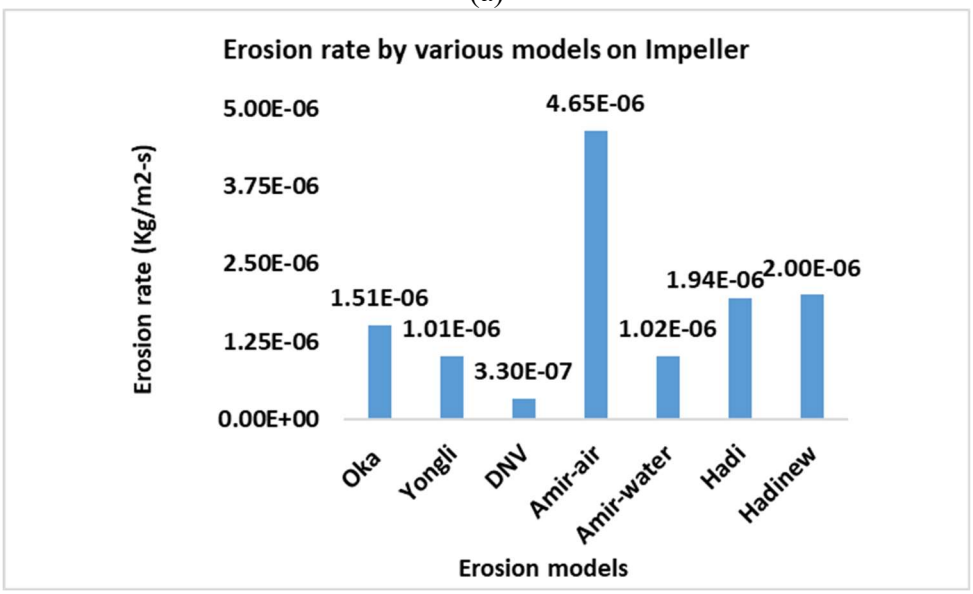

(b)

Figure 4.4: Comparison of ER values obtained from various models, (a) Diffuser, (b) Impeller

Impact parameters such as the number of hits (frequency), angle of impact, and impact velocity are also depicted using the UDF and are shown in Figure 4.5. The impact angle is between 0-5°on any point on the impeller-diffuser geometry. The velocity of impact is approximately in the range of 3-5 m/s and the number of hits on the impeller-diffuser geometry is about 200-500.

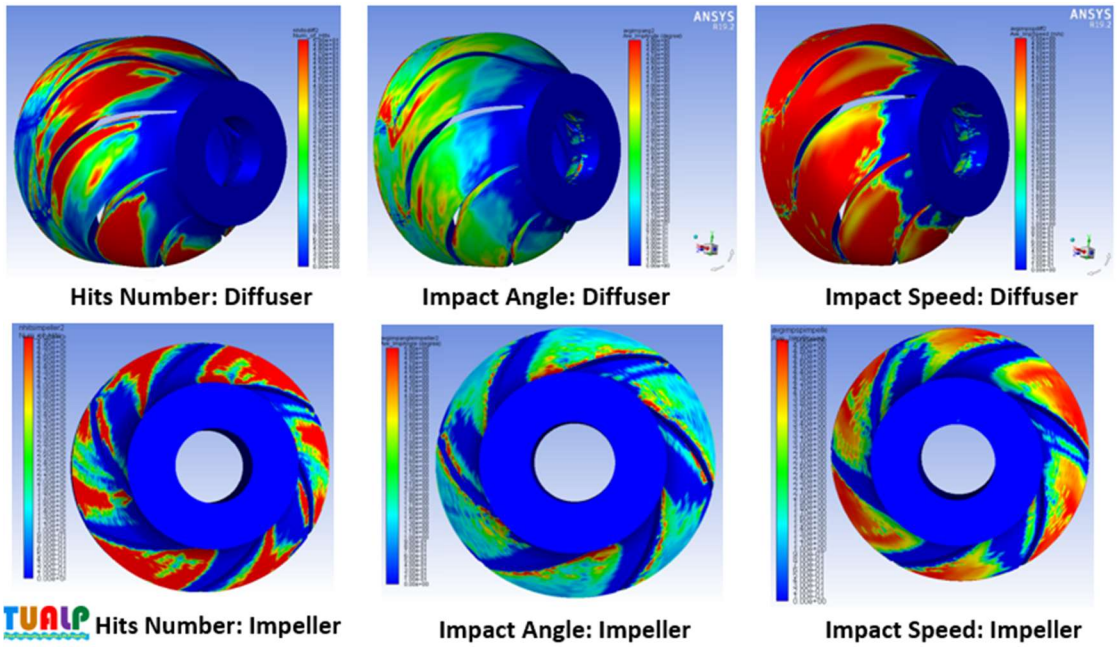

Figure 4.5: Impact parameters on diffuser and impeller geometries

The erosion rate values obtained in the current simulation for the Oka, Zhang, and DNV models were compared to the literature data of the previous test simulations. The ER predicted in the current simulation is higher for the case of both diffusers and impellers than in the previous simulation. The ER ratio however is lesser compared to the previous literature test simulation results. The case settings are generalized and maintained homogeneous to the previous case and the difference in the results is due to some minor changes such as the velocity fluctuation, and density of sand being varied. The lower erosion ratio in the current simulation shows that the erosion rate obtained on the diffuser and impellers is comparable even if it is predicted higher than in the previous case.

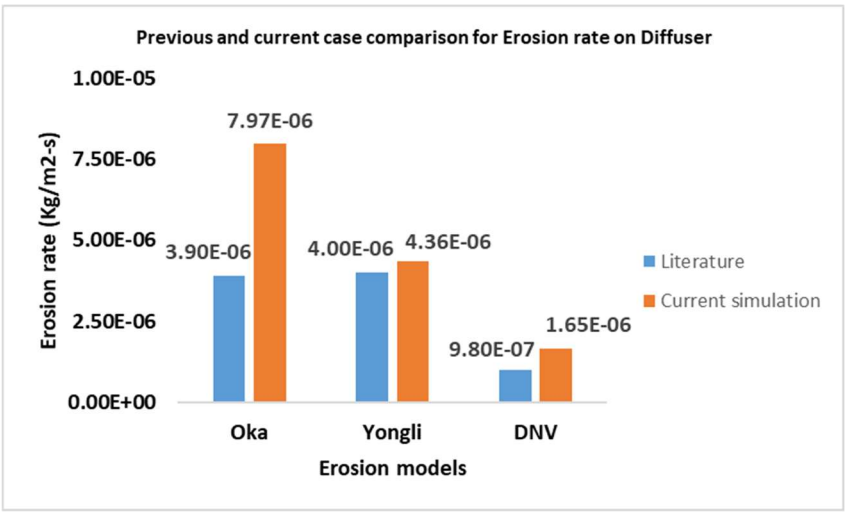

(a)

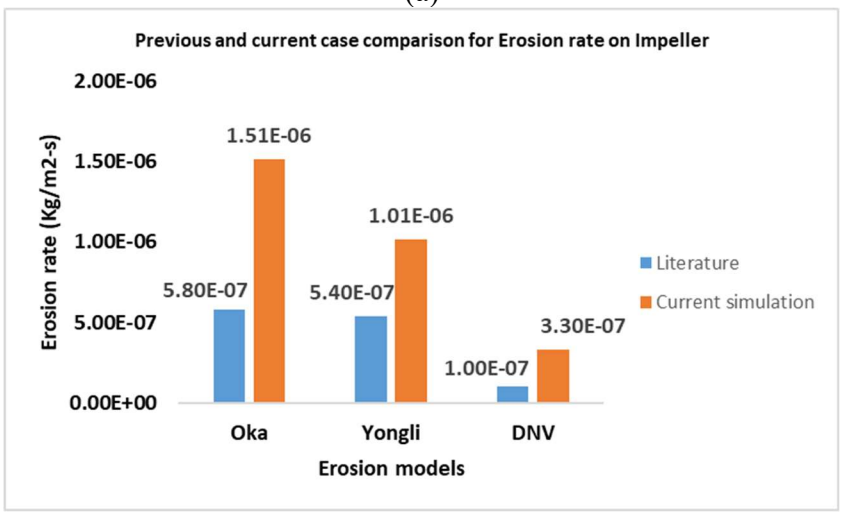

(b)

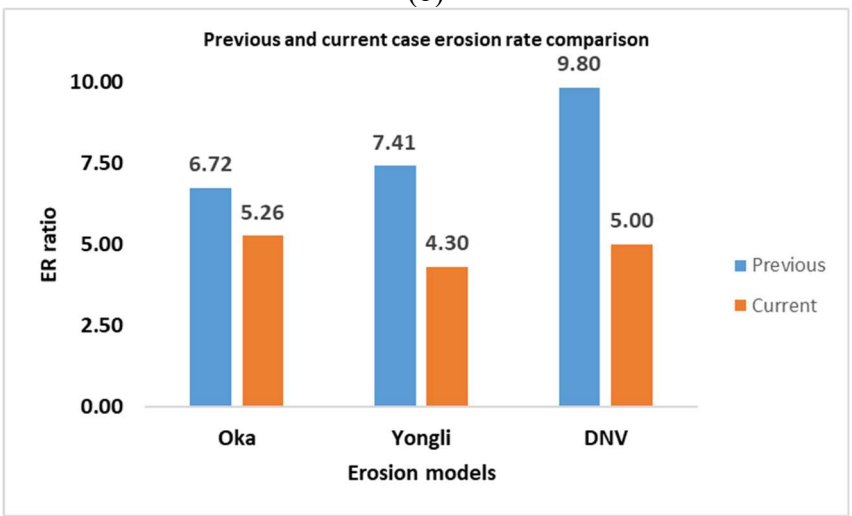

(c)

Figure 4.6: Comparison of ER values from current study and previous study in literature, (a) Diffuser, (b) Impeller, (c) ER ratio

4.2 Inlet Pre-Rotation

In the 2-stage CFD simulation, the 1st stage is generally used for flow domain generation and provides a more accurate sand distribution of the 2nd stage. Then, the erosion rate along with the pattern is observed in the 2nd stage as discussed in the above section. The results obtained from the simulations using this methodology are comparable to reality but there are still some problems such as the stage effect, non-uniform erosion pattern, ER prediction accuracy, and high time of computation. Stage effect is the difference in erosion rate values between the 1st and 2nd stage impellers and diffusers which should not exist as both the stage geometries are identical and thus should have the same patterns as per the ER models. The erosional pattern observed on the 1st stage is not uniform and when compared to actual experimental test results in reality has some differences thus the patterns are inconsistent and hence the accuracy of ER prediction would also need some improvement. In addition, fluid flow and dispersed phase simulation in 2 ESP stages are more expensive and time-consuming as well.

This methodology of simulation is improvised by introducing a novel concept which can be called Inlet Pre-Rotation. The idea is to eliminate the necessity of 1st stage by configuring the sand distribution and particle velocity profile before the particles enter the 2nd stage of the geometry. Doing this would essentially reduce the computational time since it obviates the need for the 1st stage and directly allows the ER prediction in the 2nd stage. The idea is to modify the existing UDF to account for the particle velocity profile and sand distribution parameters in such a way that this UDF can be taken as input for the case and then directly proceeding to DPM tracking and observing the ER results (again from the UDF). This process speeds up the computation and is an improvement on the previous style of simulation. The velocity profiles and sand distribution can be obtained from simple analysis in the Fluent environment that is described ahead.

4.2.1 Inlet Velocity Profile

The velocity of any particle is simply the change in displacement of the particle over time. Velocity is a vector quantity and thus has a magnitude along with a particular direction associated with it. The velocity of the sand particles is crucial to the estimation of the erosion rate on the geometry. The objective of this section is to provide a user-defined inlet velocity field to consider the inlet pre-rotation effect. The fluid field velocity in all the 3 Cartesian directions is coded in the UDF to create a generalized velocity field. Firstly, the inlet velocity field of the 2nd stage impeller was analyzed. 2 diametrically oppositely placed lines are inserted on the structure to get the position vs velocity data. The lines represent the instantaneous velocity of the particle concentration on the line surface with respect to time. Another method to obtain a 3D velocity curve profile would be by inserting a plane instead of the 2D line.

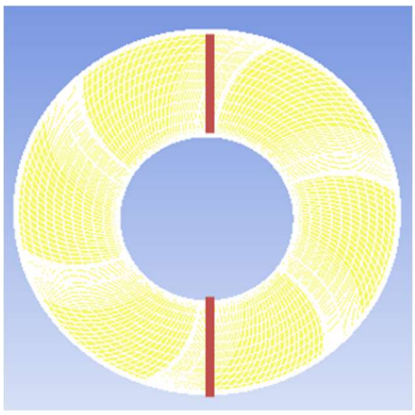

Figure 4.7: Inserted lines on the impeller-2 inlet to get velocity-position data

The velocity profiles for the X, Y, and Z directions are given below in Figure 4.8. As seen, the x and y velocity, which represent the radial velocity, is opposite along the inserted line. On the other hand, the z velocity is symmetric along the inserted line, since it represents the axial velocity that flows into the impeller inlet.

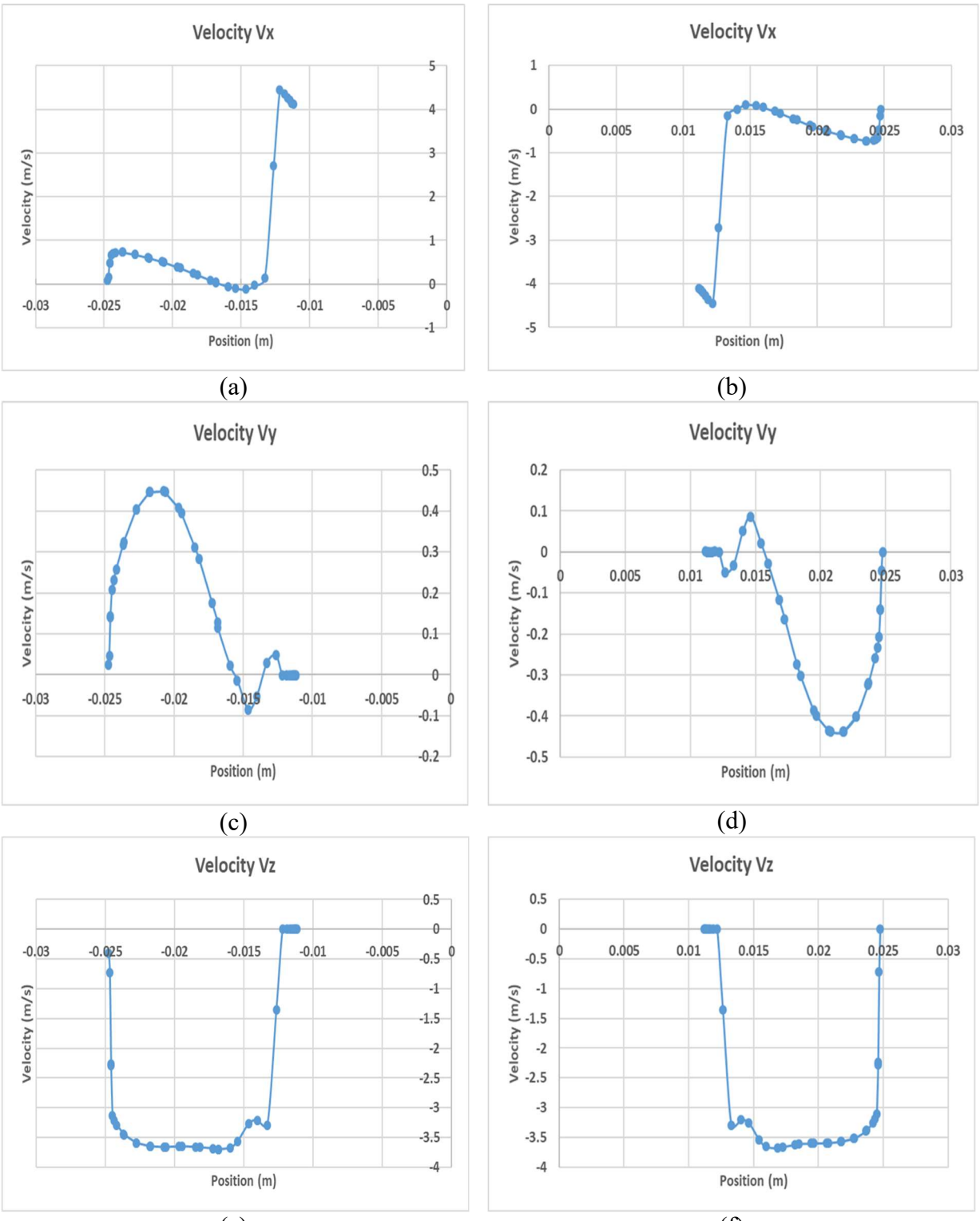

Figure 4.8: Velocity profiles obtained, (a,b) Vx, (c,d) Vy, (e,f) Vz

The obtained graphs are taken as generalized flow curves for particles and the graphs are utilized in further simplification of the inlet pre-rotation phenomena. The velocity profiles are curve-fitted using MATLAB CFTool to get a polynomial-fitting equation. MS Excel is also an option for the curve-fitting to obtain equations but the accuracy level is less compared to MATLAB. The R-squared value for the equations for X, Y, and Z velocities is higher than 0.95 for the equations obtained in MATLAB. The obtained equations are

$$Vx = -0.1598x^4 + 0.1081x^3 + 0.1538x^2 - 0.2652x + 4.278, \quad \text{(A)}$$

$$Vy = -0.2509x^8 + 0.866x^7 - 0.2675x^6 - 1.549x^5 + 1.02x^4 + 0.812x^3 - 0.5935x^2 - 0.504x + 0.4982, \quad \text{(B)}$$

and

$$Vz = -2.7411x^7 + 1.6677x^6 + 7.2671x^5 - 2.4732x^4 - 4.7983x^3 + 1.202x^2 + 0.7602x - 3.3426. \quad \text{(C)}$$

The obtained polynomial equations are coded in the UDF. The UDF file is a Microsoft Visual Studio file and the coding is done in a very simple way to include the 3 velocity profiles. The previously used UDF had 6 erosion models and impact parameter calculation equations, which is also included in the new version of UDF.

The additional inlet velocity profile curve equations make it an improvement over the old version. The equations are fed as input to the CFD case by setting the impeller inlet type to velocity inlet boundary, which previously was set as mass inlet boundary. This type of boundary condition can use the user-defined velocity profiles as described before (Figure 4.9).

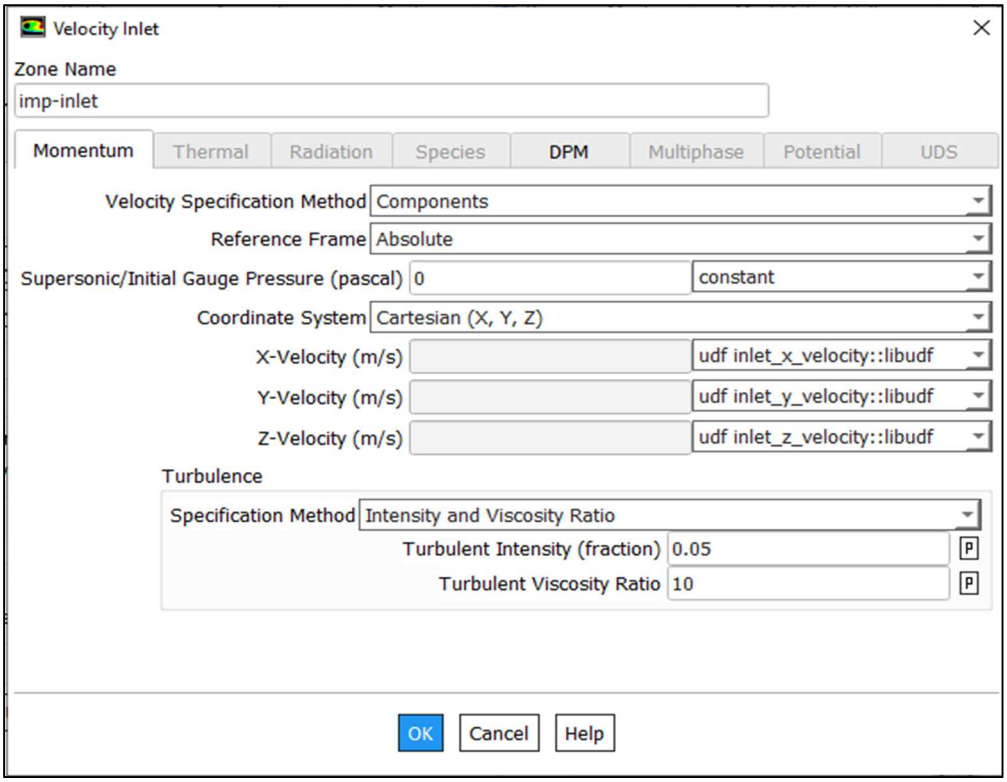

Figure 4.9: Inlet velocity boundary UDF input

Extensive simulations are run using the new UDF to compare the difference in results both qualitatively and quantitatively between the old and new UDF. The remaining case set-up parameters are kept constant so that the only difference in results would be due to the UDF inlet velocity settings, making it easier to comprehend the improvement and flaws of the same.

4.2.2 Sand Distribution

Sand particle distribution is another important factor for actively applying the inlet pre-rotation effect. Configuring the distribution of sand particles before they enter the 2nd stage helps us in estimating which parts of the geometry suffer damage more accurately. The distribution currently available in the simulation is equally spread out from inside to the outside which is of uniform orientation. But as seen from the velocity profile graphs, they are quite irregularly shaped and show higher velocity towards the outlet sand boundary in the geometry. Modelling sand

distribution to match with the velocity profile can be done by obtaining particle velocity and position based on the output. This irregularity in distribution is what the objective of the study is to attain so that the desired distribution has more concentration towards the outside of the geometry. The distribution would be like a parabolic curve with increasing concentration near the outside boundary.

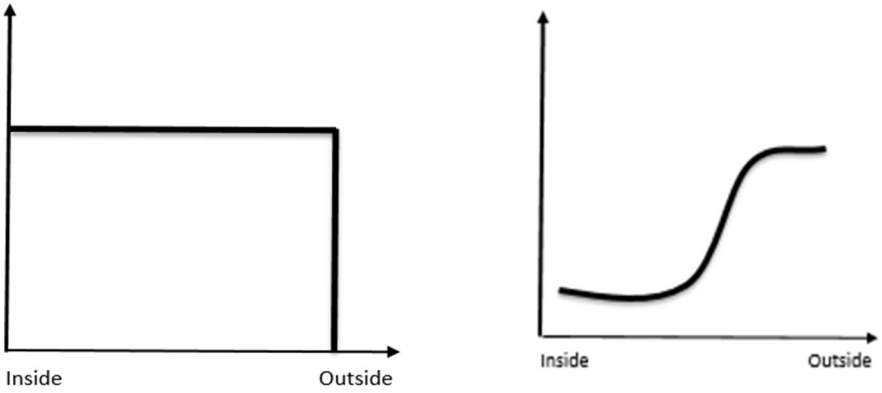

(a) (b)

Figure 4.10: Sand distribution, (a) Current, (b) Desired

This type sand distribution can be modeled by developing an injection file which can be used as an input file for particle injection. In the current case, the sand particles are inserted normally into the surface in the Z-direction. The outlet particle position and velocity can be simulated and used to create an injection file as discussed above using the discrete phase tools available in Ansys Fluent.

Although this idea has not been tried in real-life yet due to time limitations, it has a clear and simple theoretical basis that can be easily put into practice. The plan is to create an injection file that changes how particles are injected in DPM tracking. Instead of inserting particles straight into the surface, the file will be used to control their injection.. However, it's essential to mention that the current analysis doesn't include the criteria for sand distribution, which should be addressed in future studies for better accuracy.

4.2.3 Simulation results using new UDF and comparison with previous case of old UDF

Simulations were run using the modified UDF and the new methodology followed involved an additional step before applying the previous 3-step CFD methodology, which used modified UDF as a velocity inlet for the X, Y, and Z velocities. To ensure accurate comparisons, we kept the case setup parameters consistent throughout the simulations. By doing this, we could avoid any discrepancies in the results that might arise from altering those parameters. This approach allowed us to focus solely on understanding the impact of the modified UDF and the inlet pre-rotation on the simulation results without interference from other factors.

Figure 4.11 illustrates the outcomes of the simulation conducted with the new modified UDF. It presents the patterns and ER values obtained on the diffuser geometry. Similarly, Figure 4.12 showcases the results on the impeller.

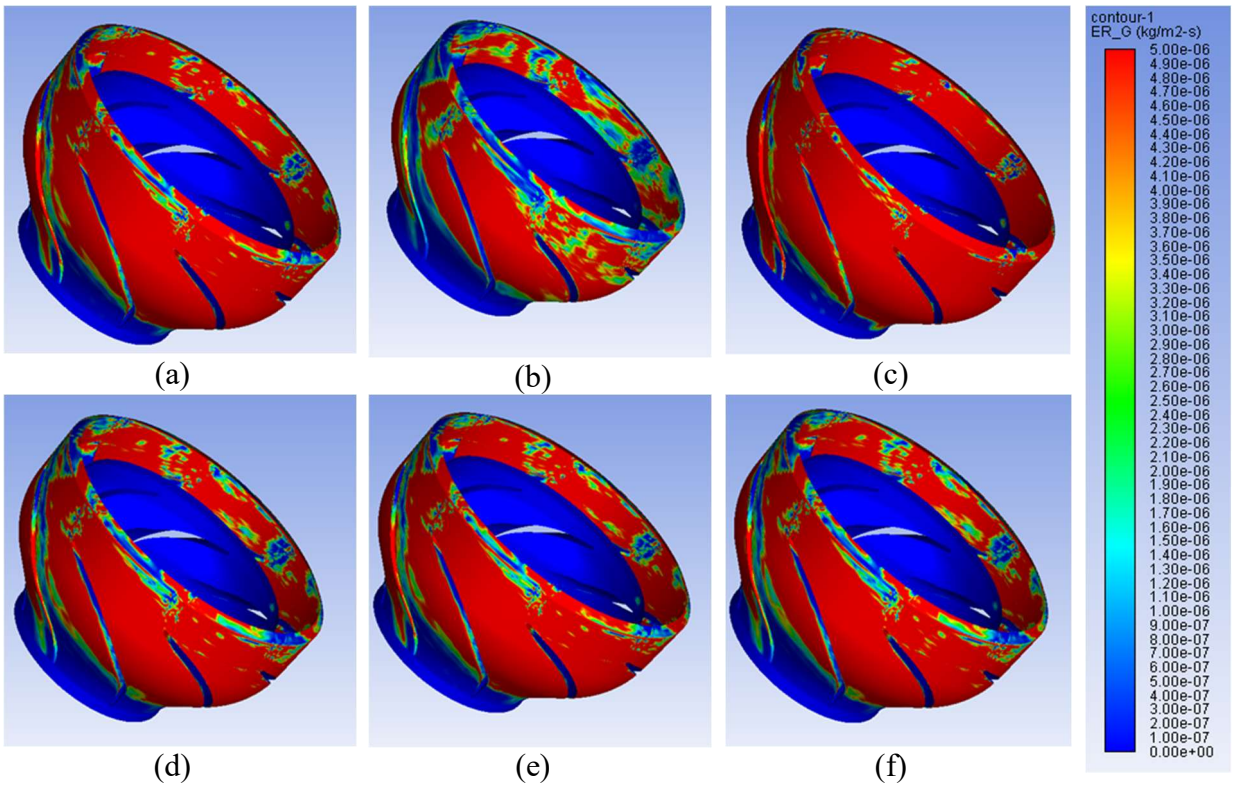

(a) (b) (c)

(d) (e) (f)

Figure 4.11: Erosion rate with new UDF from various models on diffusers, (a) Hadi, (b) DNV, (c) Amir-Air, (d) Amir-Water, (e) Oka, (f) Zhang

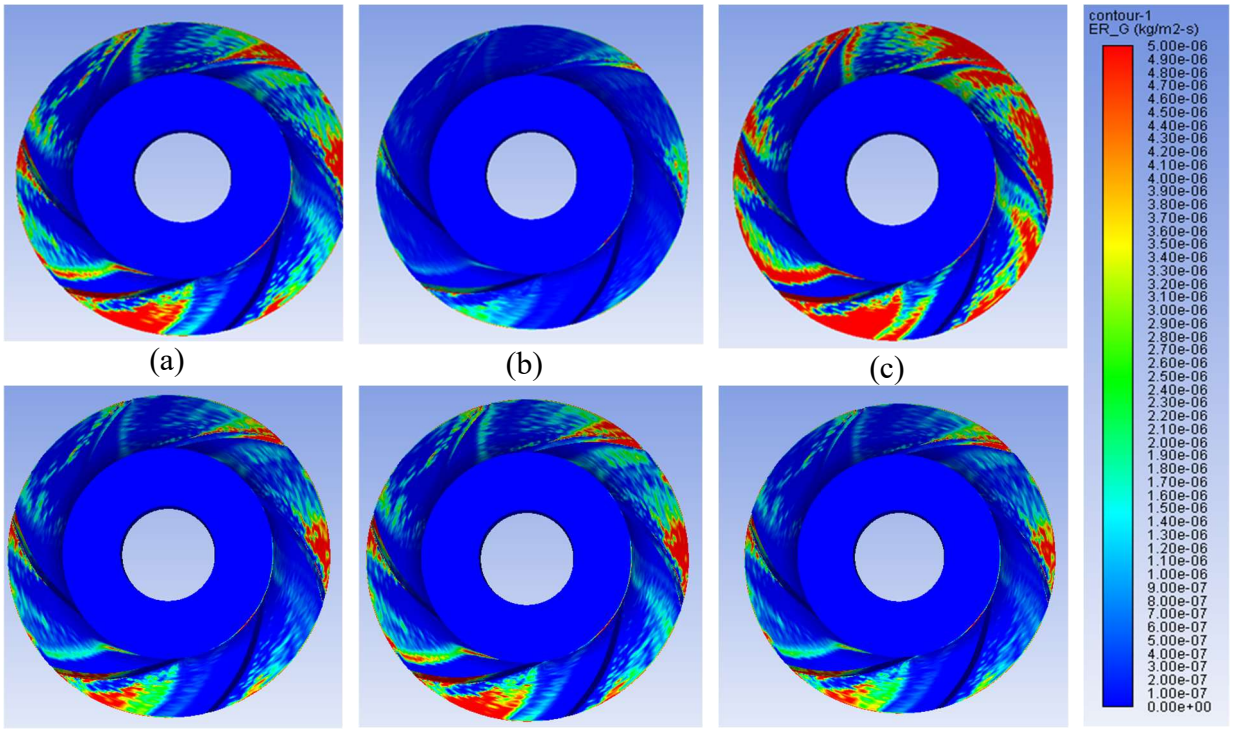

(a) (b) (c)

(d) (e) (f)

Figure 4.12: Erosion rate with new UDF from various models on diffusers, (a) Hadi, (b) DNV, (c) Amir-Air, (d) Amir-Water, (e) Oka, (f) Zhang

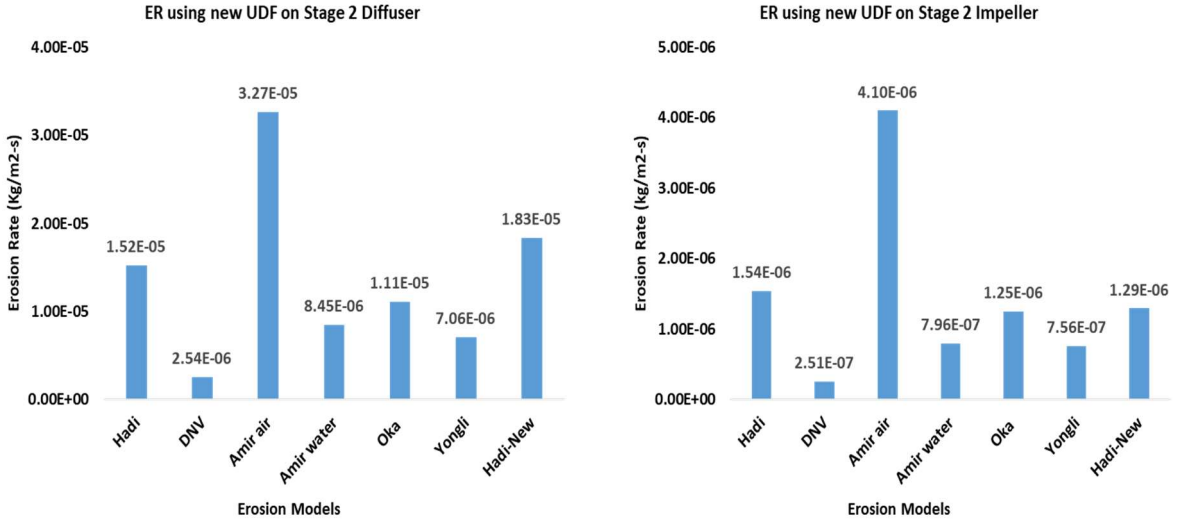

(a) (b)

Figure 4.13: Comparison of ER values obtained with new UDF from various models, (a) Diffuser, (b) Impeller

The trend of maximum and minimum prediction was similar to that of the old case and in the new UDF simulation. Amir Air still predicts the highest erosion rate and the DNV model

predicts the lowest erosion rate. The Oka model predicts the erosion rate most comparable to actual experimental test data and the Oka model results shall be used to qualitatively compare the old and new UDFs for the differences

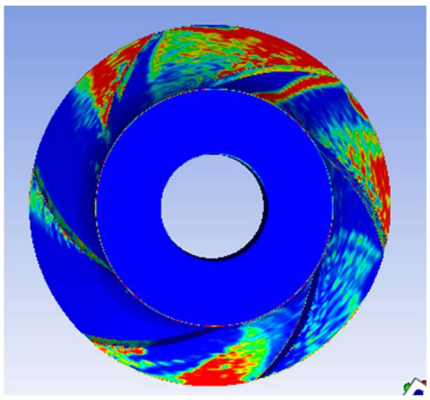

(a)

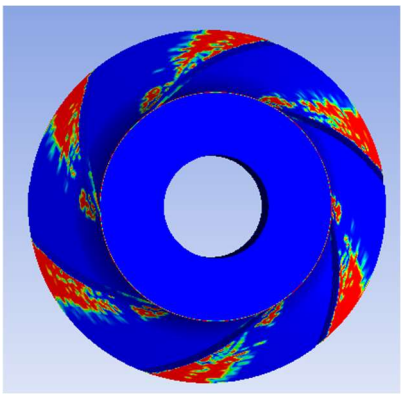

(b)

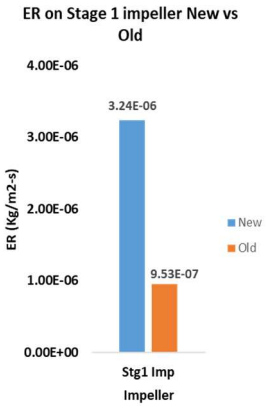

(c)

Figure 4.14: Comparison of new and old UDF ER on stage 1 impeller, (a) New, (b) Old, (c) Graphical comparison

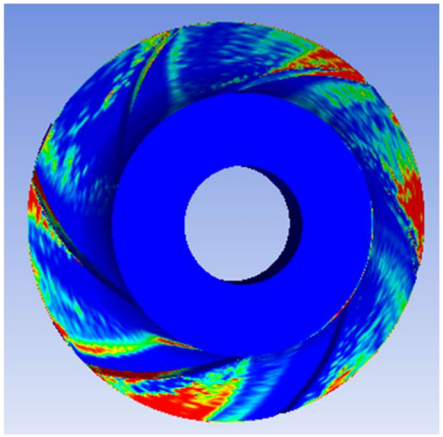

(a)

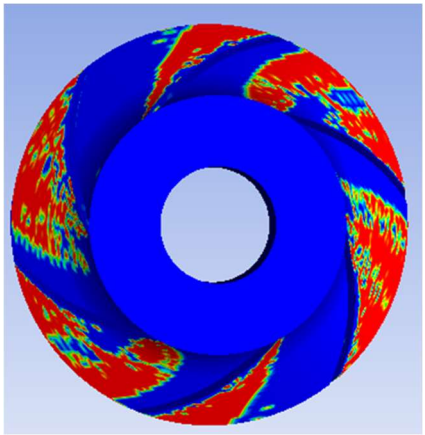

(b)

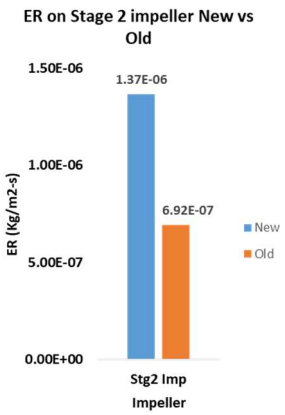

(c)

Figure 4.15: Comparison of new and old UDF ER on stage 2 impeller, (a) New, (b) Old, (c) Graphical comparison

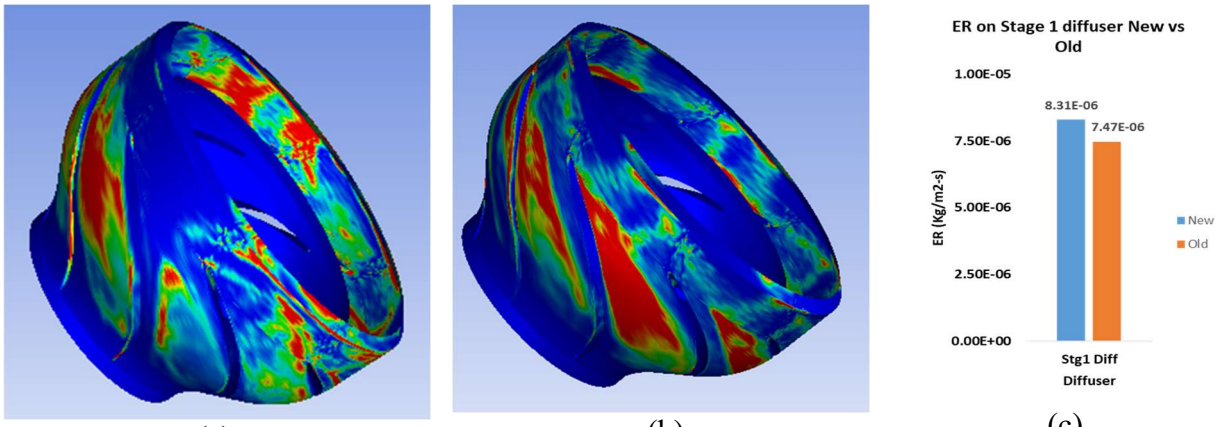

(a) (b) (c)

Figure 4.16: Comparison of new and old UDF ER on stage 1 diffuser, (a) New, (b) Old, (c) Graphical comparison

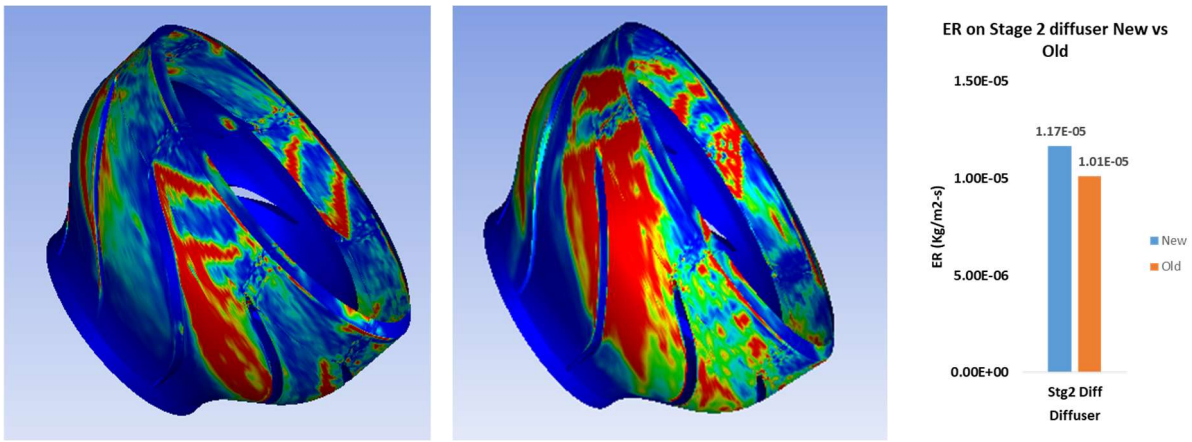

(a) (b) (c)

Figure 4.17: Comparison of new and old UDF ER on stage 2 diffuser, (a) New, (b) Old, (c) Graphical comparison

It was observed that the new UDF predicts a much higher erosion rate for impellers of both stages than the old UDF and the pattern is more uniform in the old UDF which does not take into account the inlet pre-rotation effect. The difference in values is approximately 60%. For the case of diffusers, the new UDF predicts comparable ER values to the old UDF, and also the pattern is more consistent. The difference is about significantly less about only 8%. This drastic difference in diffusers and impellers is on a complete geometry basis and is further studied in detail individual part-wise.

4.2.3.1 Stage ER ratio: ER ratio is the ratio of erosion rate observed on the diffuser to the erosion rate observed on the impeller

Table 4.2: Stage ER ratio comparison between new and old UDF

ER- Oka	New UDF			Old UDF		
Stages	Impeller	Diffuser	ER ratio	Impeller	Diffuser	ER ratio
1	3.24E-6	8.31E-6	2.56	9.53E-7	7.47E-6	7.84
2	1.37E-6	1.17E-5	8.54	6.92E-7	1.01E-5	14.6

The ER ratio obtained in the new UDF is closer to the actual experimentally obtained ER ratio value (3.8-4) whereas in the old UDF, the ER ratio has a much higher percentage of error when compared to actuality.

4.2.3.2 Stage Effect comparison: Stage effect is described as the difference between the ER on the impeller and diffuser of the 1st and 2nd stages. Theoretically, the ER on the first and second stages should be close or identical. In following table, less difference represents less stage effect.

Table 4.3: Stage effect comparison between new and old UDF

ER- Oka	New UDF			Old UDF		
Stages	1	2	Difference	1	2	Difference
Impeller	3.24E-6	1.37E-6	57.71%	9.53E-7	7.47E-6	37.71%
Diffuser	8.31E-6	1.17E-5	28.97%	6.92E-7	1.01E-5	26.03%

As seen, the new UDF does not reduce the stage effect, which indicates the inlet particle distribution and velocity profile effect cannot be neglected. Therefore, the particle inlet UDF needs to be improved in future studies. To eliminate the stage effect, sand distribution is the dominant over velocity profile and the stage effect needs to be checked once the distribution profile has been created as an injection file and applied in the simulation.

4.2.3.3 Stage surface comparison: There are 3 main surfaces of interest on the impeller-diffuser geometry, i.e. shroud, hub, and blade. Each of them shows a pattern of erosion that can be

compared to actual photos after the experimental test. This comparison is more qualitative and less quantitative as compared to the previous ones and the photos are visually observed to compare with actuality. The experimental result photos were taken after continuous sand operation to check the erosion patterns and are now used to compare with the CFD simulations.

Table 4.4: Stage effect comparison on impeller surfaces between new and old UDF

ER- Oka	New UDF			Old UDF		
Geometry Surface	1	2	Difference	1	2	Difference
Shroud	2.61E-06	1.83E-06	42.62 %	1.72E-06	6.62E-07	159.81 %
Hub	4.90E-06	5.08E-07	864.56 %	6.37E-07	1.99E-07	220.1 %
Blade	2.57E-06	1.61E-06	59.62 %	6.11E-07	1.04E-06	41.25 %

Table 4.5: Stage effect comparison on diffuser surfaces between new and old UDF

ER- Oka	New UDF			Old UDF		
Geometry Surface	1	2	Difference	1	2	Difference
Shroud	1.76E-05	2.57E-05	31.51 %	1.61E-05	2.10E-05	23.33 %
Hub	1.08E-07	3.00E-08	260 %	5.63E-08	1.64E-07	65.67 %
Blade	1.84E-06	1.23E-06	49.59 %	1.33E-06	2.61E-06	49.04 %

Observed from the tables above, the ER values are individual structure-wise compared. Similarly, the lower difference represents an improvement that helps reduce the stage effect on erosion simulation. The new UDF shows improvements on the impeller blade and shroud, while the difference mainly comes from the impeller hub. On the diffuser, the new UDF has less effect since the fluid flow in the impeller flow domain helps reduce the UDF effect. The hub simulation stage difference of New UDF reduced from 800% to 200%, which proves that the fluid field in the impeller flow domain helps reduce the error. It is presumably the user-defined velocity profile near the hub area is not accurate enough and needs to be improved in the future. However, that near blade and shroud surface proves an improvement of the erosion simulation validity.

Qualitative comparison with actual experimental results is shown in the figures below where photos are compared with CFD simulation results on the shroud, hub, and blade of the impeller-diffuser geometry respectively.

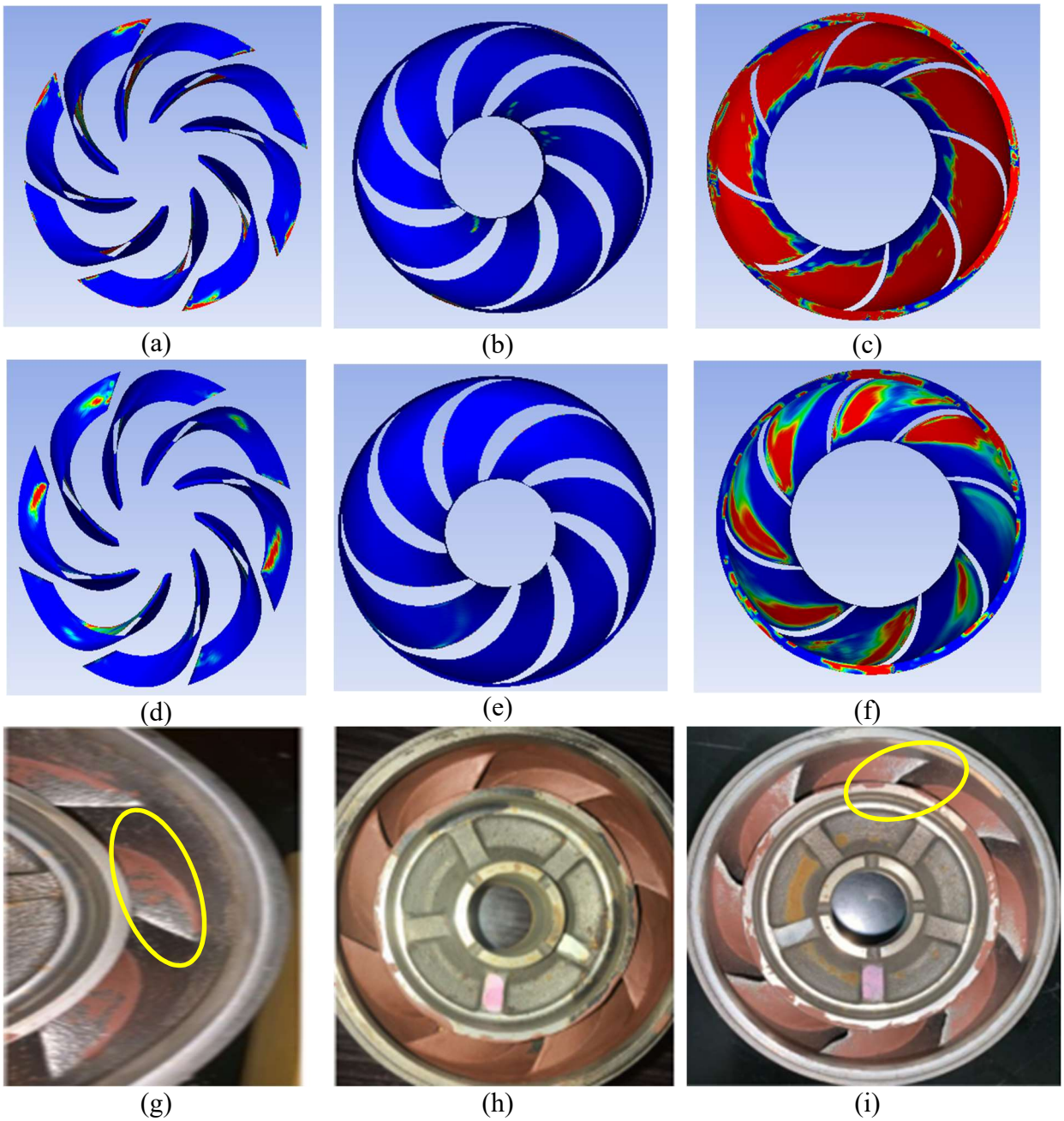

Figure 4.18: Comparison of diffuser surfaces between new and old UDF with actual experimental photos, (a) Blade (New UDF), (b) Hub (New UDF), (c) Shroud (New UDF), (d) Blade (Old UDF), (e) Hub (Old UDF), (f) Shroud (Old UDF), (g) Blade (Test), (h) Hub (Test), (i) Shroud (Test)

As seen from the diffuser erosion patterns in Figure 4.18, the 1st row presents results of simulation using the old UDF, 2nd row shows results using the new UDF and the last row shows actual experimental photos taken after erosion tests. It is seen that the erosional pattern obtained

in the new UDF is more practically consistent with experimental photos. One such surface is the diffuser shroud which reflects severe damage in the old UDF simulation but shows a more uniform spread-out damage trend in the modified UDF which is corroborated by the experiment. The shroud experiences damage but the old UDF overpredicts the sand damage at a higher concentration over the surface. The damage in experimental photos is a measure of paint removal from the geometry. The blade are comparable in simulations with minor differences in patterns.

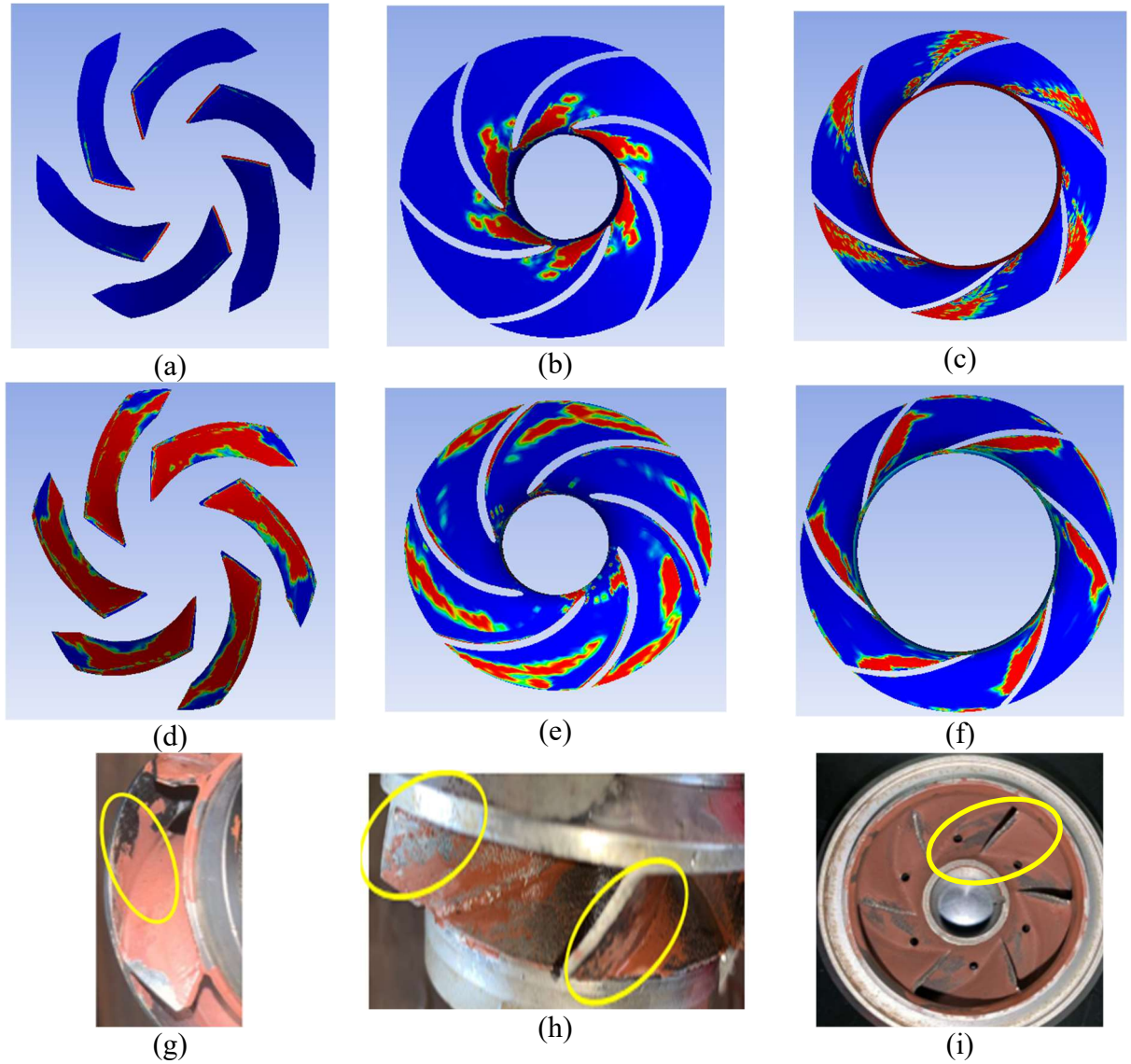

Figure 4.19: Comparison of impeller surfaces between new and old UDF with actual experimental photos, (a) Blade (New UDF), (b) Hub (New UDF), (c) Shroud (New UDF), (d) Blade (Old UDF), (e) Hub (Old UDF), (f) Shroud (Old UDF), (g) Blade (Test), (h) Hub (Test), (i) Shroud (Test)

For the impeller comparison, it was seen that the new UDF predicts much higher damage on the blade when compared with the old UDF, which is closer to the paint. The paint removal photos of blade structure from the experiments show a lot of damage which is proportional to the amount of material removed which in turn is a measure of the amount of material eroded due to sand impact. As observed in Figure 4.19, the damage on the hub is observed to be more concentrated near the bore (center) of the geometry in old UDF simulations but is more evenly spread out in the case of new UDF. The damage on the hub of an impeller in actual results is somewhat distributed but is difficult to estimate since the ER value is very low in both the simulations which matches the trend of experiments where the hub damage is less compared to shroud and blade. Overall, the new UDF's result is closer to the paint removal photos.

The validation of the CFD simulation results of the old and new UDF is an important aspect to compare the differences between the 2 methods to analyze the improvements in results obtained and the scope for further improvement. Modeling the erosion on stages of an ESP is a broad topic and the validation of simulation results with experimental results proves to be a good measure for refining the modelling process. Prediction of erosional damage on stages of an ESP is useful to understand the changes in the performance of the pump over several hours of operation under sandy flow. The inlet velocity profiles are generated by 2D lines that are inserted into the impeller inlet to obtain velocity-position data but can also be generated using 3D planes to obtain similar profiles. The inlet pre-rotation effect, in totality, can be further modified and improved by the creation of a sand injection file that might prove to produce more accurate results of ER values, as well as more uniform or consistent patterns that are observed in reality. The sand distribution is presumably to be a more dominant factor. Therefore, a further improvised hybrid case would be incorporating both the inlet velocity profile and the sand distribution profile.

CHAPTER 5

CONCLUSION AND RECOMMENDATIONS

Pump performance was monitored and analyzed after every test interval (8, 8, 16, and 32-hour) to investigate the performance deterioration. Geometrical changes and weight loss of each diffuser and impeller were also measured. The experimental data obtained and the results of CFD simulation are interpreted and the following conclusions can be drawn as per the observations.

Three-body abrasion damage on stage surface:

1) At BEP of the two tested ESPs, the three-body abrasion wear was similar in both pumps, impeller washers on both pumps became detached and loosened, and most of the measured geometries changed by only 0.5-1% after the test. As a result, the seal clearance of the skirt ring, balance ring, and inter-stage hub ring increased by almost 10 times.
2) Among all measured geometries, the impeller hub outer diameter (Dimension G) of both pumps decreased by 5%, indicating that more sand had accumulated in this area.
3) Despite the accumulation of sand in the impeller hub inner diameter (Dimension B), the resulting damage can be deemed insignificant because the impeller hub inner surface rotates along with the shaft without experiencing any relative movement.
4) The carbide parts, including sleeves and bearings, underwent polishing, but their outer diameters remained unchanged.
5) Overall, the abrasive damage in both ESPs are comparable, despite different BEP flow rates.

Two-body erosion damage and sand impact on primary flow channel surface:

1) The primary flow channels of both pumps exhibit evident erosion damage patterns, particularly on the blade tips, and balance holes.
2) Compared to ESP1, ESP2 impeller blade inlet tips show a more distinct “C” or “S” shape pattern. In addition, deformed blade tails and cracks were observed at the impeller outlet of ESP2, likely caused by sand impact and a manufacturing casting issue. The weight loss of ESP2 is greater.
3) In summary, erosion in ESP2 is higher due to higher BEP flowrates, which can resulting higher solid impacting speed and frequency.

Overall pump performance deterioration:

1) ChampionX and TUALP's performance tests are similar, with a decrease in head of approximately 15% for both pumps.
2) The greatest performance reduction occurred during the first 8-16 hours, which aligns with the trend of three-body abrasion damage.
3) The primary reason for the reduced pump boosting capability is the significant increase in recirculation between stages caused by abrasion damage.
4) While the erosion damage of ESP2 is more severe than ESP1, its impact on pump performance is not that obvious, which should be investigated through extension tests.

ESP erosion CFD simulation:

1) Erosion values and patterns observed are similar but still exists some dissimilarities. Different erosion models are compared in this study, Oka model has the most accurate erosion rate prediction, while Hadi models is more accurate in erosion ratio prediction (ratio between erosion on impeller and diffuser).

2) A new UDF considering inlet pre-rotation effect is developed in this study and compared to previous UDF and results in both simulation and experimental tests. In both case, the worst impacted areas are impeller blades, diffuser vanes along with the shroud and hubs of the geometries. Damage is compared with experimental paint-removal photos on the particular surfaces.
3) The ER ratio obtained in the new UDF simulation (2.5-8.5) is more closer to the one obtained in tests (3-4), while that obtained in the old UDF simulation is 8-15.
4) The erosional pattern obtained in the new UDF results is more consistent with the patterns observed from the paint-removal photos from actual experimental tests such as the severe damage on the impeller blade and the balanced erosion damage on the diffuser shroud is closer to test observations.
5) The stage effect is not completely eliminated and has worsened for the hub surfaces for the geometries. The velocity field at the inner hub surface needs to be reconfigured. The erosion pattern on the 1st stage is still non-uniform. Overall, the new UDF has a slight improvements on erosion ratio, but still need to be revised in future study.

Recommendations for future study:

1) To comprehend the damage mechanism and enhance pump design, extension tests are advisable (up to 120 hours).
2) Examination at flow rates above or below BEP can be conducted to scrutinize the impact of flow rate and thrust force.
3) The impact of varying sand concentration and sand properties can be evaluated.
4) Visualization of erosion damage on the ESP primary flow channel surface can be achieved by painting particular regions of the diffusers and impellers.

5) To investigate the sand damage effect on the pump's rotating stability, vibration sensors are recommended.
6) To reduce the impact of sand damage, improvements can be made in pump stage casting and manufacturing procedures.
7) Different pump configurations can be studied. For instance, whether it is feasible to use fewer carbide sleeves while still maintaining pump rotation in solid flows, or if it is economically viable to employ carbide sleeves at every stage.
8) The observations in this study can be used to validate CFD simulation. The pump geometry can be improved to mitigate damage in certain areas.
9) It is essential to investigate the effect of pump rotation speed, particularly for high-speed conditions (over 60 Hz).
10) Configure velocity-position data by inserting a 3D plane in the geometry in the direction of flow instead of a 2D line.
11) Obtain the particle position and velocity at the outlet boundary from DPM reports to further improve the UDF and create a sand injection file to be used for the simulation.

NOMENCLATURE

BEP	Best Efficiency Point
BPD	Barrels Per Day
CFD	Computational Fluid Dynamics
CHX	ChampionX
ER	Erosion Rate, Kg/m^2-s
ESP	Electrical Submersible Pump
GVF	Gas Volume Fraction
HP	Horsepower
Hz	Hertz
ID	Inner Diameter
OD	Outer Diameter
RPM	Rotations Per Minute
SS	Stainless Steel
TUALP	Tulsa University Artificial Lift Projects
UDF	User Defined Function
VSD	Variable Speed Drive
K, n	Experimental constants
V_p	Particle velocity, m/s
Ø	Angle of impact, degrees

dp_n	Boosting pressure per stage, psig
P_{out}	Outlet pressure, psig
P_{in}	Inlet pressure, psig
H	Pump head per stage, ft.
Q_w	Standardized flow rate, BPD
n	Number of stages
ŋ	Efficiency, %
τ	Torque, lb-in
HP	Power, HP
N	Pump rotational speed, RPM
T	Temperature, ^{0}F

BIBLIOGRAPHY

Bai, C., 2017. Rotordynamic and Erosion Study of Bearings in Electrical Submersible Pumps (Doctoral dissertation)

Beck, D., Nowitzki, W. and Shrum, J., 2019, May. Electric Submersible Pump ESP Vibration Characteristics Under Wear Conditions. In SPE Gulf Coast Section Electric Submersible Pumps Symposium? (p. D022S013R001). SPE.

Boudi, A.A., 2016, November. ESP suffers erosion due to sand production in a mature onshore oil field. In SPE Middle East Artificial Lift Conference and Exhibition. OnePetro.

Brown, K.E., 1982. Overview of artificial lift systems. Journal of Petroleum Technology, 34(10), pp.2384-2396.

Chen, A.P.A.D.Y. and Chen, Y.M., 2019. Mechanical Reliability of Electrical Submersible Pumps.

Dwyer-Joyce, R.S., Sayles, R.S. and Ioannides, E., 1994. An investigation into the mechanisms of closed three-body abrasive wear. Wear, 175(1-2), pp.133-142.

Gamboa, J. and Prado, M., 2010. Visualization study of the performance breakdown in the two-phase performance of an electrical submersible pump. In Proceedings of the 26th International Pump Users Symposium. Turbomachinery Laboratory, Texas A&M University.

Arabnejad, H., 2015. Development of erosion equations for solid particle and liquid droplet impact. Department of Mechanical Engineering.

Krüger, S., Martin, N. and Dupont, P., 2010. Assessment of wear erosion in pump impellers. In Proceedings of the 26th International Pump Users Symposium. Turbomachinery

Laboratory, Texas A&M University.

Luo, C., Cao, Y., Liu, Y., Zhong, S., Zhao, S., Liu, Z., Liu, Y. and Zheng, D., 2023. Experimental and modeling investigation on gas-liquid two-phase flow in horizontal gas wells. Journal of Energy Resources Technology, 145(1), p.013102.

Liu, Y., Upchurch, E.R., Ozbayoglu, E.M., Baldino, S., Zheng, D. and Wang, J., 2023a, March. Gas Migration Model for Non-Newtonian Fluids under Shut-in Well Conditions. In SPE/IADC Drilling Conference and Exhibition (p. D011S006R005). SPE.

Liu, Y., Upchurch, E.R., Ozbayoglu, E.M., Baldino, S., Wang, J. and Zheng, D., 2023b, March. Design and Calculation of Process Parameters in Bullheading and Pressurized Mud Cap Drilling. In SPE/IADC Drilling Conference and Exhibition (p. D011S006R002). SPE.Marsis, E. and Russell, R., 2013, June. A state-of-the-art computational fluid dynamics simulation for erosion rates prediction in a bottom hole electrical submersible pump. In SPE Canada Heavy Oil Conference (pp. SPE-165452). SPE.

Morrison, G., Carvajal, N., Saleh, R. and Bai, C., 2015. The Measured Impact of Erosion on the Rotodynamic and Performance Characteristics of a Mixed Flow ESP. In Proceedings of the 31st International Pump Users Symposium. Turbomachinery Laboratories, Texas A&M Engineering Experiment Station.

Pirouzpanah, S. and Morrison, G.L., 2014, August. Predictive erosion modeling in an ESP pump. In Fluids Engineering Division Summer Meeting (Vol. 46223, p. V01BT10A004). American Society of Mechanical Engineers.

Rajkumar, Y., Karimi, S. and Shirazi, S.A., 2021, August. Investigation of Particle Size Effects on Solid Particle Erosion of Elbows in Series for Liquid-Solid Flows. In Fluids Engineering Division Summer Meeting (Vol. 85307, p. V003T08A006). American Society of Mechanical

Engineers.

Rajkumar, Y.R., Karimi, S. and Shirazi, S.A., 2022, August. Sand Erosion Measurements and Simulations Under Churn Flow Conditions in Elbows in Series. In Fluids Engineering Division Summer Meeting (Vol. 85840, p. V002T04A018). American Society of Mechanical Engineers.

Rajkumar, Y.R., Shirazi, S.A. and Karimi, S., 2020, July. Particle Size and Concentration Effects on Solid Particle Erosion With PIV Measurements of Particle Velocities. In Fluids Engineering Division Summer Meeting (Vol. 83723, p. V002T04A029). American Society of Mechanical Engineers.

Rajkumar, Y., Shirazi, S.A. and Karimi, S., 2023. Effect of pipe size on erosion measurements and predictions in liquid-dominated multiphase flows for the elbows. Wear, 523, p.204797.

Reges, G., Fontana, M., Costa, E., Lima, A., Ribeiro, M. and Schnitman, L., 2022. A new method for the vibration amplitude assessment of the ESP systems considering the vibration orbit. Journal of Petroleum Science and Engineering, 211, p.110214.

Sedrez, T.A., Rajkumar, Y.R., Shirazi, S.A., Khanouki, H.A. and McLaury, B.S., 2018, July. CFD predictions and experiments of erosion of elbows in series in liquid dominated flows. In Fluids Engineering Division Summer Meeting (Vol. 51579, p. V003T17A001). American Society of Mechanical Engineers.

Shi, Y., Zhu, J., Wang, H., Zhu, H., Zhang, J. and Zhang, H.Q., 2021. Experiments and mechanistic modeling of viscosity effect on a multistage ESP performance under viscous fluid flow. Proceedings of the Institution of Mechanical Engineers, Part A: Journal of Power and Energy, 235(8), pp.1976-1991.

Takacs, G., 2017. Electrical submersible pumps manual: design, operations, and maintenance.

Gulf professional publishing.

Wang, J., Ozbayoglu, E., Baldino, S., Liu, Y. and Zheng, D., 2023, April. Time Series Data Analysis with Recurrent Neural Network for Early Kick Detection. In Offshore Technology Conference (p. D021S020R002). OTC.

Zheng, D., Ozbayoglu, E., Miska, S.Z., Liu, Y. and Li, Y., 2022a, April. Cement sheath fatigue failure prediction by ANN-based model. In Offshore Technology Conference (p. D011S013R009). OTC.

Zheng, D., Ozbayoglu, E.M., Miska, S.Z. and Liu, Y., 2022b, October. Cement sheath fatigue failure prediction by support vector machine based model. In SPE Eastern Regional Meeting. OnePetro.

Zheng, D., Ozbayoglu, E., Baldino, S., Miska, S., Hoamidov, E., and Liu, Y., 2023a. "Cement Sheath Fatigue Failure Prediction Using Machine Learning Method", ARMA-2023-0241, June 2023

Zheng, D., Ozbayoglu, E., Baldino, S., Miska, S., and Liu, Y .,2023b. "The Influence of Casing Eccentricity on Zonal Isolation," ARMA-2023-0159, 28 June 2023bZhou, D. and Sachdeva, R., 2010. Simple model of electric submersible pump in gassy well. Journal of Petroleum Science and Engineering, 70(3-4), pp.204-213.

Zhu, J., Banjar, H., Xia, Z. and Zhang, H.Q., 2016. CFD simulation and experimental study of oil viscosity effect on multi-stage electrical submersible pump (ESP) performance. Journal of Petroleum Science and Engineering, 146, pp.735-745.

Zhu, H., 2019. Experiments, CFD Simulation and Modeling of Sand Wear and Performance Degradation in ESPs. The University of Tulsa.

Zhu, H., Zhu, J., Zhou, Z., Rutter, R., Forsberg, M., Gunter, S. and Zhang, H.Q., 2019, March.

Experimental study of sand erosion in multistage electrical submersible pump ESP: performance degradation, wear and vibration. In International Petroleum Technology Conference (p. D011S007R004). IPTC.

Zhu, H., Lin, Z., Peng, J., Zhang, H.Q., Zhu, J. and Zhang, J., 2020, July. A Numerical Study of Mesh Type, Size, and Near Wall Grid Thickness Effect on Performance and Erosion Simulations in an Electrical Submersible Pump (ESP). In Fluids Engineering Division Summer Meeting (Vol. 83723, p. V002T04A013). American Society of Mechanical Engineers.

Zhu, H., Zhu, J., Rutter, R. and Zhang, H.Q., 2019. A numerical study on erosion model selection and effect of pump type and sand characters in electrical submersible pumps by sandy flow. Journal of Energy Resources Technology, 141(12), p.122004.

APPENDIX A

GEOMETRICAL DIMENSIONS, SEAL CLEARANCES, AND WEIGHT LOSS

A.1 ESP1 erosion results

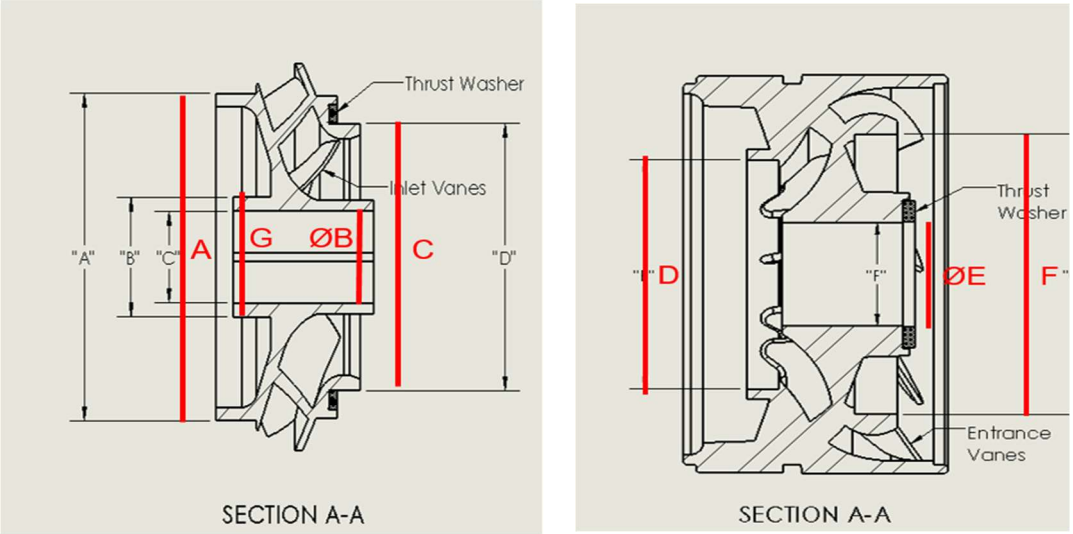

Figure A.1: Impeller and Diffuser geometries of ESP1 stages

Table A.1: Change in impeller balance ring OD (Dimension A) of ESP1

Change in Dimension A										
Stage	0h (in)	8h (in)	0-8h % change	16h (in)	8-16h % change	32h (in)	16-32h % change	64h (in)	32-64h % change	0-64h % change overall
1	2.44975	2.44525	-0.18	2.44125	-0.16	2.43975	-0.06	2.43675	-0.12	-0.53
2	2.44975	2.444	-0.23	2.44125	-0.11	2.43975	-0.06	2.43775	-0.08	-0.49
3	2.4495	2.44125	-0.34	2.44075	-0.02	2.43825	-0.10	2.4355	-0.11	-0.57
4	2.4495	2.44425	-0.21	2.44075	-0.14	2.4385	-0.09	2.43625	-0.09	-0.54
5	2.45	2.4445	-0.22	2.43975	-0.19	2.439	-0.03	2.435	-0.16	-0.61
6	2.45025	2.44625	-0.16	2.44125	-0.20	2.44125	-0.00	2.438	-0.13	-0.50
7	2.45	2.44675	-0.13	2.44025	-0.27	2.43775	-0.10	2.434	-0.15	-0.65
8	2.45	2.4475	-0.10	2.44075	-0.28	2.43975	-0.04	2.4365	-0.13	-0.55
9	2.4495	2.443	-0.27	2.4385	-0.18	2.43625	-0.09	2.4315	-0.19	-0.73
10	2.45	2.4445	-0.22	2.43975	-0.19	2.43775	-0.08	2.435	-0.11	-0.61
11	2.44975	2.444	-0.23	2.4385	-0.23	2.437	-0.06	2.43175	-0.22	-0.73
12	2.45025	2.44525	-0.20	2.43875	-0.27	2.43625	-0.10	2.4325	-0.15	-0.72
13	2.4505	2.4455	-0.20	2.43875	-0.28	2.4375	-0.05	2.4335	-0.16	-0.69
14	2.45025	2.44375	-0.27	2.439	-0.19	2.436	-0.12	2.43225	-0.15	-0.73

Table A.2: Change in impeller hub ID (Dimension B) of ESP1

Change in Dimension B										
Stage	0h (in)	8h (in)	0-8h % change	16h (in)	8-16h % change	32h (in)	16-32h % change	64h (in)	32-64h % change	0-64h % change overall
1	0.72871	0.72886	0.02	0.72896	0.01	0.72931	0.05	0.72896	-0.05	0.03
2	0.72926	0.73326	0.55	0.72881	-0.61	0.72886	0.01	0.73131	0.34	0.28
3	0.73141	0.73146	0.01	0.73126	-0.03	0.73121	-0.01	0.73096	-0.03	-0.06
4	0.73226	0.73146	-0.11	0.73126	-0.03	0.73131	0.01	0.72941	-0.26	-0.39
5	0.73116	0.73066	-0.07	0.73041	-0.03	0.73036	-0.01	0.72991	-0.06	-0.17
6	0.73081	0.72941	-0.19	0.72886	-0.08	0.73041	0.21	0.72886	-0.21	-0.27
7	0.73016	0.73046	0.04	0.73001	-0.06	0.73026	0.03	0.73156	0.18	0.19
8	0.73046	0.72946	-0.14	0.73061	0.16	0.73076	0.02	0.73051	-0.03	0.01
9	0.73291	0.73016	-0.38	0.73041	0.03	0.73021	-0.03	0.73006	-0.02	-0.39
10	0.73011	0.72916	-0.13	0.73261	0.47	0.73046	-0.29	0.72801	-0.34	-0.29
11	0.72991	0.73056	0.09	0.73056	0.00	0.72961	-0.13	0.72936	-0.03	-0.08
12	0.73091	0.73031	-0.08	0.73056	0.03	0.73226	0.23	0.73171	-0.08	0.11
13	0.72901	0.72911	0.01	0.72926	0.02	0.72871	-0.08	0.72836	-0.05	-0.09
14	0.73221	0.73066	-0.21	0.73041	-0.03	0.73021	-0.03	0.72981	-0.05	-0.33

Table A.3: Change in impeller skirt ring OD (Dimension C) of ESP1

Change in Dimension C										
Stage	0h (in)	8h (in)	0-8h % change	16h (in)	8-16h % change	32h (in)	16-32h % change	64h (in)	32-64h % change	0-64h % change overall
1	2	1.9915	-0.43	1.9915	0	1.985	-0.33	1.984	-0.05	-0.8
2	1.9995	1.99275	-0.34	1.9905	-0.11	1.98625	-0.21	1.9835	-0.14	-0.8
3	2.00	1.9915	-0.46	1.98725	-0.21	1.98625	-0.05	1.9825	-0.19	-0.91
4	2	1.992	-0.4	1.9865	-0.28	1.984	-0.13	1.97875	-0.26	-1.06
5	1.999	1.99075	-0.41	1.98725	-0.18	1.9855	-0.09	1.977	-0.43	-1.1
6	1.99925	1.99475	-0.23	1.991	-0.19	1.988	-0.15	1.9855	-0.13	-0.69
7	2.001	1.993	-0.4	1.98775	-0.26	1.98675	-0.05	1.98275	-0.2	-0.91
8	1.99925	1.9925	-0.34	1.988	-0.23	1.9855	-0.13	1.98075	-0.24	-0.93
9	1.9995	1.99075	-0.44	1.98525	-0.28	1.9825	-0.14	1.97675	-0.29	-1.14
10	1.99975	1.98825	-0.58	1.98825	0	1.98525	-0.15	1.9755	-0.49	-1.21
11	1.999	1.99325	-0.29	1.9855	-0.39	1.98275	-0.14	1.9755	-0.37	-1.18
12	2	1.99275	-0.36	1.98725	-0.28	1.987	-0.01	1.97475	-0.62	-1.26
13	2.00025	1.9905	-0.49	1.9865	-0.2	1.987	0.03	1.9805	-0.33	-0.99
14	1.99975	1.99225	-0.38	1.98675	-0.28	1.98675	0	1.9795	-0.36	-1.01

Table A.4: Change in diffuser skirt ring ID (Dimension D) of ESP1

Change in Dimension D										
Stage	0h (in)	8h (in)	0-8h % change	16h (in)	8-16h % change	32h (in)	16-32h % change	64h (in)	32-64h % change	0-64h % change overall
1	2.008	2.01025	0.11	2.0245	0.71	2.02225	-0.11	2.023	0.04	0.75
2	2.0095	2.0105	0.05	2.02175	0.56	2.02275	0.05	2.02275	0	0.66
3	2.0075	2.012	0.22	2.02275	0.53	2.024	0.06	2.0205	-0.17	0.65
4	2.0095	2.01025	0.04	2.02175	0.57	2.02275	0.05	2.02275	0	0.66
5	2.0095	2.01575	0.31	2.02475	0.45	2.026	0.06	2.0265	0.02	0.85
6	2.009	2.012	0.15	2.02225	0.51	2.0235	0.06	2.02625	0.14	0.86
7	2.009	2.0105	0.07	2.0215	0.55	2.02475	0.16	2.0245	-0.01	0.77
8	2.00925	2.0004	-0.44	2.0185	0.9	2.02625	0.38	2.02175	-0.22	0.62
9	2.01	2.00565	-0.22	2.0215	0.79	2.02225	0.04	2.0235	0.06	0.67
10	2.00925	2.01225	0.15	2.021	0.43	2.02375	0.14	2.0205	-0.16	0.56
11	2.00925	2.01325	0.2	2.02375	0.52	2.0235	-0.01	2.02325	-0.01	0.7
12	2.00875	2.01625	0.37	2.0225	0.31	2.0215	-0.05	2.02	-0.07	0.56
13	2.00875	2.00925	0.02	2.007	-0.11	2.00675	-0.01	2.0115	0.24	0.14
14	2.01	2.01925	0.46	2.01975	0.02	2.02575	0.3	2.026	0.01	0.8

Table A.5: Change in diffuser hub ID (Dimension E) of ESP1

Change in Dimension E										
Stage	0h (in)	8h (in)	0-8h % change	16h (in)	8-16h % change	32h (in)	16-32h % change	64h (in)	32-64h % change	0-64h % change overall
1	0.90907	0.90882	-0.03	0.90922	0.04	0.908995	-0.02	0.908995	0	-0.01
2	0.90742	0.90992	0.28	0.91127	0.15	0.912045	0.09	0.913795	0.19	0.7
3	0.907645	0.910295	0.29	0.911445	0.13	0.91232	0.1	0.913095	0.08	0.6
4	0.90897	0.90852	-0.05	0.908745	0.02	0.908295	-0.05	0.908645	0.04	-0.04
5	0.907845	0.91122	0.37	0.91262	0.15	0.913545	0.1	0.91812	0.5	1.13
6	0.90862	0.910695	0.23	0.912245	0.17	0.91252	0.03	0.91582	0.36	0.79
7	0.90852	0.90847	-0.01	0.908445	0	0.908495	0.01	0.908795	0.03	0.03
8	0.907095	0.909745	0.29	0.91247	0.3	0.91347	0.11	0.91657	0.34	1.04
9	0.90747	0.909845	0.26	0.91187	0.22	0.91302	0.13	0.913545	0.06	0.67
10	0.90832	0.908495	0.02	0.908795	0.03	0.90802	-0.09	0.908645	0.07	0.04
11	0.907445	0.90952	0.23	0.91022	0.08	0.91222	0.22	0.91442	0.24	0.77
12	0.908545	0.90847	-0.01	0.908495	0	0.90807	-0.05	0.908645	0.06	0.01
13	0.90737	0.908095	0.08	0.908745	0.07	0.91117	0.27	0.916095	0.54	0.96
14	0.908395	0.910345	0.21	0.91242	0.23	0.913495	0.12	0.914995	0.16	0.73

Table A.6: Change in diffuser balance ring ID (Dimension F) of ESP1

Change in Dimension F										
Stage	0h (in)	8h (in)	0-8h % change	16h (in)	8-16h % change	32h (in)	16-32h % change	64h (in)	32-64h % change	0-64h % change overall
1	2.45925	2.464	0.19	2.46575	0.07	2.465	-0.03	2.47125	0.25	0.49
2	2.45875	2.4665	0.32	2.46475	-0.07	2.4685	0.15	2.4705	0.08	0.48
3	2.4595	2.45775	-0.07	2.463	0.21	2.46675	0.15	2.4645	-0.09	0.2
4	2.4595	2.45525	-0.17	2.4645	0.38	2.46975	0.21	2.47425	0.18	0.6
5	2.45925	2.45475	-0.18	2.46175	0.29	2.4665	0.19	2.46925	0.11	0.41
6	2.46	2.4575	-0.1	2.46325	0.23	2.467	0.15	2.4725	0.22	0.51
7	2.45925	2.46325	0.16	2.46125	-0.08	2.4645	0.13	2.473	0.34	0.56
8	2.45975	2.4515	-0.34	2.46825	0.68	2.465	-0.13	2.47075	0.23	0.45
9	2.4595	2.45725	-0.09	2.46425	0.28	2.466	0.07	2.468	0.08	0.35
10	2.45975	2.45675	-0.12	2.46575	0.37	2.46675	0.04	2.471	0.17	0.46
11	2.4595	2.46275	0.13	2.46475	0.08	2.46875	0.16	2.4695	0.03	0.41
12	2.45975	2.462	0.09	2.46475	0.11	2.4685	0.15	2.47025	0.07	0.43
13	2.4595	2.46425	0.19	2.46525	0.04	2.46925	0.16	2.47	0.03	0.43
14	2.459	2.46	0.04	2.46275	0.11	2.4655	0.11	2.47025	0.19	0.46

Table A.7: Change in impeller hub OD (Dimension G) of ESP1

Change in Dimension G										
Stage	0h (in)	8h (in)	0-8h % change	16h (in)	8-16h % change	32h (in)	16-32h % change	64h (in)	32-64h % change	0-64h % change overall
1	0.89725	0.844	-5.93	0.84025	-0.44	0.84125	0.12	0.8405	-0.09	-6.32
2	0.8975	0.838	-6.63	0.83625	-0.21	0.83925	0.36	0.83925	0	-6.49
3	0.89775	0.8525	-5.04	0.8515	-0.12	0.84975	-0.21	0.84925	-0.06	-5.4
4	0.89775	0.8375	-6.71	0.8355	-0.24	0.83775	0.27	0.828	-1.16	-7.77
5	0.898	0.84	-6.46	0.84025	0.03	0.84375	0.42	0.83325	-1.24	-7.21
6	0.898	0.8385	-6.63	0.84	0.18	0.83875	-0.15	0.83675	-0.24	-6.82
7	0.898	0.84025	-6.43	0.85	1.16	0.84525	-0.56	0.83675	-1.01	-6.82
8	0.89875	0.846	-5.87	0.8525	0.77	0.8465	-0.7	0.84175	-0.56	-6.34
9	0.89825	0.8495	-5.43	0.85275	0.38	0.8485	-0.5	0.8405	-0.94	-6.43
10	0.89875	0.83925	-6.62	0.84475	0.66	0.84025	-0.53	0.83325	-0.83	-7.29
11	0.89825	0.84425	-6.01	0.8425	-0.21	0.8365	-0.71	0.83925	0.33	-6.57
12	0.8985	0.83775	-6.76	0.85025	1.49	0.83875	-1.35	0.834	-0.57	-7.18
13	0.89825	0.84875	-5.51	0.84425	-0.53	0.83975	-0.53	0.84225	0.3	-6.23
14	0.89825	0.8505	-5.32	0.87375	2.73	0.84025	-3.83	0.8485	0.98	-5.54

Table A.8: Change in balance ring clearance of ESP1

Clearance (balance ring)										
Stage	0h (in)	8h (in)	0-8h % change	16h (in)	8-16h % change	32h (in)	16-32h % change	64h (in)	32-64h % change	0-64h % change overall
1	0.01	0.0165	-65.00	0.02225	34.85	0.0285	28.09	0.029	1.75	190.00
2	0.009	0.0225	-150.00	0.0235	4.44	0.02875	22.34	0.03275	13.91	263.89
3	0.0095	0.01875	-97.37	0.0245	30.67	0.02525	3.06	0.0345	36.63	263.16
4	0.01	0.011	-10.00	0.02375	115.91	0.03125	31.58	0.038	21.60	280.00
5	0.00925	0.01025	-10.81	0.022	114.63	0.0275	25.00	0.03425	24.55	270.27
6	0.00975	0.01125	-15.38	0.022	95.56	0.02575	17.05	0.0345	33.98	253.85
7	0.00925	0.0165	-78.38	0.021	27.27	0.02675	27.38	0.039	45.79	321.62
8	0.00975	0.004	58.97	0.0275	587.50	0.02525	-8.18	0.03425	35.64	251.28
9	0.01	0.01425	-42.50	0.02575	80.70	0.02975	15.53	0.0365	22.69	265.00
10	0.00975	0.01225	-25.64	0.026	112.24	0.029	11.54	0.036	24.14	269.23
11	0.00975	0.01875	-92.31	0.02625	40.00	0.03175	20.95	0.03775	18.90	287.18
12	0.0095	0.01675	-76.32	0.026	55.22	0.03225	24.04	0.03775	17.05	297.37
13	0.009	0.01875	-108.33	0.0265	41.33	0.03175	19.81	0.0365	14.96	305.56
14	0.00875	0.01625	-85.71	0.02375	46.15	0.0295	24.21	0.038	28.81	334.29

Table A.9: Change in seal ring clearance of ESP1

Clearance (skirt ring)										
Stage	0h (in)	8h (in)	0-8h % change	16h (in)	8-16h % change	32h (in)	16-32h % change	64h (in)	32-64h % change	0-64h % change overall
1	0.00675	0.0205	-203.70	0.0355	73.17	0.03775	6.34	0.038	0.66	462.96
2	0.01	0.01775	-77.50	0.03125	76.06	0.0365	16.80	0.03925	7.53	292.50
3	0.008	0.01875	-134.38	0.033	76.00	0.03725	12.88	0.039	4.70	387.50
4	0.0095	0.01825	-92.11	0.03525	93.15	0.03875	9.93	0.044	13.55	363.16
5	0.0105	0.025	-138.10	0.0375	50.00	0.0405	8.00	0.0495	22.22	371.43
6	0.00975	0.01725	-76.92	0.03125	81.16	0.0355	13.60	0.04075	14.79	317.95
7	0.008	0.0175	-118.75	0.03375	92.86	0.038	12.59	0.04175	9.87	421.87
8	0.01	0.0079	21.00	0.0305	286.08	0.04075	33.61	0.041	0.61	310.00
9	0.0105	0.0149	-41.90	0.03625	143.29	0.03975	9.66	0.04675	17.61	345.24
10	0.0095	0.024	-152.63	0.03275	36.46	0.0385	17.56	0.045	16.88	373.68
11	0.01025	0.02	-95.12	0.03825	91.25	0.04075	6.54	0.04775	17.18	365.85
12	0.00875	0.0235	-168.57	0.03525	50.00	0.0345	-2.13	0.04525	31.16	417.14
13	0.0085	0.01875	-120.59	0.0205	9.33	0.01975	-3.66	0.031	56.96	264.71
14	0.01025	0.027	-163.41	0.033	22.22	0.039	18.18	0.0465	19.23	353.66

Table A.10: Change in weight of diffusers of ESP1

Change in Weight of Diffusers										
Stage	0h (in)	8h (in)	0-8h % change	16h (in)	8-16h % change	32h (in)	16-32h % change	64h (in)	32-64h % change	0-64h % change overall
1	891	889	-0.22	887	-0.22	884	-0.34	880	-0.45	-1.23
2	902	899	-0.33	898	-0.11	895	-0.33	891	-0.45	-1.22
3	915	912	-0.33	911	-0.11	909	-0.22	905	-0.44	-1.09
4	908	905	-0.33	904	-0.11	902	-0.22	897	-0.55	-1.21
5	882	879	-0.34	877	-0.23	875	-0.23	869	-0.69	-1.47
6	898	894	-0.45	893	-0.11	891	-0.22	886	-0.56	-1.34
7	913	911	-0.22	910	-0.11	907	-0.33	900	-0.77	-1.42
8	904	901	-0.33	899	-0.22	897	-0.22	893	-0.45	-1.22
9	903	900	-0.33	898	-0.22	896	-0.22	892	-0.45	-1.22
10	913	910	-0.33	909	-0.11	906	-0.33	899	-0.77	-1.53
11	895	892	-0.34	891	-0.11	888	-0.34	884	-0.45	-1.23
12	913	911	-0.22	909	-0.22	906	-0.33	901	-0.55	-1.31
13	907	906	-0.11	905	-0.11	903	-0.22	899	-0.44	-0.88
14	910	907	-0.33	905	-0.22	903	-0.22	898	-0.55	-1.32

Table A.11: Change in weight of impellers of ESP1

Change in Weight of Impellers										
Stage	0h (in)	8h (in)	0-8h % change	16h (in)	8-16h % change	32h (in)	16-32h % change	64h (in)	32-64h % change	0-64h % change overall
1	220	217	-1.36	216	-0.46	214	-0.93	211	-1.4	-4.09
2	222	219	-1.35	219	0	216	-1.37	215	-0.46	-3.15
3	224	222	-0.89	220	-0.9	219	-0.45	217	-0.91	-3.13
4	215	213	-0.93	212	-0.47	210	-0.94	208	-0.95	-3.26
5	210	208	-0.95	207	-0.48	205	-0.97	201	-1.95	-4.29
6	217	215	-0.92	214	-0.47	212	-0.93	209	-1.42	-3.69
7	214	212	-0.93	211	-0.47	209	-0.95	206	-1.44	-3.74
8	223	221	-0.9	220	-0.45	218	-0.91	215	-1.38	-3.59
9	216	214	-0.93	212	-0.93	210	-0.94	207	-1.43	-4.17
10	218	215	-1.38	214	-0.47	212	-0.93	209	-1.42	-4.13
11	209	207	-0.96	205	-0.97	203	-0.98	200	-1.48	-4.31
12	216	213	-1.39	212	-0.47	210	-0.94	207	-1.43	-4.17
13	221	219	-0.9	218	-0.46	216	-0.92	213	-1.39	-3.62
14	213	211	-0.94	209	-0.95	207	-0.96	204	-1.45	-4.23

Table A.12: Change in diameter of balance holes of ESP1

Change in diameter of balance holes										
Stage	0h (in)	8h (in)	0-8h % change	16h (in)	8-16h % change	32h (in)	16-32h % change	64h (in)	32-64h % change	0-64h % change overall
1	0.128	0.128	0.00	0.129	0.78	0.129	0.00	0.133	3.10	3.91
2	0.128	0.128	0.00	0.13	1.56	0.13	0.00	0.131	0.77	2.34
3	0.126	0.126	0.00	0.127	0.79	0.127	0.00	0.127	0.00	0.79
4	0.128	0.127	-0.78	0.128	0.79	0.128	0.00	0.128	0.00	0.00
5	0.128	0.128	0.00	0.13	1.56	0.13	0.00	0.131	0.77	2.34
6	0.129	0.127	-1.55	0.13	2.36	0.13	0.00	0.131	0.77	1.55
7	0.128	0.128	0.00	0.128	0.00	0.128	0.00	0.128	0.00	0.00
8	0.13	0.13	0.00	0.13	0.00	0.13	0.00	0.131	0.77	0.77
9	0.13	0.13	0.00	0.13	0.00	0.13	0.00	0.13	0.00	0.00
10	0.128	0.128	0.00	0.128	0.00	0.128	0.00	0.128	0.00	0.00
11	0.132	0.132	0.00	0.13	-1.52	0.131	0.77	0.132	0.76	0.00
12	0.126	0.126	0.00	0.126	0.00	0.126	0.00	0.126	0.00	0.00
13	0.127	0.127	0.00	0.128	0.79	0.128	0.00	0.129	0.78	1.57
14	0.127	0.127	0.00	0.128	0.79	0.128	0.00	0.129	0.78	1.57

A.2 ESP2 erosion results

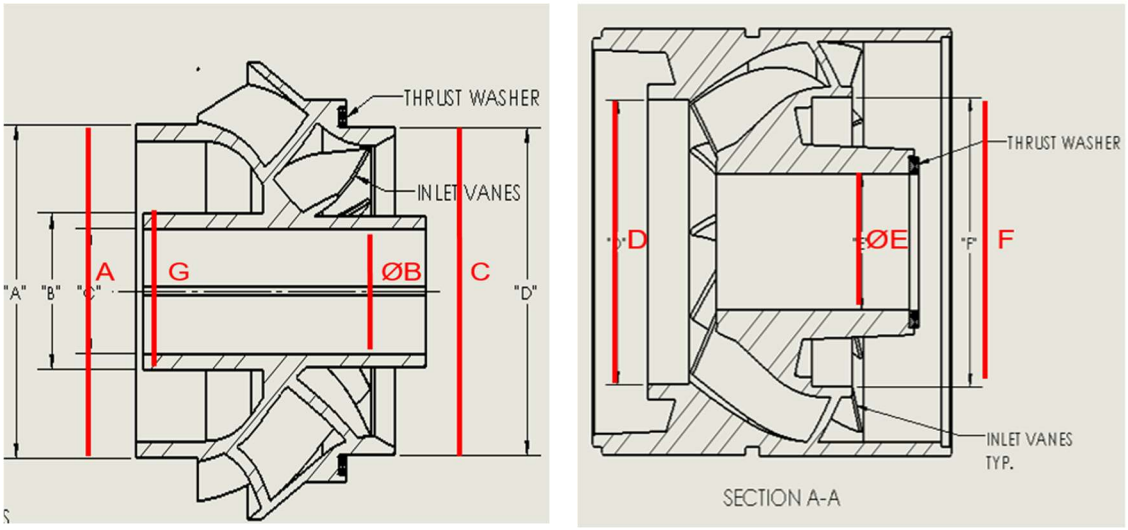

Figure A.2: Impeller and Diffuser geometries of ESP2 stages

Table A.13: Change in impeller balance ring OD (Dimension A) of ESP2

Change in Dimension A										
Stage	0h (in)	8h (in)	0-8h % change	16h (in)	8-16h % change	32h (in)	16-32h % change	64h (in)	32-64h % change	0-64h % change overall
1	2.35	2.3465	-0.15	2.345	-0.06	2.342	-0.13	2.34025	-0.07	-0.41
2	2.34925	2.34675	-0.11	2.34525	-0.06	2.34325	-0.09	2.34325	0	-0.26
3	2.35025	2.348	-0.1	2.34575	-0.1	2.3445	-0.05	2.3425	-0.09	-0.33
4	2.35	2.34675	-0.14	2.3465	-0.01	2.34375	-0.12	2.34225	-0.06	-0.33
5	2.3505	2.34825	-0.1	2.34625	-0.09	2.34425	-0.09	2.3425	-0.07	-0.34
6	2.35	2.34725	-0.12	2.34575	-0.06	2.34375	-0.09	2.3435	-0.01	-0.28
7	2.3505	2.34925	-0.05	2.34575	-0.15	2.3445	-0.05	2.34475	0.01	-0.24
8	2.34875	2.34875	0	2.3455	-0.14	2.344	-0.06	2.3395	-0.19	-0.39

Table A.14: Change in impeller hub ID (Dimension B) of ESP2

Change in Dimension B										
Stage	0h (in)	8h (in)	0-8h % change	16h (in)	8-16h % change	32h (in)	16-32h % change	64h (in)	32-64h % change	0-64h % change overall
1	0.87722	0.87737	0.02	0.8755	-0.21	0.87475	-0.09	0.87575	0.11	-0.17
2	0.87787	0.87802	0.02	0.87675	-0.14	0.875	-0.2	0.8765	0.17	-0.16
3	0.87982	0.87727	-0.29	0.8755	-0.2	0.87475	-0.09	0.875	0.03	-0.55
4	0.87767	0.87772	0.01	0.873	-0.54	0.87625	0.37	0.8775	0.14	-0.02
5	0.88022	0.87732	-0.33	0.87375	-0.41	0.87525	0.17	0.8775	0.26	-0.31
6	0.87777	0.87807	0.03	0.873	-0.58	0.876	0.34	0.87625	0.03	-0.17
7	0.87752	0.87757	0.01	0.8745	-0.35	0.87525	0.09	0.87675	0.17	-0.09
8	0.87812	0.87807	-0.01	0.875	-0.35	0.876	0.11	0.8765	0.06	-0.18

Table A.15: Change in impeller skirt ring OD (Dimension C) of ESP2

Change in Dimension C										
Stage	0h (in)	8h (in)	0-8h % change	16h (in)	8-16h % change	32h (in)	16-32h % change	64h (in)	32-64h % change	0-64h % change overall
1	2.30975	2.30525	-0.19	2.3025	-0.12	2.29975	-0.12	2.2985	-0.05	-0.49
2	2.31025	2.3045	-0.25	2.30325	-0.05	2.3	-0.14	2.299	-0.04	-0.49
3	2.31025	2.30575	-0.19	2.304	-0.08	2.3015	-0.11	2.2995	-0.09	-0.47
4	2.3105	2.30375	-0.29	2.3025	-0.05	2.30025	-0.1	2.29825	-0.09	-0.53
5	2.31025	2.30575	-0.19	2.30425	-0.07	2.30225	-0.09	2.29975	-0.11	-0.45
6	2.31075	2.30525	-0.24	2.30425	-0.04	2.30125	-0.13	2.29925	-0.09	-0.5
7	2.31025	2.3055	-0.21	2.30325	-0.1	2.30125	-0.09	2.299	-0.1	-0.49
8	2.3105	2.30475	-0.25	2.30325	-0.07	2.3025	-0.03	2.298	-0.2	-0.54

Table A.16: Change in diffuser skirt ring ID (Dimension D) of ESP2

Change in Dimension D										
Stage	0h (in)	8h (in)	0-8h % change	16h (in)	8-16h % change	32h (in)	16-32h % change	64h (in)	32-64h % change	0-64h % change overall
1	2.30525	2.3145	0.4	2.31975	0.23	2.321	0.05	2.33325	0.53	1.21
2	2.30725	2.3205	0.57	2.32225	0.08	2.33	0.33	2.3335	0.15	1.14
3	2.314	2.322	0.35	2.321	-0.04	2.327	0.26	2.32825	0.05	0.62
4	2.31425	2.32625	0.52	2.329	0.12	2.329	0	2.3315	0.11	0.75
5	2.31675	2.32425	0.32	2.32825	0.17	2.32925	0.04	2.33325	0.17	0.71
6	2.31875	2.32475	0.26	2.3255	0.03	2.32925	0.16	2.3345	0.23	0.68
7	2.31325	2.32225	0.39	2.326	0.16	2.3285	0.11	2.32975	0.05	0.71
8	2.3165	2.31875	0.1	2.318	-0.03	2.3155	-0.11	2.3175	0.09	0.04

Table A.17: Change in diffuser hub ID (Dimension E) of ESP2

Change in Dimension E										
Stage	0h (in)	8h (in)	0-8h % change	16h (in)	8-16h % change	32h (in)	16-32h % change	64h (in)	32-64h % change	0-64h % change overall
1	1.11003	1.11268	0.24	1.11225	-0.04	1.115	0.25	1.1205	0.49	0.94
2	1.110755	1.11268	0.17	1.115	0.21	1.11825	0.29	1.1205	0.20	0.88
3	1.11028	1.112355	0.19	1.115	0.24	1.1185	0.31	1.122	0.31	1.06
4	1.109505	1.11153	0.18	1.11	-0.14	1.113	0.27	1.1185	0.49	0.81
5	1.110505	1.112355	0.17	1.1155	0.28	1.118	0.22	1.121	0.27	0.95
6	1.11038	1.11243	0.18	1.1145	0.19	1.11625	0.16	1.122	0.52	1.05
7	1.109405	1.11243	0.27	1.113	0.05	1.11525	0.20	1.12	0.43	0.96
8	1.11043	1.112755	0.21	1.11425	0.13	1.1175	0.29	1.124	0.58	1.22

Table A.18: Change in diffuser balance ring ID (Dimension F) of ESP2

Change in Dimension F										
Stage	0h (in)	8h (in)	0-8h % change	16h (in)	8-16h % change	32h (in)	16-32h % change	64h (in)	32-64h % change	0-64h % change overall
1	2.35695	2.361	0.17	2.36375	0.12	2.37025	0.27	2.372	0.07	0.64
2	2.35575	2.36375	0.34	2.36625	0.11	2.36975	0.15	2.365	-0.20	0.39
3	2.3563	2.364	0.33	2.3645	0.02	2.36775	0.14	2.37	0.10	0.58
4	2.358	2.36275	0.20	2.364	0.05	2.36925	0.22	2.37475	0.23	0.71
5	2.3526	2.36125	0.37	2.3655	0.18	2.36975	0.18	2.37075	0.04	0.77
6	2.3565	2.36475	0.35	2.3655	0.03	2.36775	0.10	2.3735	0.24	0.72
7	2.35535	2.3615	0.26	2.36575	0.18	2.3705	0.20	2.37125	0.03	0.68
8	2.3556	2.36175	0.26	2.3635	0.07	2.36875	0.22	2.3715	0.12	0.67

Table A.19: Change in impeller hub OD (Dimension G) of ESP2

Change in Dimension G										
Stage	0h (in)	8h (in)	0-8h % change	16h (in)	8-16h % change	32h (in)	16-32h % change	64h (in)	32-64h % change	0-64h % change overall
1	1.1	1.0995	-0.05	1.0925	-0.64	1.0825	-0.92	1.075	-0.69	-2.27
2	1.099	1.09925	0.02	1.0725	-2.43	1.07	-0.23	1.0475	-2.1	-4.69
3	1.09975	1.101	0.11	1.1025	0.14	1.0875	-1.36	1.055	-2.99	-4.07
4	1.0985	1.0998	0.12	1.0725	-2.48	1.025	-4.43	1.005	-1.95	-8.51
5	1.098	1.0875	-0.96	1.0975	0.92	1.06	-3.42	1.0425	-1.65	-5.05
6	1.10075	1.085	-1.43	1.0675	-1.61	1.0375	-2.81	1.0575	1.93	-3.93
7	1.09875	1.0875	-1.02	1.09575	0.76	1.065	-2.81	1.06	-0.47	-3.53
8	1.10075	1.0875	-1.2	1.09	0.23	1.0575	-2.98	1.0625	0.47	-3.47

Table A.20: Change in balance ring clearance of ESP2

Clearance (balance ring)										
Stage	0h (in)	8h (in)	0-8h % change	16h (in)	8-16h % change	32h (in)	16-32h % change	64h (in)	32-64h % change	0-64h % change overall
1	0.00695	0.0145	-108.63	0.01875	-29.31	0.02825	-50.67	0.03175	-12.39	-356.83
2	0.0065	0.017	-161.54	0.021	-23.53	0.0265	-26.19	0.02175	17.92	-234.62
3	0.00605	0.016	-164.46	0.01875	-17.19	0.02325	-24.00	0.0275	-18.28	-354.55
4	0.008	0.016	-100.00	0.0175	-9.38	0.0255	-45.71	0.0325	-27.45	-306.25
5	0.0021	0.013	-519.05	0.01925	-48.08	0.0255	-32.47	0.02825	-10.78	-1245.24
6	0.0065	0.0175	-169.23	0.01975	-12.86	0.024	-21.52	0.03	-25.00	-361.54
7	0.00485	0.01225	-152.58	0.02	-63.27	0.026	-30.00	0.0265	-1.92	-446.39
8	0.00685	0.013	-89.78	0.018	-38.46	0.02475	-37.50	0.032	-29.29	-367.15

Table A.21: Change in skirt ring clearance of ESP2

Clearance (skirt ring)										
Stage	0h (in)	8h (in)	0-8h % change	16h (in)	8-16h % change	32h (in)	16-32h % change	64h (in)	32-64h % change	0-64h % change overall
1	0.00025	0.00925	-3600.00	0.01725	-86.49	0.02125	-23.19	0.03475	-63.53	-13800.00
2	0.00475	0.016	-236.84	0.019	-18.75	0.03	-57.89	0.0345	-15.00	-626.32
3	0.00375	0.01625	-333.33	0.017	-4.62	0.0255	-50.00	0.02875	-12.75	-666.67
4	0.00375	0.0225	-500.00	0.0265	-17.78	0.02875	-8.49	0.03325	-15.65	-786.67
5	0.0065	0.0185	-184.62	0.024	-29.73	0.027	-12.50	0.0335	-24.07	-415.38
6	0.008	0.0195	-143.75	0.02125	-8.97	0.028	-31.76	0.03525	-25.89	-340.63
7	0.003	0.01675	-458.33	0.02275	-35.82	0.02725	-19.78	0.03075	-12.84	-925.00
8	0.006	0.014	-133.33	0.01475	-5.36	0.013	11.86	0.0195	-50.00	-225.00

Table A.22: Change in weight of diffusers of ESP2

Weight Loss of Diffusers										
Stage	0h (in)	8h (in)	0-8h % change	16h (in)	8-16h % change	32h (in)	16-32h % change	64h (in)	32-64h % change	0-64h % change overall
1	1317	1312	-0.38	1310	-0.15	1302	-0.61	1288	-1.08	-2.20
2	1319	1314	-0.38	1311	-0.23	1304	-0.53	1291	-1.00	-2.12
3	1320	1315	-0.38	1311	-0.30	1305	-0.46	1292	-1.00	-2.12
4	1303	1299	-0.31	1295	-0.31	1287	-0.62	1272	-1.17	-2.38
5	1320	1316	-0.30	1311	-0.38	1303	-0.61	1288	-1.15	-2.42
6	1320	1316	-0.30	1312	-0.30	1305	-0.53	1292	-1.00	-2.12
7	1323	1318	-0.38	1313	-0.38	1305	-0.61	1290	-1.15	-2.49
8	1319	1315	-0.30	1311	-0.30	1305	-0.46	1294	-0.84	-1.90

Table A.23: Change in weight of impellers of ESP2

Weight Loss of Impellers										
Stage	0h (in)	8h (in)	0-8h % change	16h (in)	8-16h % change	32h (in)	16-32h % change	64h (in)	32-64h % change	0-64h % change overall
1	456	454	-0.44	453	-0.22	448	-1.10	443	-1.12	-2.85
2	453	450	-0.66	448	-0.44	443	-1.12	437	-1.35	-3.53
3	455	453	-0.44	451	-0.44	447	-0.89	441	-1.34	-3.08
4	452	449	-0.66	447	-0.45	443	-0.89	437	-1.35	-3.32
5	458	455	-0.66	452	-0.66	449	-0.66	443	-1.34	-3.28
6	460	458	-0.43	455	-0.66	451	-0.88	446	-1.11	-3.04
7	454	453	-0.22	450	-0.66	446	-0.89	442	-0.90	-2.64
8	449	447	-0.45	444	-0.67	442	-0.45	432	-2.26	-3.79

Table A.24: Change in diameter of balance holes of ESP2

Change in diameter of balance holes										
Stage	0h (in)	8h (in)	0-8h % change	16h (in)	8-16h % change	32h (in)	16-32h % change	64h (in)	32-64h % change	0-64h % change overall
1	0.128	0.129	0.78	0.129	0.00	0.129	0.00	0.129	0.00	0.78
2	0.128	0.128	0.00	0.129	0.78	0.128	-0.78	0.13	1.56	1.56
3	0.128	0.129	0.78	0.129	0.00	0.128	-0.78	0.13	1.56	1.56
4	0.128	0.128	0.00	0.129	0.78	0.129	0.00	0.129	0.00	0.78
5	0.128	0.129	0.78	0.129	0.00	0.129	0.00	0.129	0.00	0.78
6	0.128	0.128	0.00	0.129	0.78	0.129	0.00	0.13	0.78	1.56
7	0.128	0.128	0.00	0.128	0.00	0.128	0.00	0.129	0.78	0.78
8	0.128	0.128	0.00	0.129	0.78	0.129	0.00	0.129	0.00	0.78

APPENDIX B

DETERIORATION OF PERFORMANCE PARAMETERS

B.1 ESP1 performance data (calibrated to 3600 RPM)

Table B.1: Change in head of ESP1

Change in head (ft.)										
Flow rate (BPD)	0h	8h	0-8h change (%)	16h	8-16h change (%)	32h	16-32h change (%)	64h	32-64h change (%)	Overall change (%)
300	37.21	33.25	-10.63	32.28	-2.91	-	-	-	-	-
1000	32.47	29.74	-8.4	29.77	0.11	27.84	-6.51	25.82	-3.27	-17.07
1700	25.96	23.75	-8.54	24.04	1.25	23.17	-3.63	21.84	-5.74	-15.88
2500	14.50	11.14	-23.2	11.67	4.78	11.19	-4.12	11.23	0.33	-22.59
2800	8.07	4.80	-40.52	5.34	11.16	5.16	-3.38	5.24	1.58	-35.11
3000	2.39	1.69	-29.32	1.60	-5.17	1.64	2.57	1.62	-1.41	-32.22

Table B.2: Change in efficiency of ESP1

Change in efficiency (%)										
Flow rate (BPD)	0h	8h	0-8h change (%)	16h	8-16h change (%)	32h	16-32h change (%)	64h	32-64h change (%)	Overall change (%)
300	20.11	18.52	-7.89	29.36	58.51	-	-	-	-	-
1000	52.11	46.80	-10.18	46.18	-1.33	52.81	14.34	47.84	-9.41	-8.20
1700	60.67	55.20	-9.02	55.37	0.32	57.14	3.2	50.14	-12.25	-17.35
2500	48.03	38.93	-18.95	40.99	5.31	42.04	2.55	38.83	-7.62	-19.14
2800	30.62	19.84	-35.21	22.27	12.26	23.19	4.1	21.60	-6.84	-29.47
3000	9.97	7.49	-24.87	7.39	-1.29	8.15	10.28	7.47	-8.43	-25.11

Table B.3: Change in horsepower of ESP1

Change in horsepower (HP)										
Flow rate (BPD)	0h	8h	0-8h change (%)	16h	8-16h change (%)	32h	16-32h change (%)	64h	32-64h change (%)	Overall change (%)
300	5.49	5.62	2.34	6.13	9.16	-	-	-	-	-
1000	6.21	6.65	7	6.67	0.34	7.04	5.6	7.06	0.21	13.62
1700	7.24	7.62	5.33	7.70	0.98	7.67	-0.3	7.73	0.78	6.88
2500	7.55	7.40	-2.03	7.42	0.31	7.46	0.44	7.54	1.1	-0.20
2800	7.34	7.02	-4.38	7.03	0.08	7.03	0.08	7.10	0.99	-3.28
3000	7.16	6.85	-4.42	6.74	-1.48	6.74	-0.12	6.76	0.33	-5.64

Table B.4: Change in torque of ESP1

Change in torque (lb-in)										
Flow rate (BPD)	0h	8h	0-8h change (%)	16h	8-16h change (%)	32h	16-32h change (%)	64h	32-64h change (%)	Overall change (%)
300	98.17	96.99	-1.2	105.69	8.96	-	-	-	-	-
1000	111.17	115.14	3.57	115.69	0.48	121.98	5.44	122.25	0.22	9.97
1700	129.84	132.55	2.09	133.19	0.48	132.98	-0.16	133.65	0.5	2.94
2500	134.84	129.11	-4.25	128.69	-0.32	129.08	0.31	130.55	1.14	-3.18
2800	131.67	122.41	-7.03	121.69	-0.59	121.48	-0.17	123.05	1.29	-6.55
3000	129.00	119.39	-7.46	116.69	-2.26	116.68	-0.01	117.05	0.32	-9.27

B.2 ESP2 performance data (calibrated to 3600 RPM)

Table B.5: Change in head of ESP2

Change in head (ft.)										
Flow rate (BPD)	0h	8h	0-8h change (%)	16h	8-16h change (%)	32h	16-32h change (%)	64h	32-64h change (%)	Overall change (%)
7500	17.57	17.42	-0.89	18.05	3.63	17.76	-1.61	15.57	-12.31	-11.38
6000	24.83	23.79	-4.17	23.58	-0.9	22.81	-3.26	21.83	-4.28	-12.07
4500	28.50	26.59	-6.69	25.77	-3.09	25.51	-0.99	24.23	-5.02	-14.96
3000	29.51	28.96	-1.86	28.58	-1.3	28.98	1.41	28.35	-2.18	-3.91
1500	39.29	36.02	-8.32	36.11	0.23	34.83	-3.53	33.76	-3.08	-14.08
500	38.53	36.88	-4.27	35.97	-2.47	35.33	-1.78	34.81	-1.47	-9.64

Table B.6: Change in efficiency of ESP2

Change in efficiency (%)										
Flow rate (BPD)	0h	8h	0-8h change (%)	16h	8-16h change (%)	32h	16-32h change (%)	64h	32-64h change (%)	Overall change (%)
7500	53.23	53.00	-0.41	56.47	6.54	56.56	0.15	50.97	-9.88	-4.25
6000	63.69	61.40	-3.6	61.81	0.67	61.95	0.22	59.38	-4.15	-6.78
4500	62.46	59.73	-4.38	58.70	-1.72	59.72	1.75	56.34	-5.66	-9.80
3000	49.94	49.15	-1.58	46.88	-4.62	49.62	5.84	48.49	-2.28	-2.91
1500	32.45	31.83	-1.91	30.68	-3.63	30.42	-0.84	28.28	-7.03	-12.85
500	12.33	12.55	1.81	10.09	-19.61	10.76	6.61	11.73	9.02	-4.87

Table B.7: Change in horsepower of ESP2

Change in horsepower (HP)										
Flow rate (BPD)	0h	8h	0-8h change (%)	16h	8-16h change (%)	32h	16-32h change (%)	64h	32-64h change (%)	Overall change (%)
7500	14.86	14.78	-0.56	14.54	-1.62	14.13	-2.83	13.74	-2.72	-7.53
6000	14.08	13.94	-1.02	13.73	-1.49	13.27	-3.31	13.23	-0.35	-6.05
4500	12.43	12.02	-3.27	11.91	-0.98	11.51	-3.34	11.51	0.05	-7.37
3000	10.62	10.60	-0.17	10.70	0.92	10.46	-2.19	10.54	0.7	-0.77
1500	10.86	10.23	-5.79	10.63	3.93	10.35	-2.7	10.34	-0.09	-4.82
500	9.30	8.90	-4.32	9.50	6.8	9.30	-2.11	9.11	-2.03	-2.00

Table B.8: Change in torque of ESP2

Change in torque (lb-in)										
Flow rate (BPD)	0h	8h	0-8h change (%)	16h	8-16h change (%)	32h	16-32h change (%)	64h	32-64h change (%)	Overall change (%)
7500	256.74	255.46	-0.5	249.42	-2.36	244.15	-2.12	237.54	-2.7	-7.48
6000	242.74	240.96	-0.74	237.26	-1.54	229.15	-3.42	228.67	-0.21	-5.80
4500	213.44	207.81	-2.64	205.76	-0.99	198.98	-3.29	199.04	0.03	-6.75
3000	183.54	183.08	-0.25	184.92	1	180.81	-2.22	182.04	0.68	-0.82
1500	187.74	176.83	-5.81	183.92	4.01	178.98	-2.69	178.79	-0.1	-4.77
500	160.84	153.46	-4.59	164.26	7.04	160.98	-1.99	157.54	-2.13	-2.05

APPENDIX C

CONTINUOUS MONITORING DATA

The continuous monitoring data for each 2-hour erosion test, after which sand was replaced, are plotted in this section. As seen, head, efficiency and horsepower changed smoothly in the test.

C.1 ESP1 continuous monitoring data

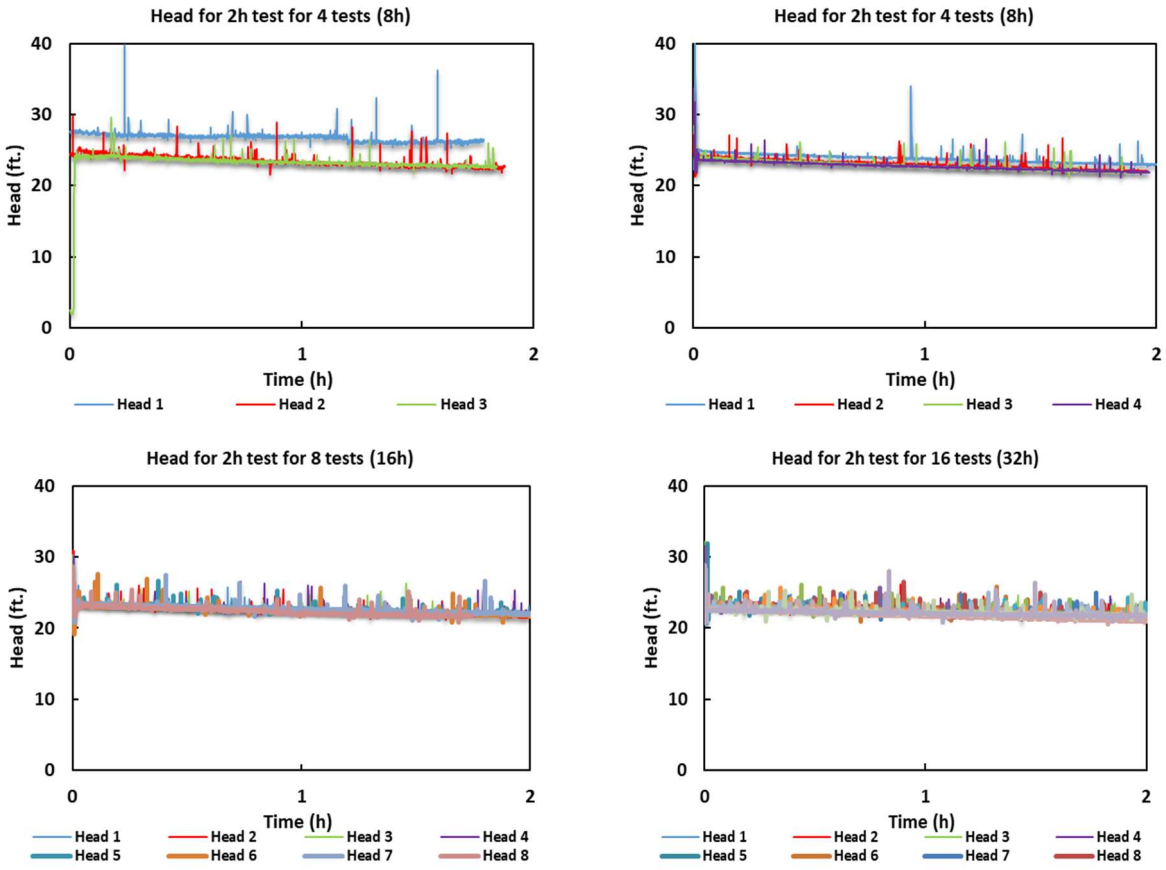

Figure C.1: Monitoring head at ESP1 BEP for various testing periods

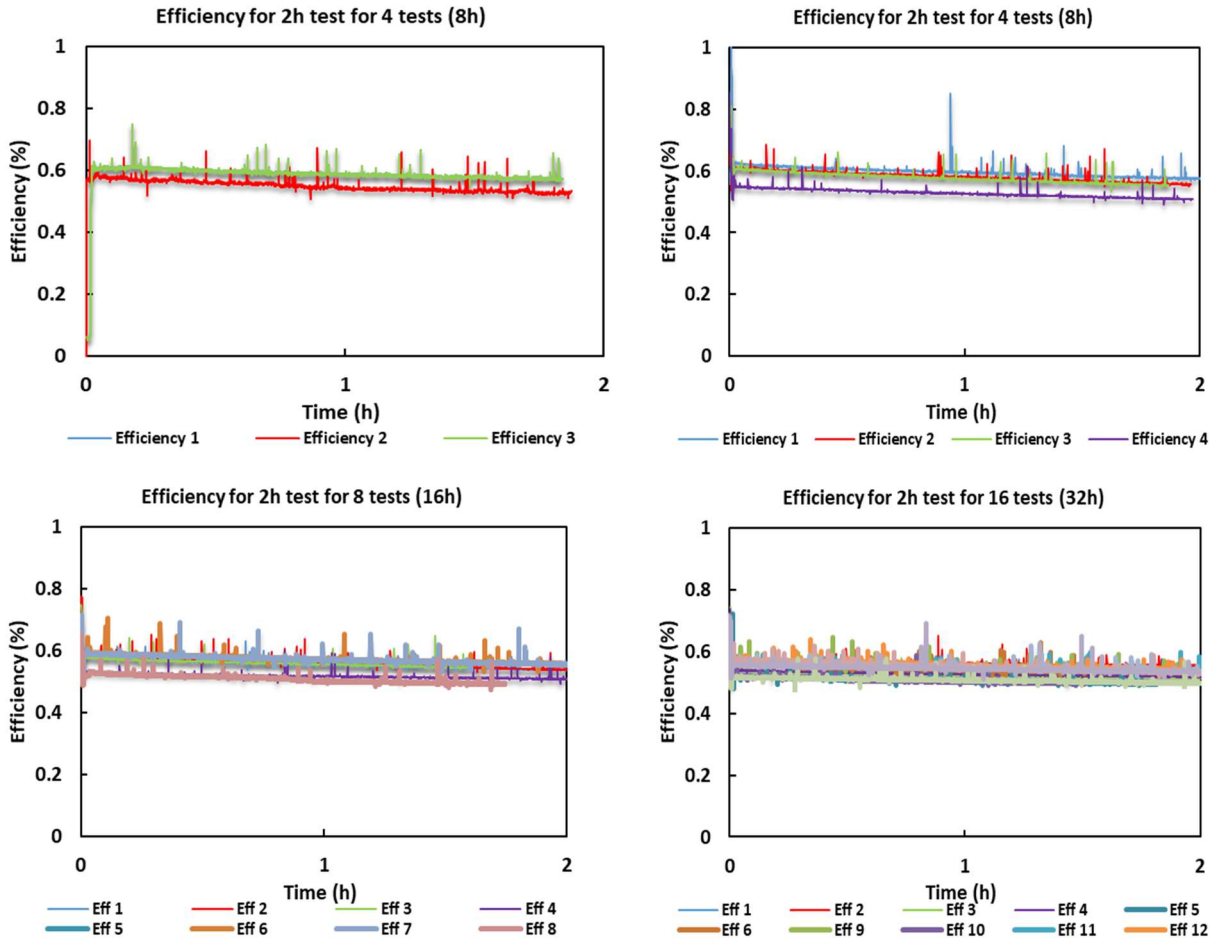

Figure C.2: Monitoring efficiency at ESP1 BEP for various testing periods

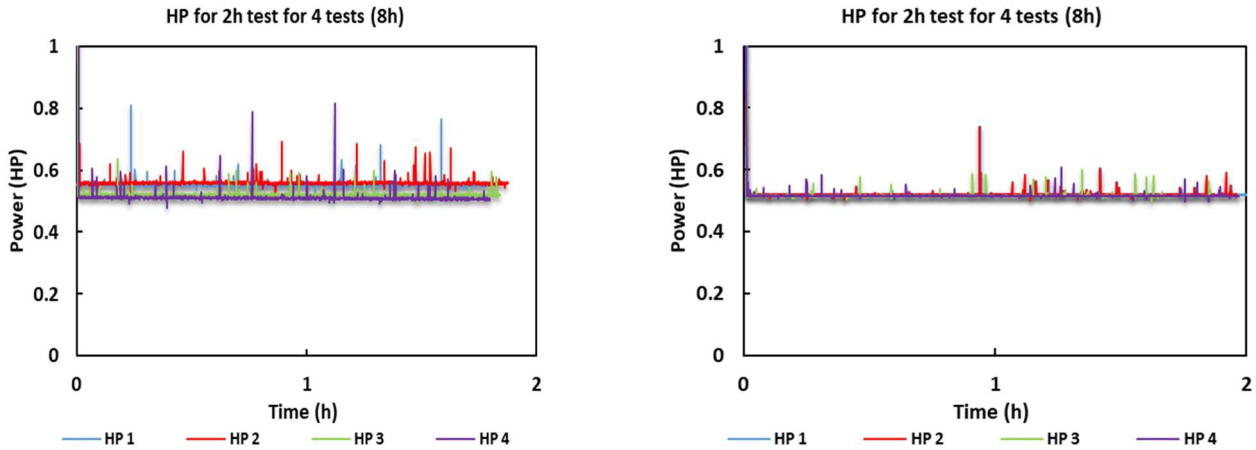

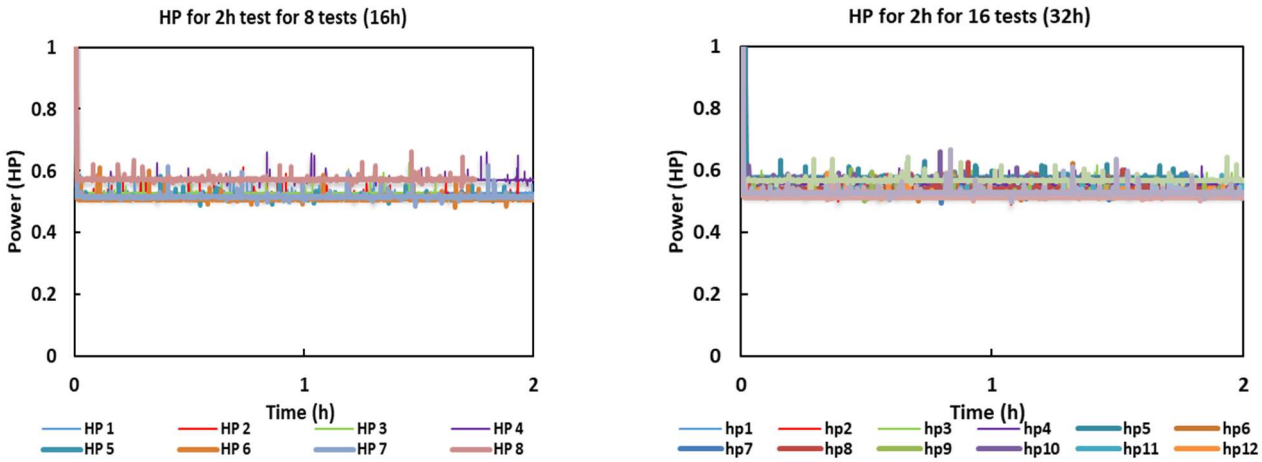

Figure C.3: Monitoring horsepower at ESP1 BEP for various testing periods

C.2 ESP2 continuous monitoring data

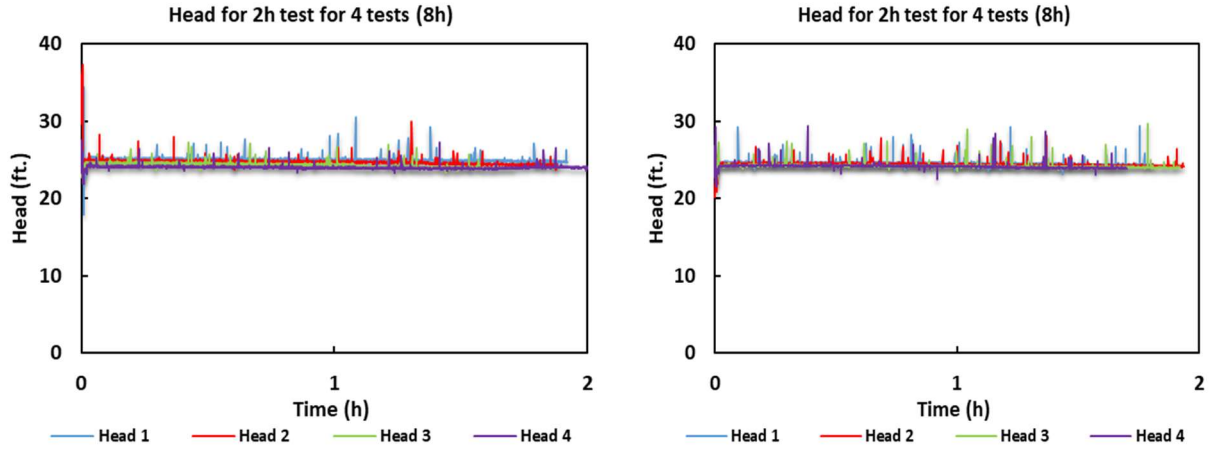

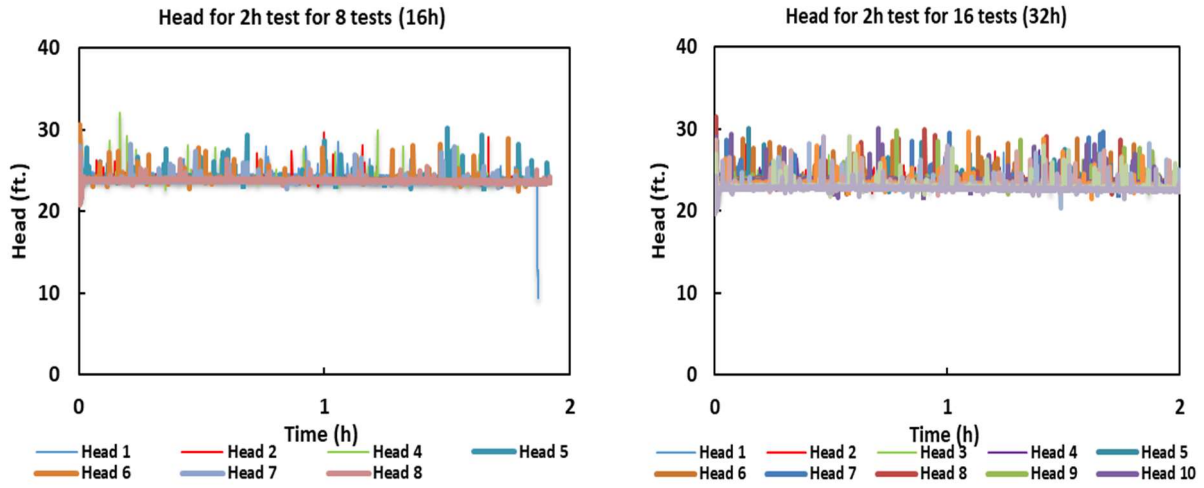

Figure C.4: Monitoring head at ESP2 BEP for various testing periods

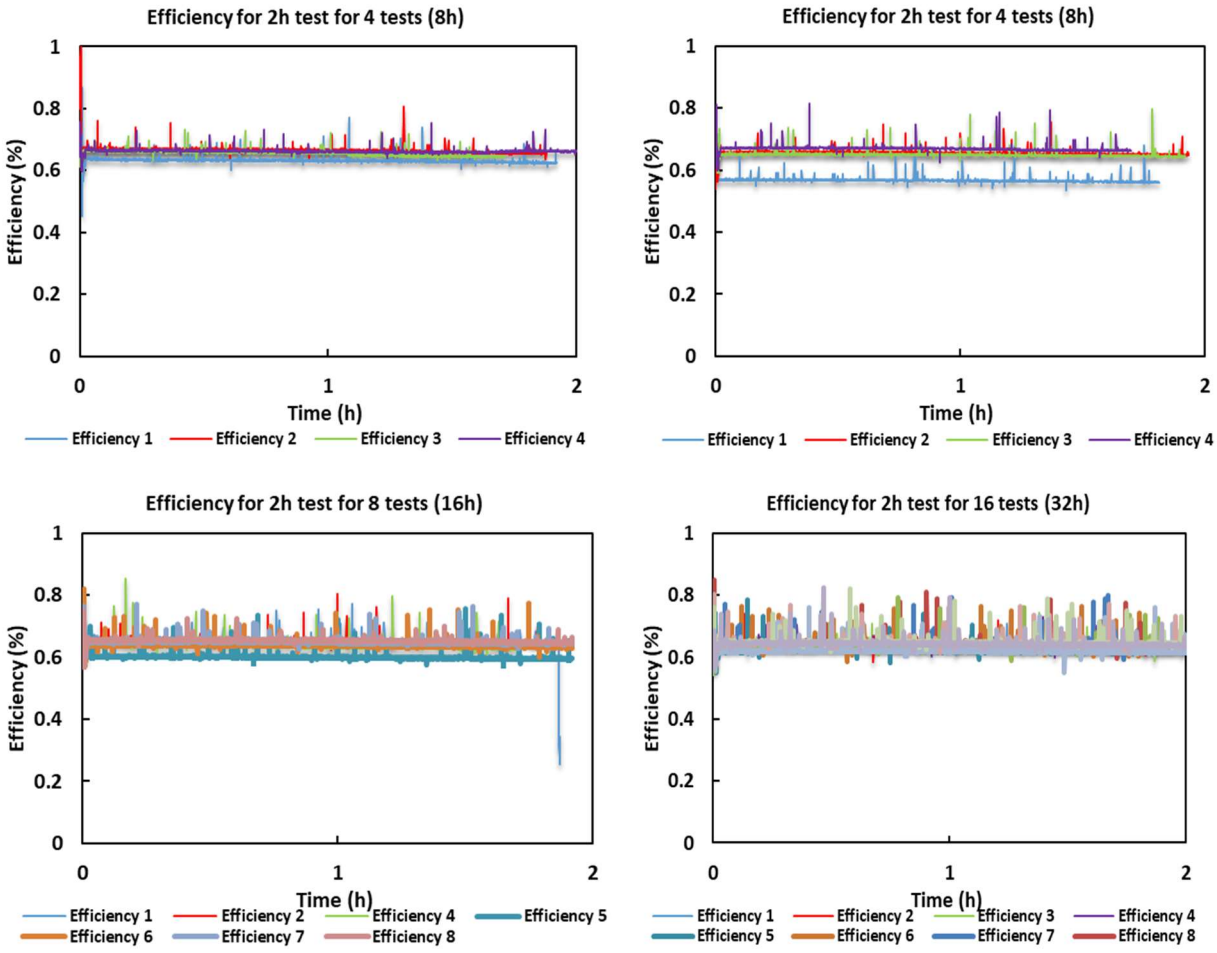

Figure C.5: Monitoring efficiency at ESP2 BEP for various testing periods

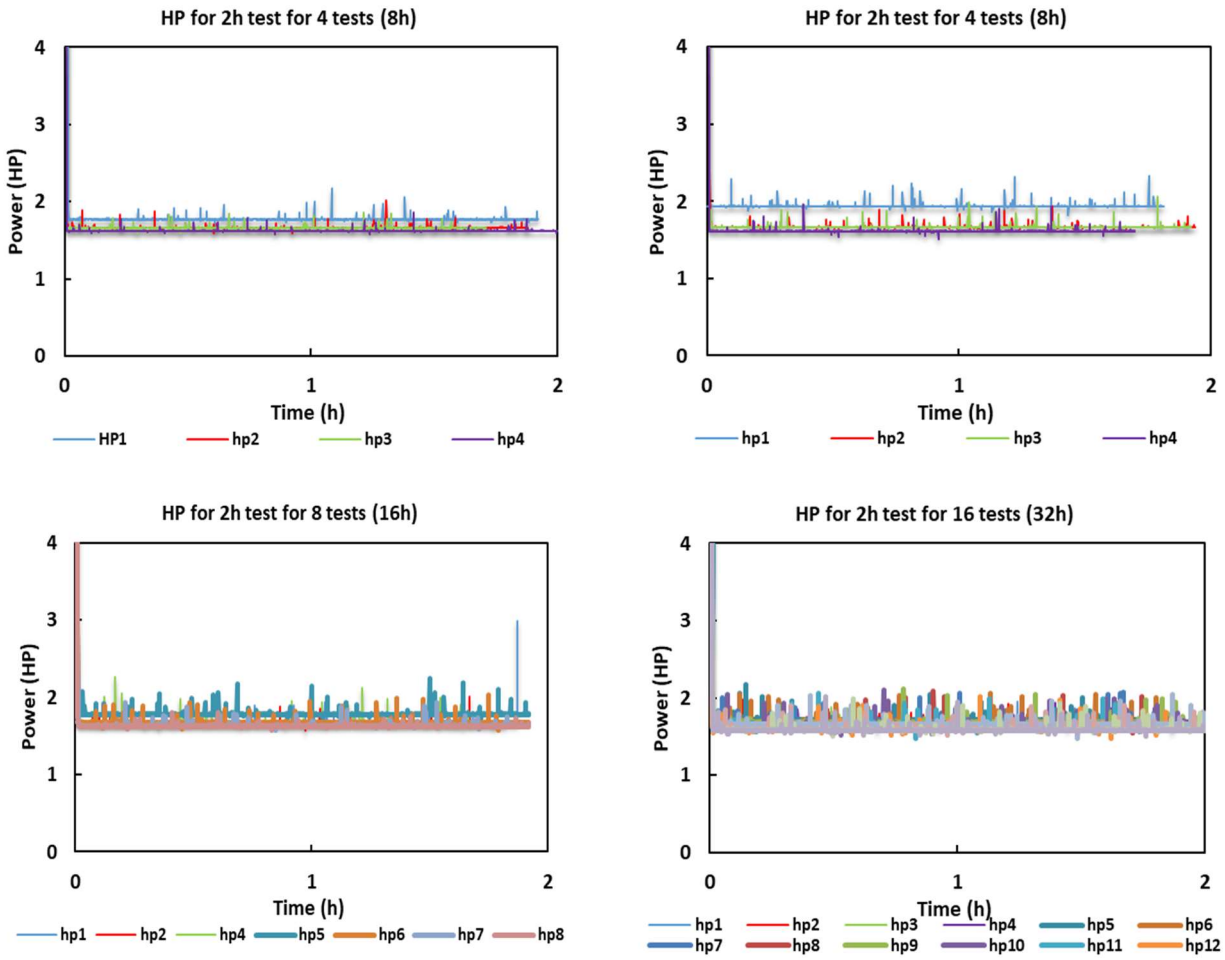

Figure C.6: Monitoring horsepower at ESP2 BEP for various testing periods

APPENDIX D

STAGE DISASSEMBLY PHOTOS AFTER TESTING INTERVALS

After every testing interval, stages were removed from the ESP pump and photos were taken of individual diffuser-impeller units for observing the areas and patterns developed due to sand wearing. Photos of shaft and other components such as bearings and sleeves are also taken to note any changes which are generally ignorable

D.1 ESP1

(a)

(b)

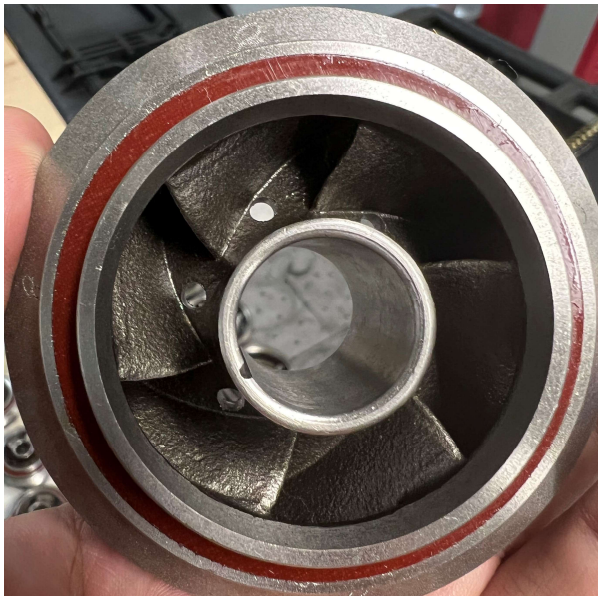

(c)

(d)

Figure D.1: Initial photos of ESP1 stages pre-testing, (a) Diffuser front, (b) Diffuser back, (c) Impeller front, (d) Impeller back

(a)

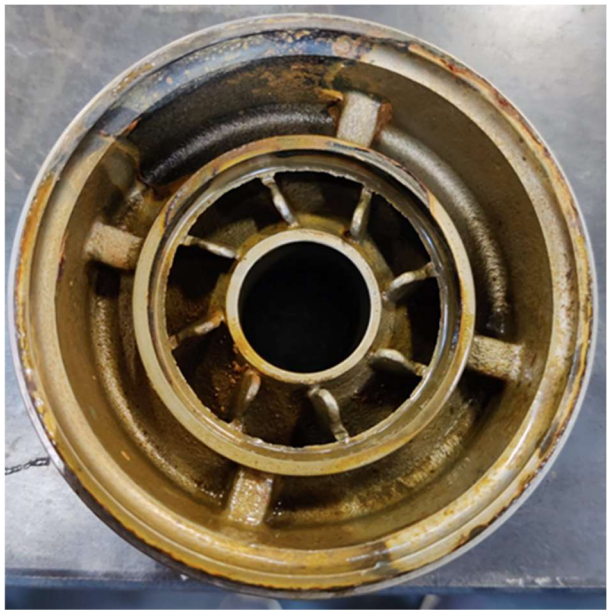

(b)

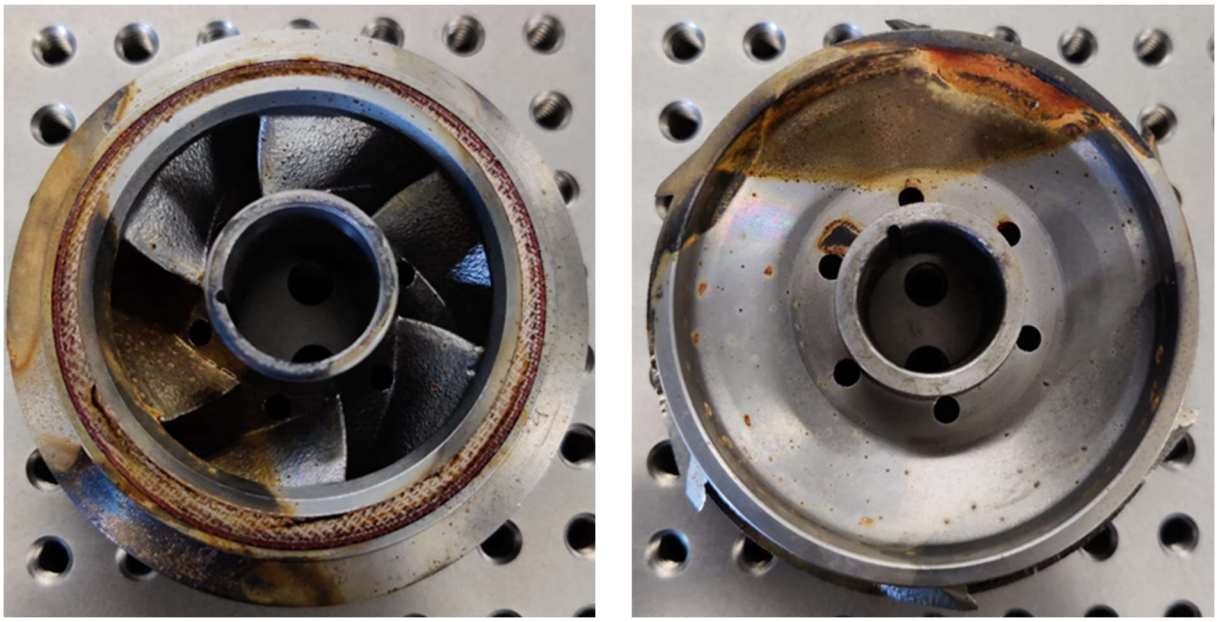

(c) (d)

Figure D.2: 8-hour test photos of ESP1, (a) Diffuser front, (b) Diffuser back, (c) Impeller front, (d) Impeller back

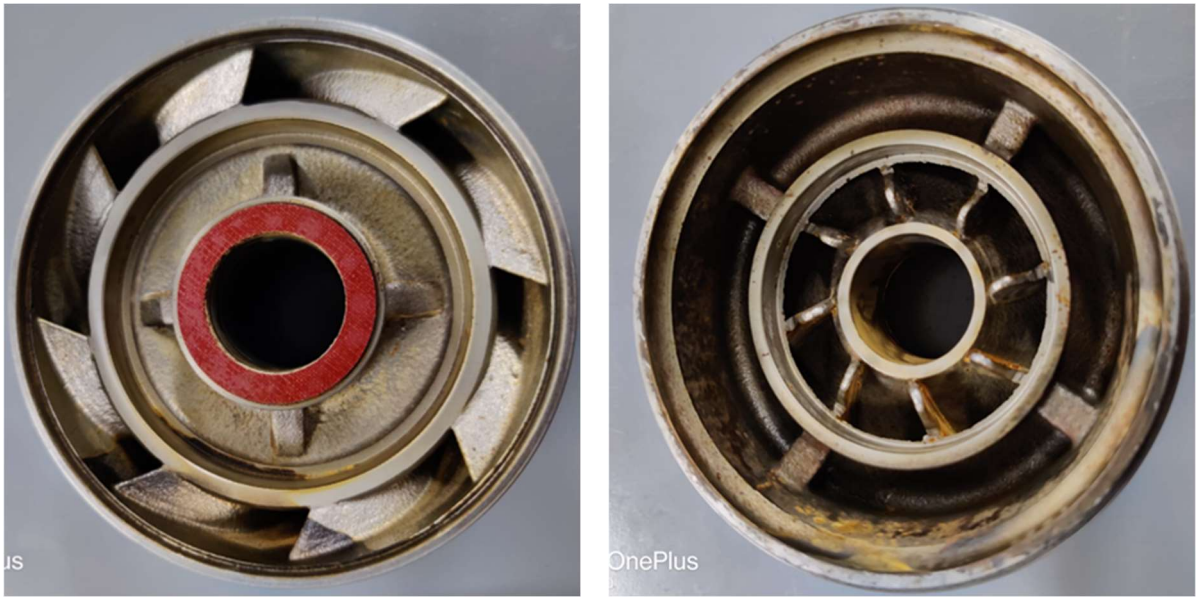

(a) (b)

(c) (d)

Figure D.3: 16-hour test photos of ESP1, (a) Diffuser front, (b) Diffuser back, (c) Impeller front, (d) Impeller back

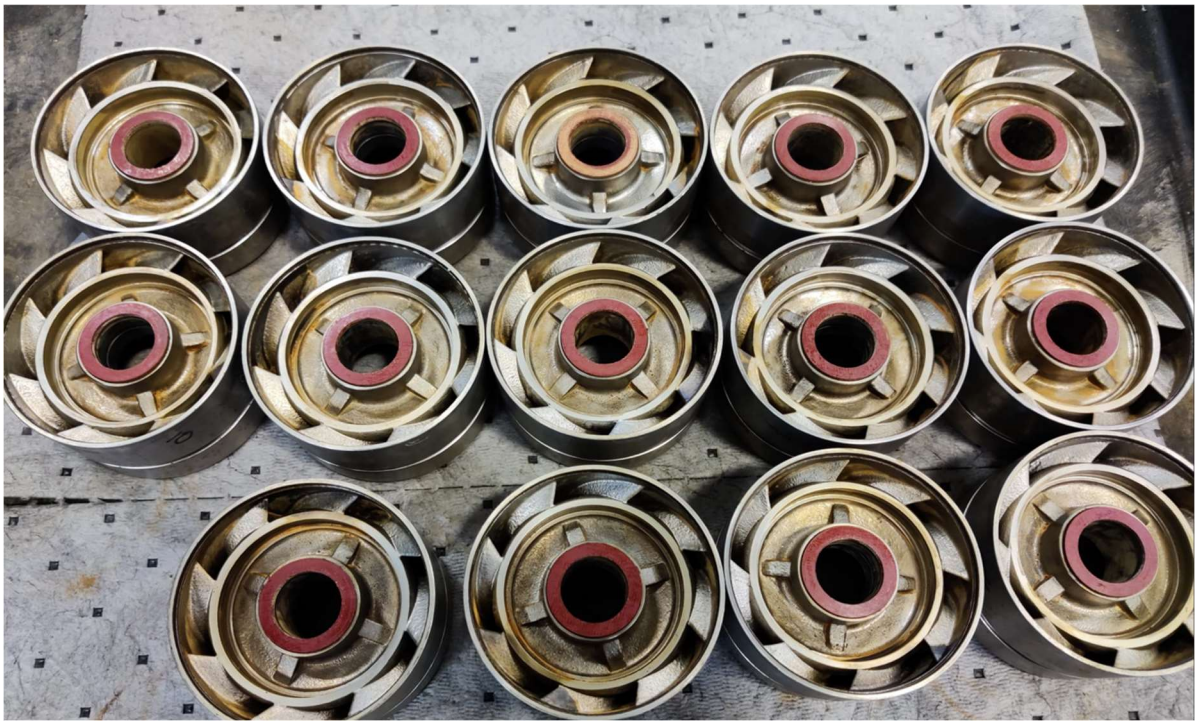

(a)

(b)

Figure D.4: 32-hour test photos of ESP1, (a) Diffusers, (b) Impellers

(a)

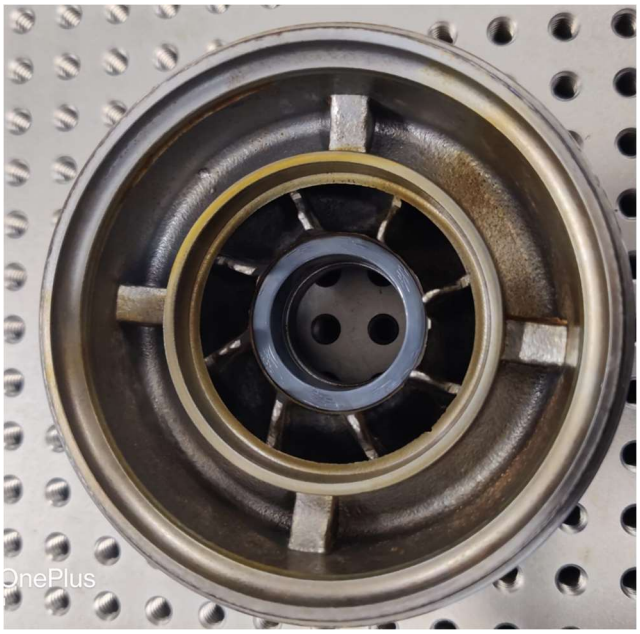

(b)

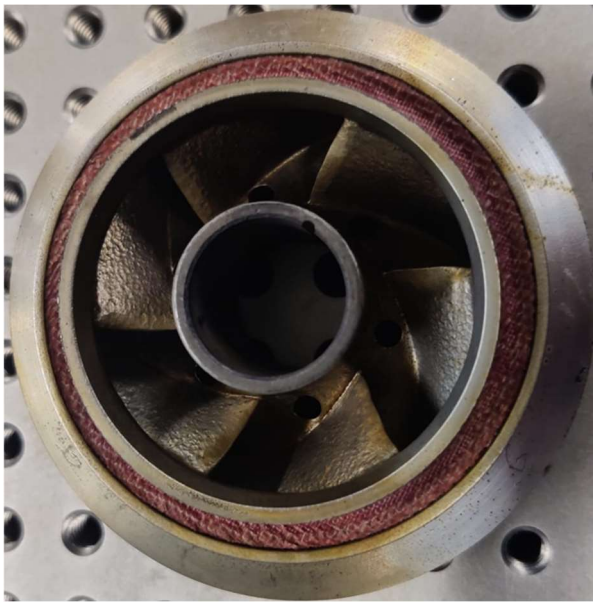

(c)

(d)

Figure D.5: 64-hour test photos of ESP1, (a) Diffuser front, (b) Diffuser back, (c) Impeller front, (d) Impeller back

(a)

(b)

Figure D.6: Miscellaneous parts, (a) Shaft, (b) Sleeves and bushings

D.2 ESP2

(a)

(b)

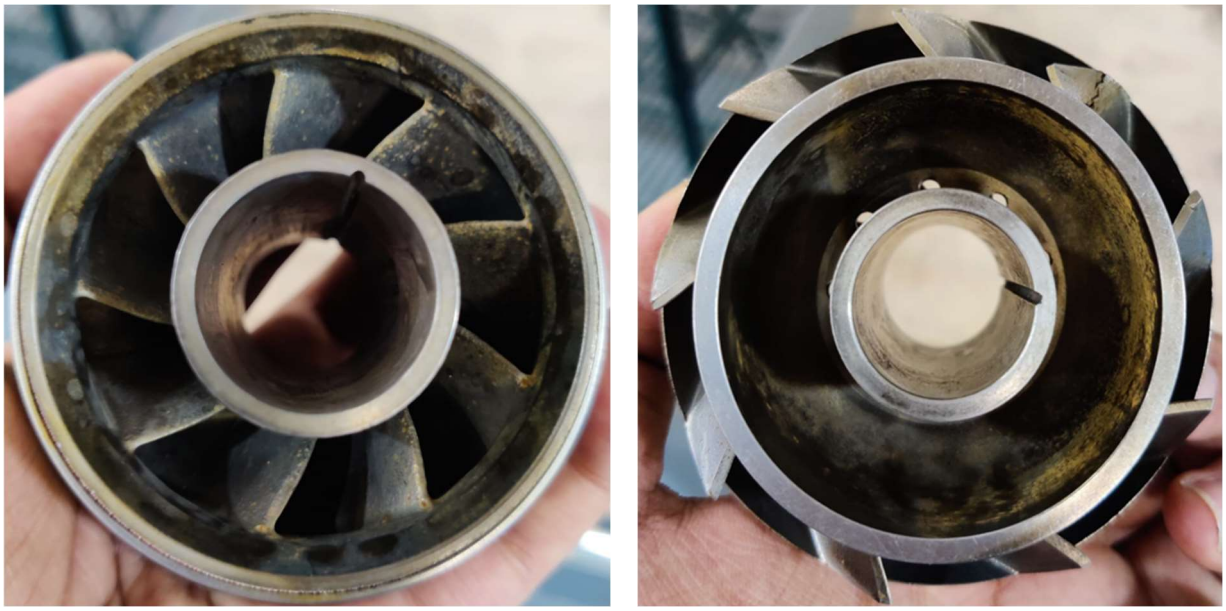

(c) (d)

Figure D.7: 8-hour test photos of ESP2, (a) Diffuser front, (b) Diffuser back, (c) Impeller front, (d) Impeller back

(a) (b)

(c) (d)

Figure D.8: 16-hour test photos of ESP2, (a) Diffuser front, (b) Diffuser back, (c) Impeller front, (d) Impeller back

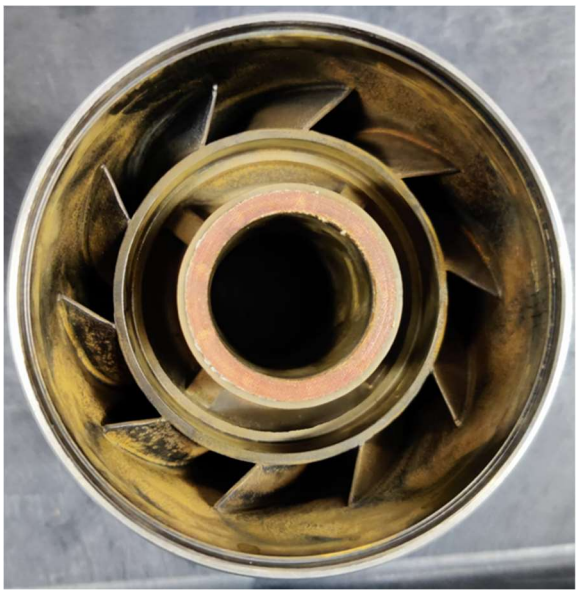

(a) (b)

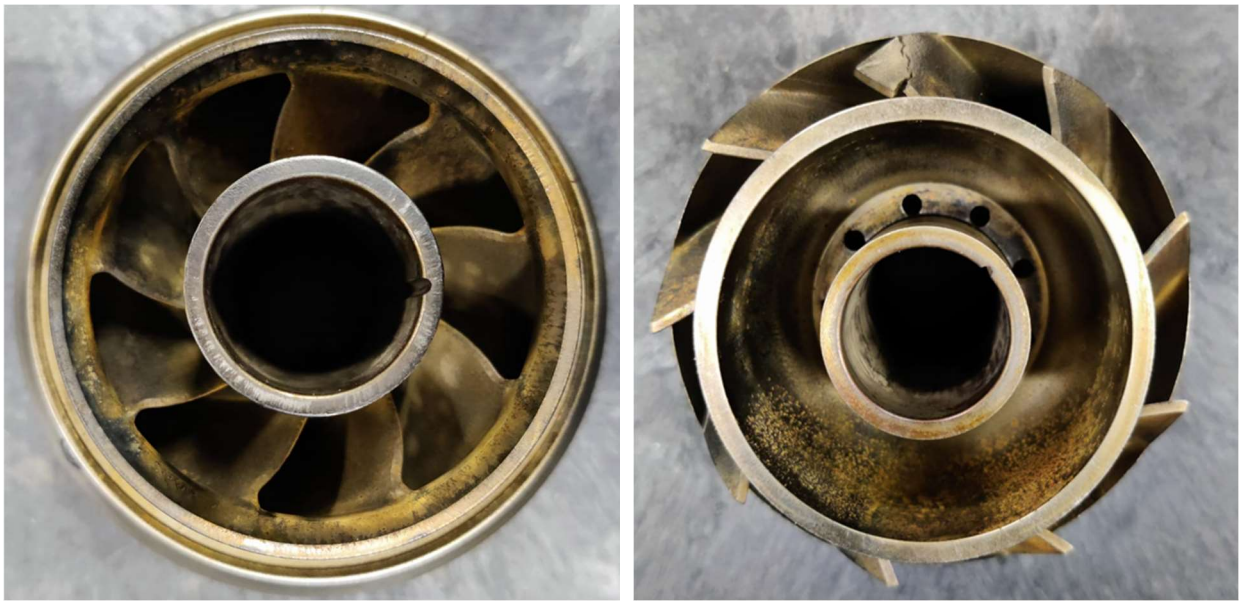

(c) (d)

Figure D.9: 32-hour test photos of ESP2, (a) Diffuser front, (b) Diffuser back, (c) Impeller front, (d) Impeller back

(a)

(b)

Figure D.10: 64-hour test photos of ESP2, (a) Diffusers, (b) Impellers

(a)

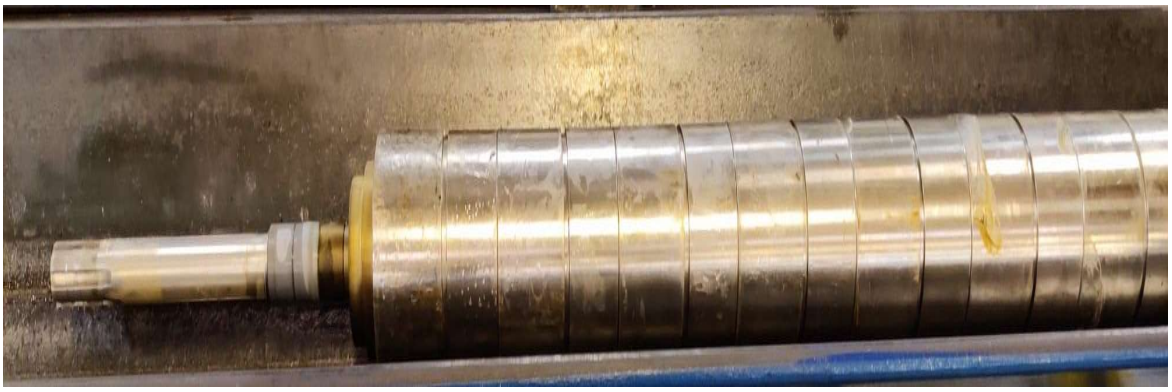

(b)

Figure D.11: Miscellaneous parts, (a) Shaft, (b) Sleeves and bearings

APPENDIX E

MATHEMATICAL EQUATIONS FOR CALCULATIONS

Equations used for the calculations of parameters for both pumps are presented in this section. Calculation equations of the basic performance parameters such as the head (Eq. E.1 and Eq. E.2), efficiency (Eq. E.3), and brake horsepower (Eq. E.4) are:

$$dp_n = \frac{P_{out} - P_{in}}{n}, \tag{E.1}$$

$$H = dp_n * \frac{144}{62.4}, \tag{E.2}$$

$$ŋ = \frac{\left(\frac{dp_n \times Q_w \times n}{0.434 \times 3960 \times 34.2857}\right)}{\left(\frac{\tau_{ESp} \times 3600}{63025}\right)} \tag{E.3}$$

and

$$HP = \frac{N \times \tau_{ESP}}{63025 \times ŋ}. \tag{E.4}$$

The calculation of head, efficiency, and brake horsepower is standardized to 3600 RPM using pump Affinity Laws below:

$$\frac{Q_1}{Q_2} = \left(\frac{N_1}{N_2}\right), \tag{E.5}$$

$$\frac{dP_1}{dP_2} = \left(\frac{N_1}{N_2}\right)^2, \tag{E.6}$$

$$\frac{HP_1}{HP_2} = \left(\frac{N_1}{N_2}\right)^3. \tag{E.7}$$

The torque measured in the tests is the total combined torque of the thrust chamber and ESP. By running the thrust chamber without any ESP, the following calibration equations are obtained:

$$\tau_{thrust\ chamber} = -0.1875 \times T_{thrust\ chamber} + 36.025 \tag{E.8}$$

and

$$\tau_{ESP} = \tau_{Total} - \tau_{thrust\ chamber}. \tag{E.9}$$